Thermal Microfluidic Devices; Design, Fabrication and Applications

Benyamin Davaji
Marquette University

THERMAL MICROFLUIDIC DEVICES; DESIGN, FABRICATION AND APPLICATIONS

by

Benyamin Davaji, B.S., M.S.

A Dissertation submitted to the Faculty of the Graduate School,

Marquette University,

in Partial Fulfillment of the Requirements for

the Degree of Doctor of Philosophy

Milwaukee, Wisconsin

May 2016

ABSTRACT

THERMAL MICROFLUIDIC DEVICES;
DESIGN, FABRICATION AND APPLICATIONS

Benyamin Davaji, B.S., M.S.

Marquette University, 2016

This thesis investigates the thermal actuation and temperature measurement methods in microfluidic devices. We designed and fabricated microfluidic devices with various functionalities such as: bio sensing, particle counting, microscale calorimetry, and cellular temperature measurement. All of these functionalities use thermal measurement methods.

When quantitative measurements are required, the label-free nature of thermal measurement methods, along with its simple readout, make it a powerful candidate for lab on a chip and bio sensing/detection applications. In this work, thermal measurement methods are used to characterize bio-samples, measure concentrations, study thermal responses, and even perform particle cytometry.

However, thermal measurement methods are known for their low speed and low sensitivity characteristics, which are influenced by thermal properties of materials and structural design. On the microscale, we designed and fabricated microfluidic structures with modified thermal properties to achieve low response times and high sensitivity. To optimize our devices, we analyzed the thermal responses of the designed structures using a first order equivalent electrical circuit model. We then compared the results of the model to the fabricated device responses. To increase the functionality of our device, we used a number of temperature measurement techniques; thermal wave analysis, AC calorimetry, time of flight measurement, and the continuous recording of differential temperature.

In this work, we fabricated an on-chip calorimeter with a 200 nL chamber volume and measured specific heat and thermal conductivity of water and glycerol. Also, we measured the thermal properties of the ionic liquids with the calorimeter. Moreover, we fabricated a calorimetric microfluidic biosensor to detect and measure the glucose levels of blood with concentrations of 0.05 to 0.3% wt/vol. We applied the same method to measure DNA concentration in buffer solution and a protein binding reaction. Also, we developed a method to count the number of particles passing through a micro channel while simultaneously measuring the size deference between particles by measuring changes in thermal conductivity. We fabricated a microfluidic platform to capture a single cell to measure the temperature of the cell in response to an external stimulation.

ACKNOWLEDGEMENTS

Benyamin Davaji, B.S., M.S.

I would like to take this opportunity to thanks my parents, Anamohammad Davaji and Tayebe Mashreghi and family, Elham, Asieh and Danial, for their priceless support and patience during my graduate school work since 2007. I want to thank my Ph. D advisor, Prof. Chung Hoon Lee for everything he has thought me in past 3 years. I also wanted to thank all of the Nanoscale Devices Laboratory previous and current members of the Nanoscale Devices Laboratory, specifically: Dr. Junhyun Han, Heyjeong Bak, Mohammadali Malakoutian, Andrew Kolb, Tsenguun Byambadorj, Trevor Thiess and Michael Bachmann.

In addition I want to thank all of my Ph. D dissertation committee members, Dr. James Richie, Dr. Fabien Josse, Dr. John Borg and Dr. Amit Lal for their constructive criticism and valuable feedback.

Finally, I wanted to thank, Dr. Erfan Dashtimoghadam, Kemaleddin Farrokhnia, John Neuman, Alireza Fatemi, Ian Morrissey, Thomas Burke and all other friends who helped me on this dissertation and finally, without their support this could be a lot harder to accomplish.

Benyamin Davaji
Milwaukee, WI.

TABLE OF CONTENTS

LIST OF TABLES

LIST OF FIGURES

Chapter 1 Introduction

One of the most exciting parts of scientific research is extending our understanding of nature through discovery of novel ideas and developing new technologies. Both new ideas by theorists and novel tools by experimentalists have revolutionized the sciences. Which one drives scientific research is the fundamental question: concepts or tools. Freeman Dyson divided scientists based on their approach into two categories: Kuhnians and Galisonians, named after two scientific revelation theorists, Thomas Kuhn and Peter Galison, respectively (Dyson 2012). The Kuhnians are theorists who are looking to drive the scientific research by developing new ideas. On the other hand, the Galisonians are experimentalist researchers with strong belief in dominating the scientific advances by developing new tools.

Currently, it is not possible to clearly identify the contribution share of Kuhnian science versus Galisonian science. Fortunately, science is witnessing the strong progresses in both directions in 21st century (Dyson 2012). However, Dyson believes “new directions in science are launched by new tools much more often than those by new concepts. The effect of a tool-driven revolution is to discover new things that have to be explained” (Dyson 1998). This argument highlights the importance of tool-driven research without neglecting the contributions of concept-driven research.

This dissertation investigates thermal microfluidic technology and offers fundamental new capabilities as a powerful tool to enhance the functionality of microfluidic devices. Thermal microfluidic technology is the science and technology of performing thermal measurements on extremely small quantities of liquids or suspensions, where the microfluidic devices are used to handle and prepare the samples. This work is a tool-driven research based on the introduction, and it lays among many others tool driven researches on “Galisonians planet”.

This chapter starts with an introduction to the thermal measurement technology and reviews the scope of applications of thermal measurement techniques. Then, microfluidic

technology is reviewed with emphasis on advantages of applications. Identifying the limits and potentials of thermal microfluidic devices and developing a general design approach for overcoming these limits leads to the utilization of its potential. This is the motivation of research presented in following section. Finally, the structure of the context of this dissertation is explained in the last section of this chapter.

1.1 Thermal Measurement

In general, thermal measurement methods and thermal analysis are measurement techniques for investigating the properties of samples using heat. The origin of heat as a physical quantity is discussed in chapter 2, where the heat transfer phenomena and main heat transfer modes are introduced.

Since heat is not a directly measurable physical quantity, the heat transfer and temperature changes are commonly investigated instead. Various thermal measurement techniques are developed for measuring the physical properties of materials or for investigating the chemical reactions and physical interactions.

Thermal measurements are direct measurement techniques that produce quantitative results and offer considerable advantages. The advantages of thermal measurements and thermal analysis are presented later in chapter 2.

However, thermal techniques are commonly known to be slow due to the thermal properties of measuring tools and samples. Another known issue with thermal measurement techniques is the ambient effects, where the thermal isolations are a challenge in many applications.

The main goal of this research is to investigate the feasibility of thermal measurement methods for diverse measurement and detection applications in the microscale by defining design considerations for developing measurement tools based on thermal methods.

To achieve this goal and investigate the capabilities of the thermal methods, microfluidic devices with thermal measurement methods for four different applications are developed. Microfluidic technology based on substantial capabilities in handling and processing samples in small scale are used as the base for implementing thermal measurement technique.

The presented research is structured slightly different from others. Here where the implementation of thermal measurement methods by investigating the applicability of such techniques is the main concept. Then, in this work, the feasibility of proposed measurement methods are studied by developing, characterizing, and evaluating the output results of four different devices to verify the practicality of the concept of thermal measurement.

1.2 Microfluidic Technology

Microfluidic technology is the science and technology to handle, manupulate, and process small quantities (10^{-18} to 10^{-9} liters) of substances in the dimensions of a few hundred nanometers to hundreds of microns (Whitesides 2006). Based on application and functionality, microfluidic devices have been recognized with different names: Lab on a Chip (LOC), Miniaturized Total Analysis System (μTAS), and Point of Care (POC) diagnosis devices (Erickson & Li 2004; Sackmann et al. 2014). Typically, miniturized reaction chambers, micro channels or a network of microchannels, micro valves, micropumps, and sample inlet and outlet interfaces are the most common parts of microfluidic systems.

Microfluidic technology offeres many advantages, to name a few: rapid sample processing and precise control over fluid, which implise substantially smaller required sample and reagent. Considering these advantages, microfluidic technology at the beginning promised considerable optimism for revolutionizing diagnostics and biological research (Sackmann et al. 2014). The microfluidic system can be combined with simple sensors and/or complex detection systems to deliver the expected analytical functionalities (Whitesides 2006).

Microfluidic technology originated from five different fields in science and enginering: microelectronics, molecular biology, molecular analysis, biodefense (Whitesides 2006), and fluid mechanics. However, the microelectronic and semiconductor industries started the fabrication of microscale devices using standard micromachining techniques (Sackmann et al. 2014). The on-chip gas chromatography and inkjet printers are pioneer projects in the field that shaped the roadmap of current developments in microfluidic technology (Erickson & Li 2004). Combining integration and miniaturization from microelectronics with the groundbreaking power of microanalytical methods in chemical analysis, microfluidic systems belong in the category of powerful/emerging technologies. The recent developments in molecular biology, genomics, and the research/investigations in the field of biodefense to overcome the chemical and biological threats also contributed deeply into the field. They contribiuted not only as a consumer to use the technology, but also by bringing the development experience back to the feild (Whitesides 2006).

The field of microfluidics offers new capabilities in handling and processing the fluid samples, which brings unique possibilities. The main advantage of microfluidic systems is the small quantities of the required sample and reagent. The short analysis time, low cost, high throughput, and high sensitivity are the other advantages of microfluidic systems.

Microfluidic research became one of the very common interdisciplinary research topics that brought people from different fields together. Industrial applications of microfluidic technology are increasingly growing (Chin et al. 2012). The microfluidic products are not dominating the field yet and the reasons are not clear to scientists, engineers, and developers (Whitesides 2006). Like most scientific fields, microfluidic technology has its disadvantages and necessary tradeoffs, however, the advantages far outweigh the disadvantages.

1.3 Motivation of Research

Microfluidic technology, as presented in the introduction section, offers fundamentally new capabilities to handle, control, and manipulate very small quantities of samples and reagents (Whitesides 2006). These new capabilities are broadly used for research in life science and diagnostic technology (Temiz et al. 2015) [ref]. However, the developed detection and sensing methods for microfluidic technology are limiting this fast growing technology. Thermal measurement offers many advantages that make it suitable to integrate with microfluidic technology for detection and sensing. In the rest of this section, the main advantages of thermal microfluidic devices are discussed.

Chemical and biochemical reactions result in enthalpy change. The absorbed or released energy causes temperature change. Measuring this temperature change is a key to understanding the progress of chemical or biochemical reactions. This technique makes thermal measurement a good candidate for detection of reactions and interactions. However, the applications of thermal measurements are not limited to the study of reactions and interactions, but we can find or design a reaction for investigating the existence and concentration of different species.

Understanding of cellular and intercellular interactions are essential for many therapeutic and diagnostic studies. Researchers in fields like tissue engineering, regenerative medicine, drug discovery, drug delivery, and disease detection are investigating cellular and/or intercellular responses. The cellular and intercellular responses often investigated in a large group or a suspension of cells. Recent reports show the independent applications and importance of studying the cellular responses at the single cell level, the tissue level, and also at the organ level. Regardless of the population, it is known that many intercellular processes are causing a temperature change, such as the gene expression and cell division which are exothermic processes (Okabe et al. 2012)(Is et al. 2012). Thermal microfluidic devices are capable of measuring this temperature change without disturbing the cell or group of cells.

Furthermore, the temperature measurement methods in bio-detection are label-free techniques. Label-free detection approaches avoid additional labeling steps, where it is essential for labeled detection methods to develop or find a stable label for attaching to a biomarker or chemical complex. The labels could be simple color dyes, complex quantum dots, gold nanoparticles, or radioactive inks. These labels often need external excitation for detection and imaging. The label free methods avoid these complexities. The label-free nature of thermal measurement makes thermal measurements suitable for lab-on-a-chip (LOC) and point of care (POC) applications.

Measuring the concentration of quantities is an important role for many diagnostic devices. Currently, producing the quantitative measurement results is a key challenge for portable devices, where the size of devices are limited. The majority of POC devices currently use optical detection methods, which produce qualitative measurement data or semi-quantitative measurement results. Using thermal detection method with known enthalpy change and reaction kinetics in combination with precise volume control in microfluidic devices results in quantitatively measured data. The quantitative output offered by thermal measurement methods makes it well suited for many diagnostic applications and analytical devices.

The other application of thermal microfluidic devices is calorimetry at microscale. Calorimetry is known as a powerful tool to investigate the state variables of materials by controlling and measuring heat transfer. Calorimetry is used for studying chemical reactions , physical changes , and phase transitions in materials. The calorimetry techniques are intensively investigated for a number of different measurements in bulk. However, microscale calorimeters are in early stages of development. There are few early researches reported with focus on scaling down the calorimeter system to achieve highly controlled fluid handling, low required quantities of samples and reagents, and increasing precision. However, the complexities of thermal isolation and sensitivity of the measurement issues have yet to be addressed.

Thermal microfluidic technology has started at the earlier stage mainly for basic calorimetry applications. Calorimetric techniques in microscale offered new capabilities such as using thermal conductivity measurement to count the particles or cells and perform cytometry in microfluidic channels or measuring the thermal diffusivity for cellular viability.

The complexities associated with thermal measurement methods include the spatial and temporal resolution of measurement and the sensitivity vary from a simple resistor technique to atomically precise machined probes or state of the art florescent particles techniques. Microfluidic technology enables the use of simple thermal measurements that avoid complexities in fabrication and integration. Developing a device for a wide range of thermal measurement applications remains a challenge. Thermal microfluidic devices are facing a trade-off between the spatial and thermal temperature measurement resolution and the sensitivity of measurement. Thermal microfluidic devices could be designed and fabricated considering the measurement requirements with offering simple fabrication and measurement. Details of design and fabrication of thermal microfluidic devices are covered in chapters 3 and 4, respectively. It is shown that simplicity can be achieved in design and development of portable thermal microfluidic devices.

In this section, the advantages of using thermal measurement methods for detection in microfluidic devices are presented. The major benefits of thermal microfluidic devices are the label-free nature of detection, non-invasive temperature measurement, qualitative measurement results, and the capability of detecting and measuring concentration of species when small quantities of samples and reagents are available. These characteristics are the main motivation of this research. Our approach for designing and developing the microfluidic system with mentioned characteristics is briefly reviewed in the next section, where the in-depth investigation is left for later chapters.

1.4 Approach

As explained in previous sections, thermal measurement characteristics as a system are a function of thermal properties of material, physical dimension of system, temperature sensor properties, and measurement techniques. Having multiple design variables makes the engineering trade-off essential to design and develop an applicable device for each specific application. For a better understanding of the thermal microfluidic device as a system, an equivalent model is used in this work. The analogy between heat transfer parameters of a system and electrical current and potential lead us to use a first order equivalent circuit to analyze the thermal microfluidic system.

In Chapter 2, the thermal design characteristics of the system, including thermal resistance, thermal mass, and thermal time constant of measurement are introduced. Using the developed equivalent circuit, design considerations to achieve applicable thermal characteristics for thermal microfluidic devices are defined. Thermal microfluidic devices are designed and restructured by applying the defined design consideration in material selection and structure design.

The majority of current microfluidic devices are polymer based devices, which are mostly developed using soft lithography techniques. However, unfavorable thermal properties (large thermal mass) of polymer based microchannel and poor thermal conductivity of such materials at sensor interfaces limit the measurement speed and result in relaxation of temperature to device and ambient. In this work, a combination of silicon based materials and polymers are used to reduce the thermal mass, increase the thermal isolation, and reduce the thermal time constant. The possibility of using porous materials with high flexibility in thermal microfluidic devices is also investigated. These investigations led to the design and development of the first paper-based microfluidic sensor with calorimetric detection.

Designing a microfluidic platform with optimized thermal isolation and small mass can be achieved by modifying and redesigning the structure of microfluidic channels and cavities.

The silicon 3D micromachining technology and thin film deposition technology allows us to develop very thin (500 nm) suspended structures, without losing the mechanical strength of the microchannel. The developed 3D micro-machined on chip calorimeter is published in scientific journal paper (Davaji et al. 2014). The same micro fabrication technique is combined with soft lithography technology and a microfluidic platform capable of measuring thermal conductivity for micro particle detection and cytometry is introduced for the first time.

The focus in this work is to develop devices for bio sensing, lab-on-a-chip (LOC) applications, and point of care (POC) applications. In our approach, we used resistive temperature detector (RTD) sensors. The operation temperature range and required linearity in the range, simplicity of the fabrication and integration of the RTD sensors were lead to this selection. The RTD sensor has good linearity compared to thermistors and offers sensitivity compared to thermocouples within the range. Moreover, fabrication of a RTD device at micro scale is simple and less expensive compared to other technologies. The RTD device can also operate as a heat source and can be actively used for thermal actuation in thermal microfluidic devices.

Thermal measurements and calorimetric technology in bulk are well stablished. Many different measurement techniques are developed and characterized for measuring different functionalities. In this work, we adapt AC calorimetry, thermal wave analysis (TWA) techniques and heat penetration time measurement or time of flight (ToF) measurement techniques. Combining these techniques, thermal microfluidic devices were developed and are able to offer different functionalities.

Signal amplification plays an important role in biosensor devices, devices can detect signals with smaller amplitudes than limit of detection (LoD). In our approach, we intended not to use any external label or excitation. In this work, we take advantages of the label-free nature of temperature measurement is preferred over using complex labels.

1.5 Organization of the Dissertation

This dissertation is divided into five chapters, where each chapter's materials are organized to be self-contained and, at the same time, the flow of context is prioritized. In the first chapter, the dissertation starts by introducing microfluidic technology and thermal measurements by reviewing existing work and looking at the limitations and challenges. In the second chapter, our approach and design principle to overcome the existing challenges are presented. In the next chapter, the fabrication and characterization of the microfluidic devices with integrated thermal measurement methods are designed. The measurement results and discussion of our work for each device is explicitly presented in the next chapter. The final chapter reviews the ongoing and future works along with highlighting the potential application. The organization of the context within each chapter is presented in the next few pages.

In the first chapter, the microfluidic technology and its applications are introduced with in-depth review of previous work. The thermal measurements and application sections are located in the next section. The potentials when the microfluidics and thermal measurement methods are combined and the background of existing work with emphasis on highlighting the advantages and disadvantages are reviewed in the next sections. In the last part of the first chapter, the motivation for this thesis and our approach to overcome the current issues and challenges, with slight touch on details of the process, are presented.

Chapter 2 covers thermal microfluidic device design and characterization in detail. The chapter starts by introducing the heat transfer phenomena and covers the fundamentals for three basic heat transfer mechanisms. The thermal characteristics and properties of microfluidic devices in the next section provide the requirements for thermal devices. The electrical analogy and first order equivalent circuit model for analyzing the heat transfer in microfluidic devices are the final part of this section.

Chapter 2 continues by presenting the considerations for thermal microfluidic device design, where a combination of material selection and micromachining techniques are used for redesigning and optimizing the microfluidic structures. The sources of measurement noise in thermal microfluidic devices are reviewed in the next section. This chapter ends by presenting the thermal measurement techniques, which makes it possible to measure different observables using the same device.

Chapter 3 provides fundamental descriptions of design and operation of fabricated thermal microfluidic devices in this work. This chapter shows how the thermal measurement methods are integrated with microfluidic devices to perform different functions. In this work, four applications for thermal microfluidic devices are investigated. The investigated applications are On-chip micro calorimeter, thermal particle detector, paper-based thermal biosensor, and microfluidic platform for continuous monitoring of a single cell temperature response. Since design criteria and functionality for devices in each application vary, the details are presented independently for each applications in this chapter.

The on-chip calorimeter design and operational principle are presented in the first section of this chapter. The next section covers the operational principle and the design of a novel device, which uses thermal measurement for detecting particles in a microfluidic channel. In the following section, we introduce a paper-based calorimetric biosensor. The final section of chapter 3 covers the design and operational principles of the developed microfluidic platform for capturing a single cell for measuring cell temperature change.

Chapter 4 contains the details of device fabrication and thermal measurement experiments for each application. This chapter also covers each application individually, where the sections are organized in the same order as the previous chapter. The experimental section for each application begins with device fabrication details, followed by sample preparation and experimental setup descriptions. For each application, the measurement results are presented. At

the end of each section, the experimental results are evaluated for each individual application in the discussion section.

Chapter 5, the final chapter, provides a summary of presented research. The first part contains a summary for each developed device as well as a general conclusion for thermal microfluidic devices. The ongoing experimental work is introduced briefly in the next section. This ongoing investigation will be published and/or transferred to junior colleagues at Nanoscale Devices Laboratory in Marquette University. In continuation, the potential applications for developed devices and introduced thermal microfluidic technology are discussed. This section is organized to present the potential of thermal microfluidic technology in two categories. First potential applications are introduced in the form of future work, which does not require significant changes in device structure. The second category discusses the future of this technology and aims to draw a big picture of applicable domains for thermal microfluidic technology.

Chapter 2 Device Design and Thermal Considerations

Fundamental understanding of the origin of heat and heat transfer phenomena is essential for designing devices where thermal measurement methods are used for detection and quantization. In addition to understanding the fundamentals, a model is required for thermal analysis to implement the thermal considerations in designs. Finally, the proper knowledge on available materials for device fabrication is vital information for designing feasible structures.

This chapter elaborates on providing the scientific background for heat transfer phenomena in microfluidic devices, introduces a model for thermal device considerations, and provides the material properties and fabrication process for thermal microfluidic device fabrication.

Section 1 introduces the fundamentals of heat transfer phenomena by reviewing the basic mechanism of heat transfer. In the second section, thermal microfluidic devices from a systematic viewpoint is studied, where an equivalent circuit model is introduced. The thermal circuit model is used for developing a set of design considerations, which allows performing thermal measurements in microfluidic devices without losing information.

Finally, the last section covers the available materials for microfluidic device fabrication with slight touch on their fabrication processes. The provided information on the materials and characteristics assists the introduced criteria to become practical realization instead of remaining theoretical.

2.1 Heat Transfer Phenomena

Interactions between any system and its surroundings results in system energy change. The law of conservation states that energy can not be created or destroyed. Therefore, these interactions cause energy transfer through heat and work. To design thermal microfluidic devices, understanding of heat and heat transfer modes is essential.

Thermodynamics is the science of studying energy transport dealing with the end states of interactions. It also studies the heat transfer modes and heat transfer rates, which are very important in designing a thermal measurement experiment. However, it does not provide microscopic view the nature of heat transfer and time rate of these interactions.

Phonons are the vibration of the atoms or molecules in condensed matter. Igor Tamm, a Russian physicist, suggested the concept of phonons for the first time in 1932. The microscopic nature of these vibrational states are caused by particle interactions; interactions of phonons and electrons in metals and phonon scattering in semiconductors and insulators. In other words, this heat transfer requires the collision between energy carriers; electrons and phonon in metals, and phonons in semiconductors and insulators. The detailed investigation of interactions of particles is required for exact microscopic understanding of heat transfer. However, macroscopic heat transfer is adequate for describing heat transfer on the macro scale.

In this section, the three main heat transfer mechanisms: conduction, convection, and radiation, are reviewed. This section will provide the background prerequisites for an understanding of the thermal characteristics of a system, presented in the next section, where an equivalent circuit and electrical analogy is used to design thermal microfluidic devices.

2.1.1 Conduction

Heat conduction is the microscopic transport of energy from higher energy particles to lower energy particles within the substance, where the substance is not experiencing any macroscopic flow or displacement. In other words, heat conduction is the transport of vibrational states within the substance in absence of any mass transport neither forced by flow nor diffusive (Incropera et al. 2006).

Conduction heat transfer is the dominant mode of heat transfer in solids. Therefore, in thermal microfluidic devices, at the microchannel walls and through the membranes, conduction is the main heat transfer mechanism.

A temperature gradient in the substance causes conduction, where heat flux goes from higher to lower temperature regimes. Fourier's law of heat conduction, proposed by French physicist Jean-Baptiste Joseph Fourier in 1822, explains the proportional relationship of the local heat flux density $\vec{q}$ to the negative gradient of temperature by introducing the thermal conductivity parameter (k):

$$\vec{q} = -k\nabla T \tag{2.1}$$

where $\vec{q}$ is local heat flux density $\left(W/m^2\right)$, k is thermal conductivity of a substance $\left(W/m \cdot K\right)$,and T is the temperature in Kelvin.

For one dimensional heat conduction, we can simplify Equation (2.1). If we consider only one dimensional heat transfer in the x direction, then we have:

$$q_x = -k\frac{dT}{dx} \tag{2.2}$$

Using Equation (2.2), the heat transfer rate in the x direction and perpendicular to the surface area A is defined by:

$$\dot{Q} = \frac{\Delta Q}{\Delta T} = qA = -kA\frac{\Delta T}{\Delta x} \tag{2.3}$$

The one dimensional form of Fourier's law can be extended to 3D equations in space. In addition, considering a 3D temperature distribution is closer to the real word temperature distribution realization. By using a 3D temperature distribution in the material, equation (2.1) can be re-written as:

$$\vec{q} = -k \cdot \nabla T = -k \cdot \left(\frac{\partial T}{\partial x}\hat{i}_x + \frac{\partial T}{\partial y}\hat{i}_y + \frac{\partial T}{\partial z}\hat{i}_z \right) \tag{2.4}$$

Heat flux for each direction can be written as:

$$q_x = -k\left(\frac{\partial T}{\partial x}\right), q_y = -k\left(\frac{\partial T}{\partial y}\right), q_z = -k\left(\frac{\partial T}{\partial z}\right) \tag{2.5}$$

Heat flux density and heat transfer rate in solid structures can be calculated for known materials, using measured gradients of temperature and measured values of heat conductivity. Also it is shown that the same concept can be used on 3D structures to get the heat flux density and heat transfer rates. In the next sections, after introducing the convention and radiation heat transfers, the concept of thermal resistance is introduced. This allows for convenient adoption of an electrical equivalent circuit to model the heat transfer.

2.1.2 Convection

Convective heat transfer is the macroscopic transfer between a surface and a moving fluid. It describes the flow of energy (vibrational states) from high-energy region to the low energy within in the substance, while experiencing mass transport. The convective heat transfer can be forced in the presence of external flow or natural convection when the flow velocity is induced due to the temperature gradient. Commonly, in natural convective heat transfer, fluid

velocity rises and then falls as it moves away from heat source. Both natural and forced convection heat transfer modes are illustrated in Figure 2.1.

Understanding the modes of convective heat transfer, natural and forced, requires an understanding of the characteristics of the working fluid. In conduction heat transfer, thermal conductivity of a substance is used as the material property to describe the heat flux. There are two parameters required to study convective heat transfer in a system; material properties and flow profile. In this work, a 3D notation, $\vec{u}(x, y, z)$, is used to describe the velocity profile of fluid. Fluid velocity is unable to describe fluid characteristics, where the viscosity and geometrical structure of the fluid plays an extensive role. Reynold's number as a dimensionless measure for characterizing fluids is widely used in fluid mechanics, and microfluidic is not an exception. Reynold's number is defined as:

$$\mathrm{Re}_{\mathrm{D}} = \left(\frac{\rho \cdot U_D \cdot L}{\mu} \right) \tag{2.6}$$

where ρ is the density of fluid in $\left({}^{kg}/_{m^3} \right)$, U_D is the maximum velocity of fluid in the D direction in $\left({}^{m}/_{s} \right)$, L is the characteristic length of structure selected based on the geometry in (m), and μ is the dynamic viscosity of fluid in $\left({}^{kg}/_{m \cdot s} \right)$. It is preferred to use only one parameter to describe fluid material properties. Commonly, kinematic viscosity $\vartheta \left({}^{m^2}/_{s} \right)$ is used instead of dynamic viscosity and fluid density and can be written as:

$$\mathrm{Re}_{\mathrm{D}} = \left(\frac{U_D \cdot L}{\upsilon} \right) \tag{2.7}$$

where the kinematic viscosity is defined as:

$$\nu = \left(\frac{\mu}{\rho} \right) \tag{2.8}$$

The Reynold's number predicts the fluid characteristics, where the fluid properties (density and viscosity), fluid velocity profile, and geometry of the fluid path are all considered. For a flat plate, if the Reynold's number is less than one it is considered Stokes flows or creeping motion, where the analytical solutions for fluid velocity boundary layers are available. In Stokes flows, the inertial forces are small compared to the viscous forces. The lubrication in mechanical systems, flow of lava, paint flow, and swimming of microorganisms such as sperm in a fluid are examples of creeping motion.

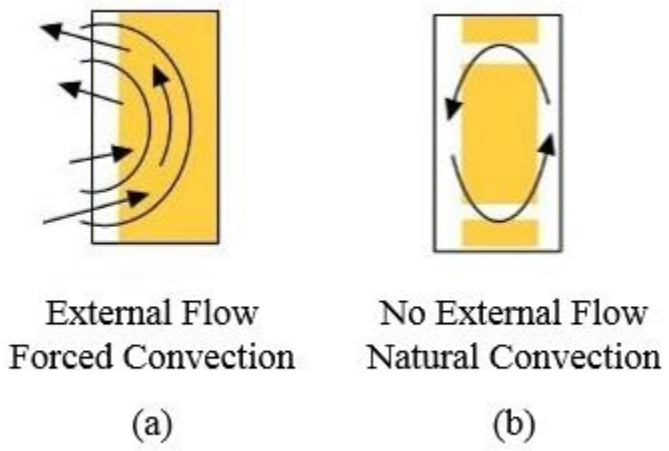

Figure 2-1 Forced Convection and natural convection heat transfer [Public Domain Figure].

.

Similarly, flat plate flows with Reynold's number greater than one and less than 2,200 are considered laminar flows. In two dimensions, laminar flow can be described as parallel fluid flow, where the layers are not experiencing any disruption or mixing from other layers. Both velocity and thermal boundary layers of the flows in the laminar region can be calculated analytically for simple structures and by computational fluid dynamics (CFD) methods for complicated structures. Considering the small velocities in microfluidic channels, flow fields in fabricated devices in this work are considered laminar flows.

The region where the Reynold's number is greater than 4,000 is considered a turbulent flow region. Turbulent flow regimes show complete chaotic properties, where the local fluid pressures and velocities are experiencing rapid changes in time and space. There is no solution developed for this region and it is described as "the most important unsolved problem of classical physics" by Nobel laureate Richard Feynman. The region between the laminar and turbulent regions is described as the transient regime. The provided flow regimes and Reynold's number will be used in the rest of this work to explain the heat transfer in microfluidic devices.

The rate of convective heat transfer between a surface and a fluid can be calculated from Newton's law of cooling, proposed in 1701 by British physicist and mathematician, Isaac Newton. Newton's law of cooling introduces convective heat transfer coefficient, h_c , in $\left(W/m^2 \cdot K\right)$ as an equation constant to describe the convective heat transfer rate:

$$\dot{Q} = h_c \cdot A \cdot \Delta T \tag{2.9}$$

where A is the area of the object through which heat is being transferred $\left(m^2\right)$ and ΔT is the difference between surface temperature and local fluid temperature in Kelvin. Since heat transfer is calculated over an area, it is common to use the average convective heat transfer coefficient, $\bar{h}_c$, over the area and rewrite equation (2.9) as:

$$\dot{Q} = \bar{h}_c \cdot A \cdot \Delta T \tag{2.10}$$

Unlike the thermal conductivity, the convective heat transfer coefficient should be calculated with respect to the geometry and often needs practical correction factors. The average convective heat transfer coefficient for the total surface is estimated by calculating the local convective heat transfer coefficient and averaging it over the surface.

In fluids, convection is not always the only heat transfer mode. Conduction can cause heat transfer in fluids as well. Often microfluidic devices experience both conduction and convection,

and must be analyzed as conjugate heat transfer. A dimensionless parameter, the Biot number named after a French physicist Jean-Baptiste Biot, suggests the ratio of conduction to convection heat transfer:

$$Bi = \left(\frac{h \cdot L}{k} \right) \tag{2.11}$$

where L is the characteristic length in (m), h and k are the heat transfer coefficient and thermal conductivity, respectively.

A Biot number less than 0.1 indicates the dominant effect is the conduction mode; here, the convective heat transfer is negligible. For greater Biot numbers, both modes must to be considered for a reasonable prediction of heat transfer.

2.1.3 Thermal Radiation

Phonons, as massless particles, could be studied as electromagnetic waves radiating in the space. Heat transfer by radiation of photons is named thermal radiation. In contrast to the other (conduction and convective) modes of heat transfer, the thermal radiation is not due to the thermal gradient in the matter. The thermal radiation does not require any transfer medium.

All forms of matter emit thermal radiation to space from its surface area depending on the surface's temperature. The Stefan-Boltzmann law explains the relationship of the radiation heat transfer rate from the surface of a black body to space by introducing the Stefan-Boltzmann constant, σ, where the fourth power of absolute temperature is directly proportional to rate of radiation heat transfer. The emitted thermal energy from the surface is described by Stefan-Boltzmann law:

$$\dot{Q} = \sigma \cdot A \cdot T^4 \tag{2.12}$$

$$\sigma = 5.76 \times 10^8 \left(\frac{W}{m^2 \cdot K^4} \right) \tag{2.13}$$

where $\dot{Q}$ is the rate of radiated heat transfer in (W) and T is absolute temperature of the surface.

In thermal radiation as stated, the heat transfer rate is proportional to the fourth power of absolute temperature. Thermal radiation models are used to explain the heat loss of substances in a vacuum and the solar radiation. It is also very important in many industrial heating, cooling, and drying processes. However, considering the operating temperature of thermal microfluidic devices, which are mainly designed for bio sample analysis, thermal radiation does not play a key role in heat transfer. Considering the negligible effects of thermal emissions, conduction and convection heat transfers are mainly used to analyze and design the thermal microfluidic devices in this work.

2.2 Thermal System Analysis

Earlier in this chapter, heat is described as the vibrational states of particles within the substance. Transferring these vibrational states from a high energy region to a low energy region is heat transfer, where it causes a change in local temperature. Even though temperature change can be measured, the direct measurement of heat is not feasible. Therefore, the measured temperature change in the system is used to calculate the heat transfer.

Understanding the heat transfer in a system allows one to design different types of measurements such as using a heat source and investigating the heat transfer throughout the sample (thermal analysis) or studying generated heat within a chemical reaction, physical interaction or biological metabolism (calorimetry). For both types of measurements, the

measurement system parameters and characteristics must be designed to optimize the results and identify design considerations.

This section investigates thermal microfluidic devices as a system and introduces thermal characterization for this system. Furthermore, a model is used to identify the effect of each parameter and system characteristics on the output response of the system.

2.2.1 Thermal Resistance

Thermal conductivity is a transport property of the material that describes the ability of the material to transfer energy by diffusion. Thermal conductivity is a physical property that is related to the structure of matter. In bulk form of materials, thermal conductivity is slightly dependent on temperature. However, at micro- and nanoscale levels, the thermal conductivity is affected by scattering. Thermal conductivity in thin films is decreased compared to materials in bulk, where the scattering at physical boundaries results in the redirecting particle propagation (Incropera et al. 2006).

Rearranging Fourier's law, thermal conductivity in the x direction is defined as:

$$k_x = -\left(\frac{q}{\frac{\Delta T}{\Delta x}} \right)\Bigg|_{\Delta x = L} = -\left(\frac{\dot{Q} \cdot L}{A \cdot \Delta T} \right) \tag{2.14}$$

The analogy between heat transfer due to the temperature difference and electric current flow due to the electric potential difference, suggests one can deal with Fourier's law of heat conduction like Ohm's law, where Ohm's law describes electrical resistance as:

$$R = \left(\frac{V}{I} \right) \tag{2.15}$$

Based on the analogy, convective thermal resistance can be described as the ratio of temperature difference to the heat transfer rate:

$$R_{cond,x} = \left(\frac{1}{k_x}\right) = \left(\frac{\Delta T}{\dot{Q}}\right) \tag{2.16}$$

Using Equation (2.14), Equation (2.16) rearranged for conduction thermal resistance in the x direction:

$$R_{cond,x} = \left(\frac{L}{k_x \cdot A}\right) \tag{2.17}$$

the thermal resistance term has a unit of $\left(K/W\right)$.

Applying the same analogy to Newton`s law of cooling, thermal resistance due to the convection can be describe as:

$$R_{conv,x} = \left(\frac{\Delta T}{q_x}\right) = \left(\frac{1}{h_{c.x} \cdot A}\right) \tag{2.18}$$

The concept of thermal resistance is very useful for the investigation of heat transfer in complex structures, where the total resistance of composite structures can be derived using the series and parallel resistance relations. Considering the thermal resistance for conduction and convection heat transfers, for convenience in calculations, defining a thermal resistance for radiation heat transfer from a surface is proposed. The thermal resistance for thermal radiation heat transfer is:

$$R_{rad,x} = \left(\frac{1}{h_{r,x} \cdot A}\right) \tag{2.19}$$

2.2.2 Thermal Mass

Thermal mass is another thermal property of a structure that plays a key role in thermal analysis. Thermal mass is the ability of a body to store thermal energy. Thermal mass of a body is dependent on the specific heat of the material and the mass of the body, and can be written as:

$$Q = C_{th} \cdot \Delta T \tag{2.20}$$

where Q is thermal energy in (J), C_{th} is the thermal mass in $\left(J/K\right)$ and ΔT is the temperature change in Kelvin.

Specific heat of a material is a measurable physical quantity that represents the amount of required heat to increase the temperature of a certain mass by 1 degree Kelvin. Using the definition of specific heat, Equation (2.20) can be rearranged using the definition of thermal mass:

$$C_{th} = m \cdot c_p \tag{2.21}$$

where c_p is specific heat capacity in $\left(J/kg \cdot K\right)$. Plugging Equation (2.21) into Equation (2.20) results in the following equation:

$$Q = m \cdot c_p \cdot \Delta T \tag{2.22}$$

Specific heat is a measurable physical quantity and can be measured by calorimetry techniques in constant pressure or constant volume. It is often used for material identification in thermal techniques. Specific heat is a temperature dependent quantity where the internal energy change in a substance results in a change in the specific heat. In this work, temperature dependence of the specific heat is not considered in the thermal analysis due to the applicable temperature change in thermal microfluidic devices, which are mostly designed for bio sample analysis.

2.2.3 Equivalent Circuit Model

A mathematical model, often the transfer function, is used to describe a physical system. These models are used to predict the performance of the system and optimize the performance for design criteria. In the thermal system design, the analogy between heat transfer and current flow in an electrical circuit is widely used.

Each system is considered from a network of elements where each element represents a physical property. Thermal systems are made up of two fundamental physical elements, thermal resistance and thermal capacitance. The material, structure geometry, and sample within the thermal system can be described by a system of thermal resistances and thermal capacitances.

Each physical system with fundamental elements needs a source to operate. In thermal systems, there are three different types of heat sources: power source, temperature source, and fluid flow. A power source is defined as a heat source, where the generated heat is independent of temperature. Joule heating, generated in an ideal resistive thermal element, is an example of a power source in thermal systems. A temperature source generates constant temperature independent of heat flow from or to the source. A good example for temperature source is a closed loop hotplate with a PID controller where the temperature is maintained at the set point, within the operation range, regardless of the heat flow. Mass transfer caused by fluid flow to a thermal system results in heat flow to or from the system. This heat flow is a result of temperature differences between the ambient and the system, and is proportional to the mass flow rate and specific heat of the flow.

Thermal systems consist of fundamental thermal elements and sources. Considering the introduced analogy between heat transfer and electric current flow, systems can be modeled as an electrical circuit. In this work, thermal microfluidic devices, as a system, are studied using the first order equivalent circuit model, where circuit theory is used to evaluate heat transfer. Thermal

circuit is illustrated in Figure 2.2, where the thermal system is represented by an equivalent resistance and an equivalent capacitance.

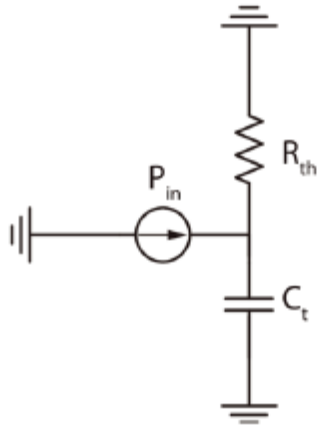

Figure 2-2 Thermal equivalent circuit model.

The total equivalent resistance and equivalent capacitance of thermal microfluidic systems are:

$$R_{th,total} = \left(\frac{1}{R_{cond}} + \frac{1}{R_{conv}} + \frac{1}{R_{rad}} \right)^{-1} \tag{2.23}$$

$$C_{th,total} = C_{structure} + C_{fluid} \tag{2.24}$$

In the following sections and chapters, this model is used to describe and investigate the performance of thermal microfluidic devices.

2.2.4 Thermal Time Constant

The main goal of this work is to develop thermal microfluidic devices for bio sample analysis through the measurement of physical interactions or chemical reaction progression. These reactions and interactions have different kinetics, so the measurements speed should be relative (faster) in time scale compare to the speed of reaction or interaction. Measurement requires a certain speed for thermal systems that the thermal elements individually are unable to

provide. Precise information on response time of thermal microfluidic devices to the temperature change is needed. This requires identifying a system parameter which describes the system response time to the temperature change.

The first order equivalent circuit is introduced for modeling a thermal microfluidic device in the previous section. Neglecting nonlinear effects in thermal components, a time constant is introduced for thermal microfluidic devices. The thermal time constant physically represents the response time of thermal microfluidic devices to the temperature change.

Time constant in a linear time invariant system is the response of a system to a step function. In a thermal circuit, the RC time constant represents the thermal time constant associated with the thermal microfluidic device. Using circuit theory, the thermal time constant is defined for thermal microfluidic systems as:

$$\tau = R_{th} \cdot C_{th} \tag{2.25}$$

where τ , the thermal time constant, represents the temperature measurement speed in microfluidic device in seconds.

As explained in the equivalent circuit model, the thermal time constant of a microfluidic system can be calculated using Equation (2.25). However, due to the assumptions in the calculations and fabrication parameter variations, this is only an estimation of actual time constant. Therefore, experiments are developed for measuring a thermal time constant in microfluidic devices.

In this work, a step response test proposed by Baliga (Davaji et al. 2014) is used for measuring the thermal time constant of fabricated devices to reduce the estimation errors. The details of a step response test for microfluidic structures are presented in the next chapter after introducing the structure and principle of operation.

2.3 Thermal Microfluidic Device Design Considerations

The thermal parameters for analyzing performance of thermal microfluidic devices were introduced in the previous section by reviewing heat transport in microfluidic systems and introducing the equivalent circuit model. A number of design considerations must be taken into account for achieving expected performance parameters. In this work, design considerations, derived from thermal system analysis, are reflected in a thermal microfluidic device through material selection and fabrication techniques. This section covers the detail of applying each of these considerations in design.

2.4 Material Selection

From its beginning in the 1980's, microfluidic technology experienced an explosive growth in the 1990's as it spread to the fields of biology, chemistry, and medical research (Ren et al. 2013). In the past decade, microfluidic technology has been revolutionized by introducing low-cost disposable devices. The material used for microfluidic devices is highly affected by the progresses in fabrication technology since the beginning of the microfluidic era (Whitesides 2006). However, the functionality demanded by microfluidic devices has changed the choice of materials in recent years. Currently, two major trends are driving the material development and selection trends for microfluidic technology: demand for highly functional micro and nanoscale platforms for research and the low-cost, portable analysis requirement for mass production (Ren et al. 2013; Whitesides 2013). This section presents the material selection consideration for thermal microfluidic devices by reviewing the previous works.

2.4.1 Conventional Materials

Microfluidic fabrication technology in the beginning was highly impacted by remarkable miniaturization capabilities offered by the semiconductor fabrication industry (Whitesides 2006). The dominant materials at the early stage of the technology were silicon and glass(Iliescu et al. 2012). The silicon processing technology provided the fabrication techniques for different structures at micro and sub microscale such as microchannel, mixers, droplet generators, filters and valves. Silicon and glass both have very good stability and non-reactivity, which make them suitable to use with different materials.

Although silicon is a very well-known material with well-established fabrication techniques, it lacks the optical access and suffers from high manufacturing costs. At the beginning of microfluidic era, silicon was widely used to fabricate complex structures to process fluids, but it was replaced with new materials very fast. Glass is a clear substrate and due to the optical transparency and it's non-reactive properties, it is widely used for microchannel fabrication(Chen et al. 2007; Kotowski et al. 2013).

Glass is an amorphous material that requires highly corrosive chemicals for micromachining, where developing an etch mask is yet a challenge for high aspect ratio etchings. Both silicon and glass are hard substrates and provide good mechanical properties but they are not gas permeable. Many biological experiments with living mammalian cells require gas permeability (Whitesides 2006).

The complexity and cost of the silicon and glass fabrication processes were what provided the momentum to search for new materials and develop new techniques to fabricate microfluidic devices (Becker & Locascio 2002). Therefore, microfluidic devices require materials that offer simple and low-cost fabrication process and at the same time, it is essential to have optical access, gas permeability, and biocompatibility.

2.4.2 Polymer-based Structures

Polymer based microfluidic devices came about several years after silicon/glass microfluidics but rapidly became the most common in the field due to their properties and are the most familiar ones to date (Ren et al. 2013). The polymers are transparent to light and offer gas permeability, and in some cases good biocompatibility. The most important benefits of polymer materials are the inexpensiveness and process simplicity. Different types of polymers are used for fabrication of microfluidic devices: elastomers, thermosets, and thermoplastics are the common polymers used in microfluidic device fabrication (Ren et al. 2013).

The most popular elastomer in microfluidic device fabrication is polydimethylsiloxane (PDMS). PDMS is a nontoxic, inert, optically transparent, and electrically insulating (nonconductive) polymer (McDonald & Whitesides 2002). The elastomeric nature of PDMS allows remarkable flexibility, which makes it perfect for fabrication of simple pneumatic valves. Introducing pneumatic valves brings a unique controllability opportunity for microfluidic devices(Whitesides 2006).

The fabrication process, the most attention-grabbing side of the PDMS, features a liquid PDMS base mixed with a crosslinking agent which can be thermally ($40-70^{\circ}C$) cured over a micro fabricated mold (Ren et al. 2013; McDonald & Whitesides 2002; Stroock & Whitesides 2002). The common fabrication process for PDMS microchannel is illustrated in Figure 2.3. Using the same techniques, a complex structure with multilayers and 3D integration can be fabricated (Thorsen et al. 2002; Unger et al. 2000).

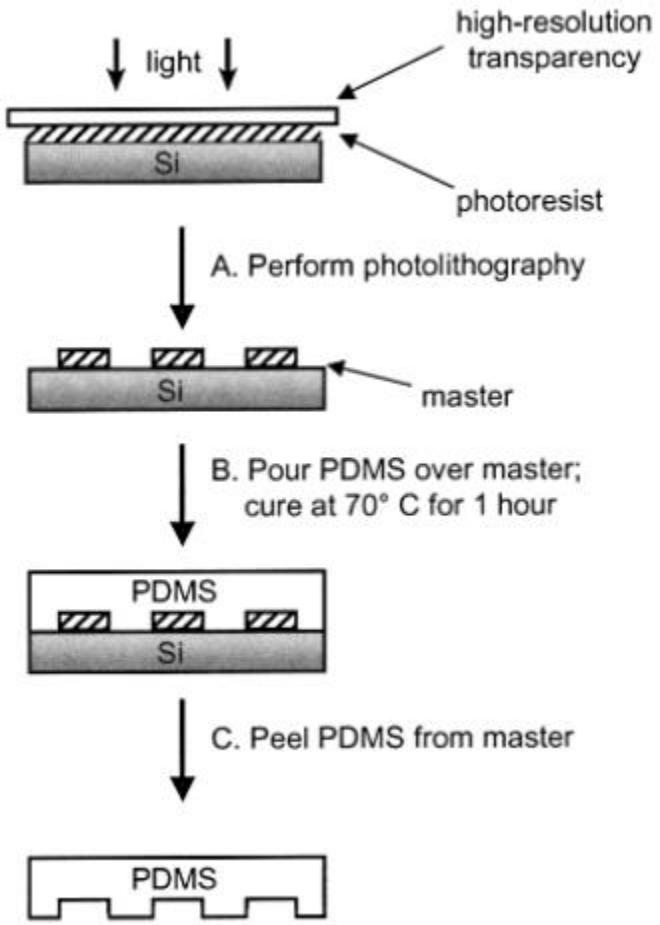

Figure 2-3 Fabrication process of PDMS microchannel using simple photoresist mold. (McDonald & Whitesides 2002)

Thermoplastics are the other group of actively used polymers to fabricate microfluidic devices. Thermoplastics can be reshaped after curing by heating them around their glass transition temperature. This exceptional thermoforming feature promotes their bonding and reshaping after curing and eases industrial production (Ren et al. 2013; Roy et al. 2011). The common thermoplastics used for microfluidic device fabrication are Polymethyl methacrylate (PMMA), Polycarbonates (PC), Polystyrene (PS), Polyethylene Terephthalate (PET), and Polyvinylchloride (PVC) (Ren et al. 2013). Thermoplastics have two major drawbacks compared to elastomers; the thermoforming requires silicon or metal micro machined molds and it creates poor contacts with the other surfaces (Becker & Locascio 2002; Ren et al. 2013).

Thermosets are the third group of commonly used polymers for microfluidic device fabrication. The most commonly used thermosets are SU8 and Polyimide, which are adopted from the silicon microfabrication process. Thermosets are commonly used as a mold for elastomer-based microfluidic device fabrications, where they serve as negative photoresist (Ren et al. 2013) (Fiorini & Chiu 2005) (Fiorini et al. 2004). SU8 is a photo cross-linkable thermoset, developed by Microchem, and capable of forming high aspect ratio structures from sub-micron to few hundredths of a micron in thickness. Photo polymerization capability of thermosets allows 3D microfabrication of microfluidic devices(Sato et al. 2006). Figure 2.4 shows the fabrication process microchannel using SU8 photoresist.

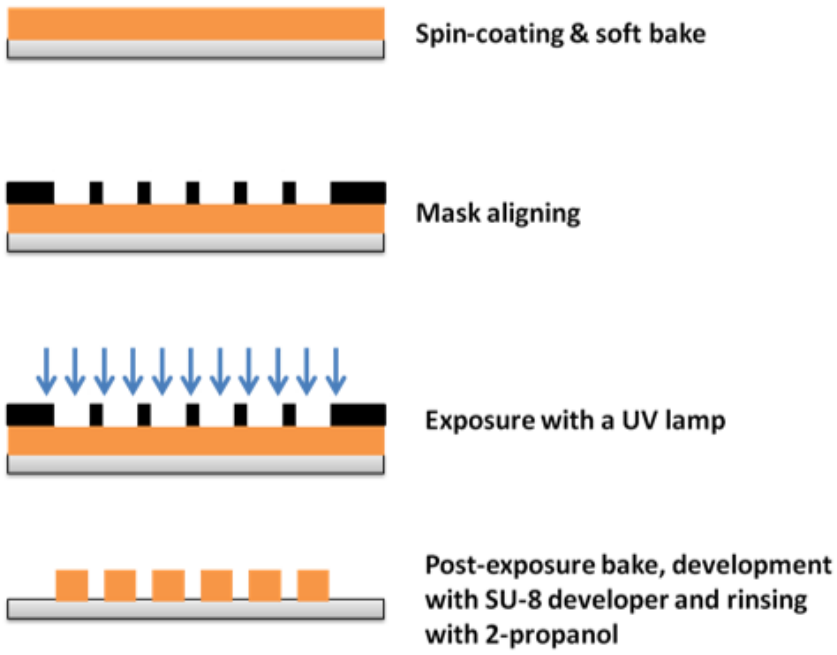

Figure 2-4 Microstructure fabrication process using SU8 and lithography process (Fiorini et al. 2004)

Thermosets, after cross-linking, form a rigid structure which makes it impossible to reshape it without damaging, results in the lack of flexibility limits in the applicability of

thermosets. The other drawback of the thermosets is high cost, which limits their applications in fabrication of microfluidic devices.

2.4.3 2D Networks as Microfluidic Substrate

Materials used for fabrication of microfluidic devices are reviewed in previous sections by highlighting the advantages and drawbacks. However, less than a decade ago, a new type of material was introduced to the field. In 2007, paper-based substrates were actually re-introduced as microfluidic channels, where the first chemical analytical techniques using paper-based substrates invented in 1943 by Martin and Synge, by developing chromatography technique.

Chapter 3 Device Design and Principle of Operation

In this work, as described in the first chapter, we investigate the ability of thermal measurement methods for detecting microscale quantities. This chapter will introduce methods and designed structures for performing thermal measurements, and cover the theoretical background. The details of fabrication and experimental setup are covered in chapter 4, where the measurement results for each measurement technique are illustrated.

This chapter introduces device designs and covers the operational principles for measuring physical or chemical processes using thermal microfluidic devices. The thermal equivalent circuit introduced in the previous chapter is used to investigate the heat transfer analysis in designed structures. Then, measurement principles for different physical and chemical quantities using heat transfer investigations are introduced.

In this chapter, operation principles of developed microfluidic devices are covered, where thermal measurement methods are implemented to measure physical and chemical quantities. The first application is an on-chip micro calorimeter, where a novel structure is used for investigating thermal properties of liquid samples. The second application is a new method for counting the suspended particles in a suspension. The operation principle and device structure for these applications are introduced in this chapter.

Chapter 3 continues by introducing the third application for thermal microfluidic devices, where the abilities and potential of thermal measurement techniques for low-cost Point of Care (POC) applications are studied. The last section introduces a microfluidic platform for measuring a single cell’s temperature response to external stimuli. This requires high control on fluid while the cell is precisely held in place. The principles of operation and the design for the structure of a single cell microfluidic platform is presented in the last section.

3.1 On-chip Micro Calorimeter

Calorimetry is a family of techniques used to measure the change of heat in a substance. Chemical reactions, physical changes and interactions result in an energy transfer and consequently a change in heat. The released or absorbed heat is not a directly measurable quantity; however, investigating the heat transfer is possible though controlling and measuring the temperature.

Through the development of heat transfer science, a number of systems have been produced to study heat transfer for performing calorimetry research. These systems often consist of a combination of heat sources (constant power) and/or temperature sources (constant temperature) and temperature sensors. Antoine-Laurent de Lavoisier, a French chemist, used the name calorimeter for the first time in 1780s. The series of experiments of Lavoisier and Pierre-Simon Marquis de Laplace, a French mathematician, to study the heat quantities associated with state change of water led to the discovery that water molecules are composed from two atoms, hydrogen and oxygen. This was the beginning of thermochemistry, which is the use of calorimetry methods in chemistry.

The origin of the current form of calorimetry was probably taken from Thermogravimetric Analysis (TGA), introduced in 1915. Thermogravimetry is the science and technique used to study the mass change of a sample due to a change in temperature, with respect to time or temperature change. Calorimetry evolved into its current form with the introduction of differential techniques, such as Differential Thermal Analysis (DTA) and Differential Scanning Calorimetry (DSC). Differential measurement resolved the precision required for absolute magnitude measurement. However, developing the temperature measurement techniques led to the development of many non-differential modes of calorimetry.

Since their first introduction, calorimetry techniques have been used for dramatically different applications, with many types of apparatus with different functionalities. Based on the

operation of a calorimeter, six main types were developed: adiabatic calorimeter, reaction calorimeter, bomb calorimeter, Calvet-type calorimeter, differential scanning calorimeter, and isothermal titration calorimeter.

The adiabatic calorimeter was originally developed to measure heat capacity of materials at low temperatures (Tan et al. 2000; Miltenburg et al. 1998). In this type of calorimeter, all of the generated heat is used to increase the temperature of the sample while the surroundings do not experience any heat changes (Hemminger & Hohne 1984). In other words, thermal leakage of the sample to the substrate and surrounding is zero. However, in a practical sense, a fully adiabatic condition is not possible and the calorimeter operates in quasi-adiabatic condition. A mathematical correction factor is often used in this type of calorimetry, where the correction factor is the ratio of the combined thermal mass of the sample and substrate to the thermal mass of the substrate (Hemminger & Hohne 1984).

The second type of calorimeters are reaction calorimeters, where a chemical reaction is investigated in an insulated environment. The high speed on-line measurement and high temperature sensitivity are the most important characteristics of this type of calorimeters (Irving & Wadsö 1964; Marison et al. 1998). Based on the methods of measuring generated heat due to the reaction, four types of reaction calorimeters are developed; heat flow, heat balance, power consumption, and constant flux.

Another type of commonly used calorimeters are bomb calorimeters, which operate similarly to reaction calorimeters. The only difference is that bomb calorimeters operate at constant volume, which allows users to measure a combustion reaction with high pressure (Magee et al. 1998; Bech et al. 2009). The main applications of bomb calorimetry are in liquid and solid fuel testing (Bech et al. 2009) and the investigation of explosives (Ostmark et al. 2002).

Calvet-type calorimeters operate based on measurement of heat flux to the ambient. The Calvet-type calorimeter is basically a three dimensional flux meter, constructed from the distribution of temperature sensors in the chamber of the calorimeter. This type of calorimeter is

largely used for high temperature analysis like the investigation of the thermodynamic properties of organic materials and enthalpies of sublimation (Mraw 1984; Santos et al. 2004).

Differential Scanning Calorimeter (DSC) is one of most commonly used calorimetry techniques. DSC consists of two identical calorimeters: a sample calorimeter and a reference calorimeter. DSC operates by measuring heat flow into the sample and comparing it to the heat flow to the reference. The twin design of DSC often operates in a temperature controlled environment. DSC has two operation modes: Differential Temperature Scanning Calorimetry (DTSC) and Differential Power Scanning Calorimetry (DPSC). The difference between these two modes is that the nature of heat source in which DTSC operates with is controllable heat flux while the DPSC operates by using a constant heat flux source (Hemminger & Hohne 1984).

DCS is used for measuring different quantities of samples like glass transition temperature, i.e. melting and boiling points, crystallization time and temperature, heat of reaction, specific heat capacity, thermal conductivity, reaction kinetics, and purity (Yinping et al. 1999; Rupp & Birringer 1987; Nassu & Gonçalves 1999; Mucha & Królikowski 2003; Thomas 2008; Blumm & Kaisersberger 2001; Barros et al. 2011; Schawe 1995).

Isothermal titration calorimeters are another type of calorimeter used for direct measurement of heat change caused by molecular interaction. This technique is widely used for interactions between proteins and small molecules such as other proteins, DNA, lipids, carbohydrates, and interactions between enzymes and inhibitors (Pierce et al. 1999; Leavitt & Freire 2001; Ladbury & Chowdhry 1996; Jelesarov & Bosshard 1999).

With the calorimetry techniques and applications of different types of calorimeters introduced, the following section covers the operational principals of micro calorimeters. The introduced thermal considerations in micro calorimeter structure fabrication is implemented and analyzed by the developed thermal circuit.

The microfluidic device in this section along with the fabrication details and measurement results were published in Biomicrofluidics Journal in 2014 by the author (Davaji et

al. 2014). Also, the experimental procedure for thermal measurement using fabricated devices was also published in the Journal of Visualized experiments (JoVE) by our group in 2015.

3.1.1 Device Design

The idea for a micro calorimeter was introduced in the early 1900s in London, when Hill published his micro calorimeter for the first time in 1911(Hill 1911). The development of micro calorimeters in the next half century appeared promising when Calvet predicted the availability of applicable micro calorimeters by the 1980s in his micro calorimetry book published in 1963 (E. et al. 1963). The predictions on the progress were legitimate, while the final practical product was not developed yet.

In the late 90s, microfluidic technology was seriously considered to perform highly complicated processes. The microfluidic technology promised valuable advantages and yet scientists and engineers were still investigating it. In the past two decades, different micro calorimeters were developed (Lee et al. 2012; Iervolino et al. 2009; Zhuravlev & Schick 2010). However, describing them is difficult due to a variety of developed techniques and fabricated devices (Lee et al. 2012).

Based on the structure of micro calorimeters (Figure 3.1), we can categorize them into two groups: open-chamber and closed-chamber. Open-chamber calorimeters are often called open micro drop calorimeters, where a small drop is placed on top of a micro machined structure. The thermal components are integrated at the location of drop. This type of calorimetry technique is user-friendly in terms of fluid handling, although the evaporation and precise volume control suffer in this configuration (Zhuravlev & Schick 2010).

Figure 3-1 Sectional view of open chamber calorimeter (a) and closed chamber calorimeter (b).

The other category, closed-chamber configuration, was able to overcome the evaporation issue and offer precise control over volume. This type of micro calorimeters uses an integrated microfluidic channel to interface the samples to the measurement cite. Based on the calorimetry method, multiple input fluid paths can be used. However, fabrication of the micro calorimeter with closed-loop configuration is extremely complicated due to the fabrication process and multiple bonding requirements.

In some cases, soft lithography is used to convert an open-chamber calorimeter structure to a closed-chamber micro calorimeter structure, where the sensitivity of measurements suffer due to the large thermal mass of polymer based micro channels. In addition, this type of planar structure has another fundamental problem. The sensor, which lies on the same plane as the heat source, interferes with the heat flow path.

This issue adds undesired complexity, requiring extra calculations and correction factors to obtain an accurate thermal measurement. Figure 3.2 illustrates different configurations of closed-chamber micro calorimeters in previous works. Although the heat flow pass in our suspended micro calorimeter chamber design is reduced by using a thin film substrate, the heat flow between the sensor and the source still experience a uniform path.

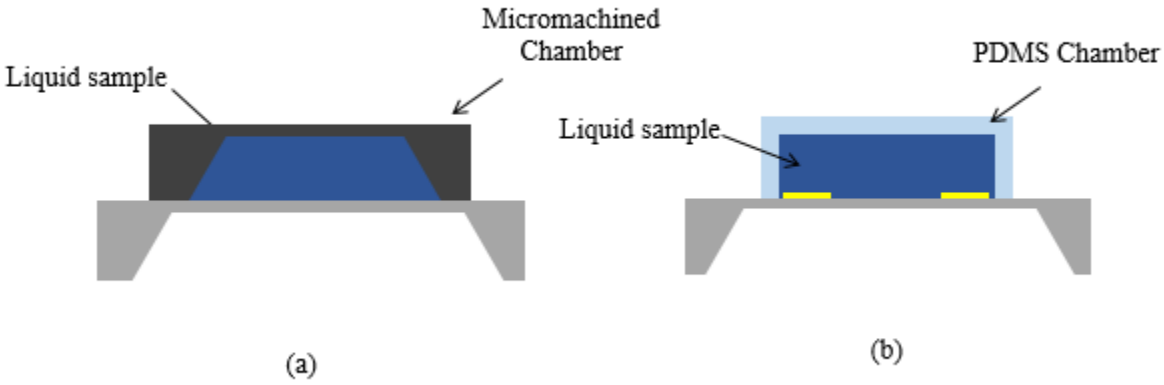

Figure 3-2 Closed chamber calorimeter configurations.

In this work, we design and develop a micro calorimeter with closed-chamber configuration, where the precise control over sample volume is preserved while the device does not suffer from evaporation. Also, for uniformity of the heat flow through the samples, thermal elements are at two different sides of the measurement chamber. Another consideration in this design is to avoid using a high polymer base microchannel, resulting in lower device sensitivity. Schematic of the designed micro calorimeter is illustrated in Figure 3.3.

In micro calorimeter design, it is important to consider the off-chip bonding in fabricating of an on-chip micro calorimeter, where it increases the complexity of fabrication processes.

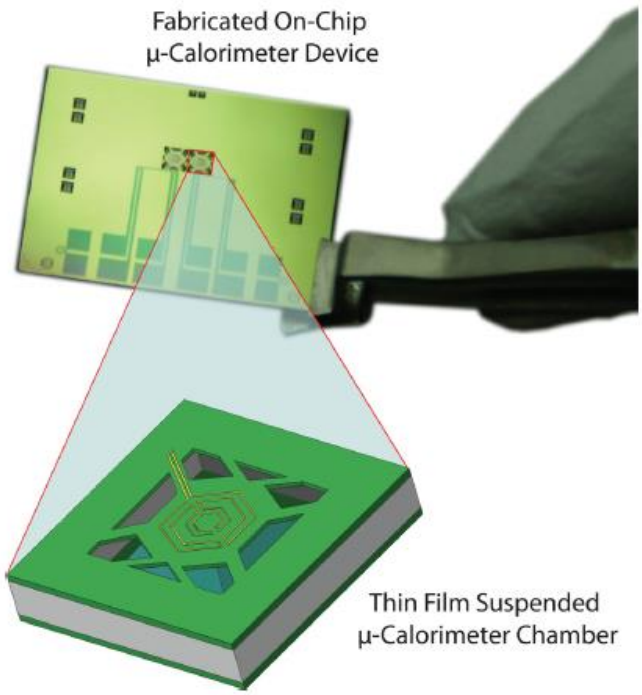

Figure 3-3 Fabricated micro calorimeter chip and close-up view of schematic of suspended thin film chamber.

In addition, to reduce the thermal mass of the structure, which increases the speed and sensitivity of micro calorimeters, the structure is fabricated only from a Silicon Nitride thin film. Also, to reduce the thermal link to the substrate and increase the thermal resistance of the chamber, the structure is suspended from substrate (handle wafer) through the implementation tethers in our design.

The fabrication process, development, and material selection for fabricating the designed structure is presented in chapter 4.

3.1.2 Micro Calorimeter Operation Principle

In the last two decades, micro calorimeters were fabricated for many measurement punctualities and different applications(Lee et al. 2012). In this study, the proposed design for a

micro calorimeter was used to measure the thermal properties of fluid samples. In this section, the measurement methods for thermal diffusivity and specific heat of fluid samples is presented.

Commonly, in micro calorimeters, thermal diffusivity measurement is implemented by 3ω (omega) measurement techniques. In 3ω measurement, the phase of temperature variation is used for measuring the thermal diffusivity. Calibration of parameters with known thermal diffusivity (standard) are required for precise measurement.

The other thermal diffusivity measurement techniques are non-steady-state techniques, where the transient variations of temperature are used for thermal diffusivity measurements. Laser flash method is a commonly used transient measurement method in micro calorimeters. Implementing the laser flash methods requires the adiabatic condition, where no thermal link to the surrounding is present. Nevertheless, in our structure, achieving adiabatic condition is not feasible due to the finite thermal resistance.

The transient methods for the non-adiabatic conditions are implemented by developing a model for the heat loss due to the thermal leakage. The developed models will supply the correction factors and make it possible to use the transient methods while having finite thermal resistance. However, in our proposed design, due to complexity of the structure and fabrication process variation, developing a model for heat loss is too complex.

In this work, heat penetration time measurement method for thermal diffusivity measurement is adopted to avoid complex heat loss analysis and reduce the effects of fabrication process variations. Heat penetration time measurement is a non-steady-state method, where the heat penetration time is measured from one side of a sample to other (through the sample) in order to determine thermal diffusivity. This technique is well suited for our design, where we have a sensor and a heater fabricated on both sides of the calorimeter chamber. By applying constant heat flux at the heater, the delay time of heat penetration through the sample is:

$$t_0 = \left[\frac{L^2}{\left(\frac{16}{\pi}\right) \cdot \alpha} \right] \tag{3.1}$$

where t_0 is time delay, L is length of the heat flow path (sample thickness), and α is thermal diffusivity of the sample in $\left(\frac{m^2}{s}\right)$. The measurement result of thermal diffusivity is presented in the next chapter after introducing the fabrication process and physical dimensions of the fabricated micro calorimeter.

Measurement setup for thermal diffusivity measurement using heat penetration time is illustrated in the Figure 3.f.

In the measurement setup shown in the diagram, the calorimeter is located inside thermal insulation to reduce the ambient noise in the measurements. A source meter is used to generate a DC pulse at the heater and at the sensor side. A current pre-amplifier is used to measure the temperature change precisely. Both signals, the DC pulse at heater and the temperature variation at the sensor, are recorded in real time by a computer controlled LabVIEW program. The recorded data from the data acquisition system is processed by a Matlab code to precisely measure the time delay by applying second derivative methods (Davaji et al. 2014).

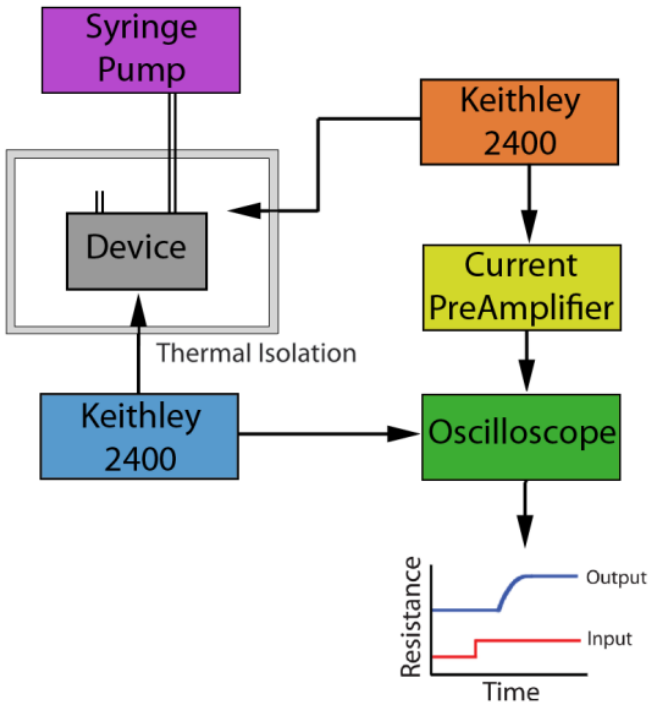

Figure 3-4 The experimental setup for thermal diffusivity measurement using heat penetration time measurement concept.

As explained at the beginning of this section, the designed micro calorimeter is capable of performing different calorimetry experiments. In the rest of this section, heat capacity measurement operation principles in micro calorimeters is covered.

For specific heat measurement, common AC calorimetry techniques are used, where an alternating temperature is applied to the heater, and the amplitude and phase of the temperature variations at the sensor side are monitored. This type of AC calorimetry is called Thermal Wave Analysis (TWA). Garden *et. al.* first reported the implementation of TWA for measuring the specific heat of a sample[ref].

TWA has two conditions: homogenous temperature distribution in a sample and quasi-adiabatic condition. The quasi-adiabatic condition is satisfied in the calorimeter by:

$$\tau_{\text{int}} \leq \frac{1}{\omega} \leq \tau \tag{3.2}$$

where ω is the frequency of applied alternating power to the heater and, τ_{int} and τ are the time it takes for heat to diffuse into the sample and thermal real action time of the sample to the environment, respectively. Having this condition satisfied in the calorimeter, a measurement for the specific heat of the sample can be determined by measuring amplitude of the AC variation of the temperature at sensor side, caused by applied alternating excitation to the heater. The specific heat relation in TWA is:

$$c_p = \frac{C_o \cdot P_{in}}{2 \cdot \omega \cdot m \cdot \Delta T_{ac}} \tag{3.3}$$

Where c_p is specific heat $\left(J \diagup kg \cdot K \right)$, C_o is a dimensionless input power correction factor, P_{in} is input power in (W) , ω is excitation frequency, m is the mass of the sample and ΔT_{AC} is temperature variations. Figure 3.5 illustrates the measurement setup for specific heat measurement.

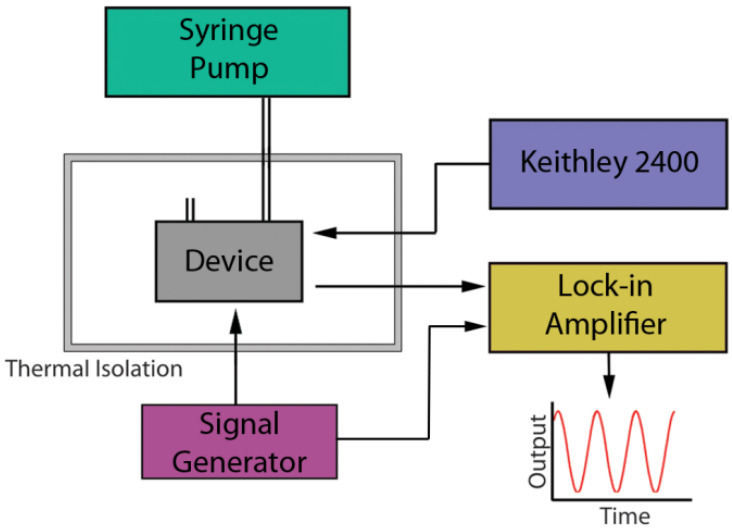

Figure 3-5 The experimental setup for specific heat measurement using Thermal Wave Analysis (TWA) technique.

As shown in the measurement setup diagram, a signal generator is used to generate alternating heat flux at the heater and a lock-in amplifier is used to detect the variation of temperature at the sensor side with high precision. The measurement result is presented in chapter 4.

3.2 Thermal Particle Detector

The first chapter explained that the capabilities of thermal measurements in small scales for different physical and chemical quantities is the focus of this research. In the previous section, we presented a micro calorimeter design for measuring thermal properties of liquid samples. In this section, we introduce the implementation of thermal conductivity measurement for micro particle detection in suspensions.

Using calorimetry, thermal conductivity can be measured. In this section, we propose to use the thermal conductivity change when particles with different thermal conductivity are added to the detection site.

Currently, optical methods are used for particle counting using a camera or photo detector. The complex optics and large size of the measurement setup has resulted in particle counting technologies being expensive. Usually this device offers another feature, cytometry, which identifies micro particles and provides the material properties and the particle sizes.

However, thermal measurement techniques can dramatically reduce the size and complexity of measurements. In this section, the operational principle and design of a microfluidic platform for thermal particle detection is presented.

The microfluidic particle detection was invented and introduced for the first time at the Nanoscale Devices Laboratory at Marquette University, in collaboration with Dr. G. Walker's group and North Carolina State University. The developed thermal method for micro particle detection is patented and the results were published in 2014 (Walker et al. 2015). The

measurement setup and experimental procedure is published in the video Journal of Visualized Experiments (JoVE) (Davaji, B., Lee 2015).

3.2.1 Device Design

For measuring the change in the thermal conductivity in a micro calorimeter, we proposed to use a simple thin film membrane structure with an integrated PDMS micro channel on top. Since the change in the thermal conductivity is measured for micro particle detection, precise measurement of absolute values of thermal conductivity is not required. The device design is optimized to reduce unnecessary fabrication complexities, where accuracy of the thermal mass and thermal time constant measurements are sacrificed as a result.

Figure 3.6 illustrates the proposed structure for fabricating a thermal particle detector. The device consists of a micro machined thin film membrane with an integrated resistive thermal element. Then, a PDMS micro channel is bonded on top of the device.

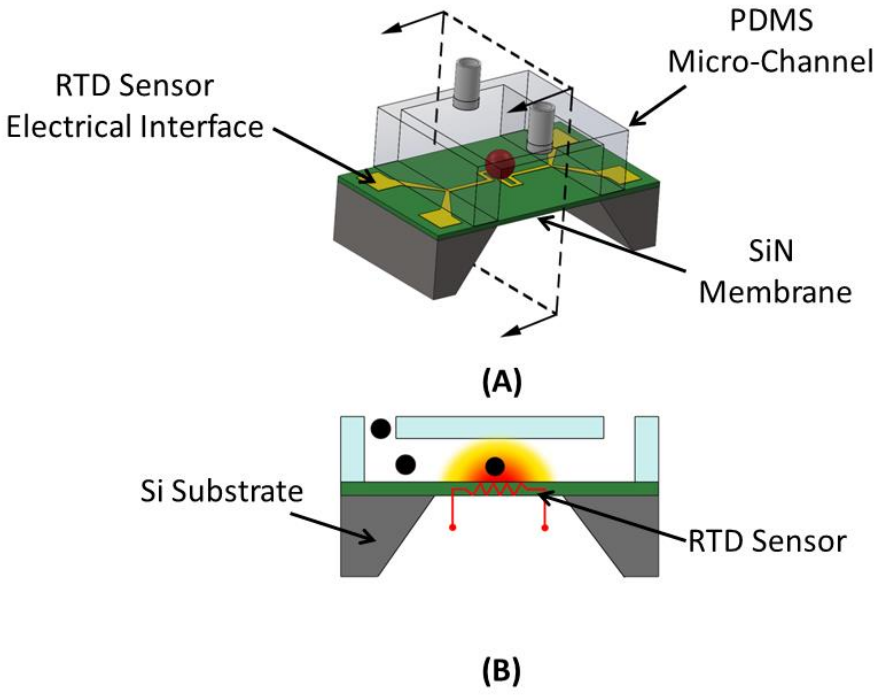

Figure 3-6 The thermal particle detector device. (A) Shows the top view and (B) sectional view.

3.2.2 Operation Principle

When the flow is passing through the channel, thermal conductivity of fluid, thermal resistance of structure, and the flow profile are affecting heat transfer in the channel. Having a stable flow in the channel, the device will experience an equilibrium condition after a finite time. In this situation, when fluid properties change, the heat transfer in the channel will be affected due to the overall thermal conductivity change in the channel.

This change in properties of the fluid could be caused by introducing a different fluid or having suspended particles within passing flow. The particles passing through the channel will result in thermal conductivity change, which can be detected using a simple proposed thermal measurement.

When a suspended particle, in this case a polymer micro sphere or a polystyrene (PS) bead, enters the micro channel, the heat transfer equilibrium is disturbed and the thermal

conductivity change will result in temperature change. This transient temperature change is measurable with thin film RTD integrated on the membrane.

The changes in total thermal conductivity will be based on the combined heat conductivity of the bead and fluid. In this research, effective medium theory (EMT) was adopted to model and calculate an average thermal conductivity of the suspension (fluid and suspended micro particle). The combined thermal conductivity can be written as (Vutha et al. 2014):

$$k_c = k_w \cdot \left[\frac{K_b \cdot (1 + 2 \cdot \phi_b) - k_w (2 \cdot \phi_b - 2)}{K_w \cdot (2 + 1 \cdot \phi_b) - k_b (2 - 2 \cdot \phi_b)} \right] \tag{3.4}$$

where the k_c , k_b and k_w are total thermal conductivities of the combined water and suspended beads, beads, and fluid, respectively.

In the experimental setup, heat transfer disturbance and heat conductivity change in the channel due to the presence of a suspended micro particle are shown in Figure 3.7

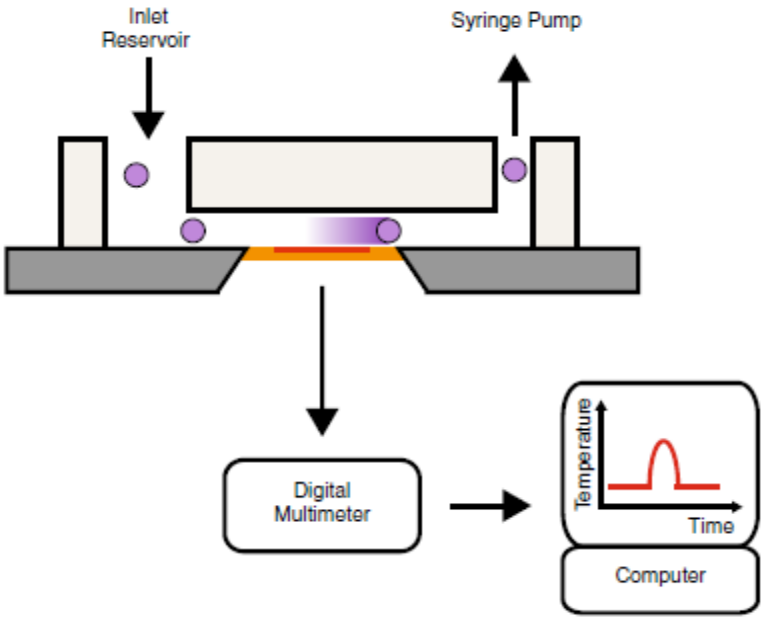

Figure 3-7 Experimental setup for thermal particle detection test.

In this device, two thin film RTD sensors are used as a heat source and as a temperature sensor. The RTD sensor is activated by constant DC current bias. The generated heat at RTD by Joule heating is used as a constant power source, where the variations of resistance of RTD due to temperature change is neglected. A source/meter instrument, in 4-wire configuration, continuously measures the RTD's resistance. The 4-wire configuration is used to bypass the effect of lead resistance change.

The source/meter is controlled by a LabVIEW program and constantly acquires measurement data. The measured resistance change profile is converted to temperature by a Matlab code.

The measurement results and discussions on device performance are presented in Chapter 4. The proposed measurement device is simple, yet effective, and requires only a resistance measurement, while industrial techniques for particle detection are very complicated and costly.

3.3 Paper-based Calorimetric Sensor

In this section, the calorimetric detection for portable applications is presented. Thermal detection techniques are used to detect chemicals and biochemical using paper-based devices. The released or absorbed heat by a reaction on a paper-based channel is used to quantify the concentration of sample. Paper-based devices are commonly used for medical diagnostic application and few successful commercialized applications are currently available in the market.

In recent years, research in the medical devices field has substantially changed by technology development. The medical devices are categorized based on their functionality in three groups: diagnostic devices, therapeutic devices, and assistive devices. All medical device fields are growing at exceedingly rapid rate in the last two decades.

Common trends are recognized in all three fields of medical devices in both medical industry and academic research. Portability is a highly demanded feature with medical devices.

Patient side diagnostic devices and point of care (PoC) therapeutic devices are both highly active fields.

The portable diagnostic devices are mostly known for the portable Glucose meter products, which play an essential and lifesaving role for diabetic patients. In addition, pregnancy strip tests, water quality strips, portable heart rate sensors, and digital blood pressure sensors are other types of portable diagnostic medical devices.

In the second category, portable therapeutic devices have developed dramatically in recent years. The progress on portable insulin micro pumps and controlled drug release implants are well known examples of portable devices.

The recent developments in portable medical device technology are mostly initiated based on the fabrication technology developments. The complexities in some of the developed techniques are the main reason that makes it difficult to implement them. The complexity of the operation, required special training, stability over time, and cost of fabrication has pushed the portable device industry toward developing simple yet effective technologies.

Paper-based devices, where the liquid sample transport on the paper substrate by capillary action is used instead of micro channels and micro pumps, is a good example of a portable and simple technology. PH test strips and pregnancy test strips are well known examples of paper-based, microfluidic devices.

This section covers the details of thermal detection technology on paper-based microfluidic devices. The thermal detection technique is proposed and used for the first time in this work and it resulted in a US patent (Lee & Davaji 2014). The paper-based calorimetric detection sensor idea and measurement results are published in Biosensors and Bioelectronics in 2014 (Davaji & Lee 2014). The experiment setup and measurement techniques are published in a video journal (Davaji, B., Lee 2015).

3.3.1 Paper-based Technology

Paper-based microfluidic technology is an unexpectedly old technology. The first paper-based chemical analytical technique was the Nobel Prize winning idea of the chromatography technique presented by Archer John Porter Martin and Richard Laurence Millington Synge in 1943. Subsequently, Muller introduced the first paper-based microfluidic immunoassay in 1949. The PH test strip, a well-identified PH measurement sensor, was invented even earlier. In 1909, Soren Peder Pauritz Sorenson, a Danish chemist, invented the paper PH test strips [ref] using the technology developed by a French scientist, Joseph Louis Gay-Lussac, in 1800s.

More recently, Whitesides group at Harvard University re-introduced and revolutionized the applications of paper-based technology by developing the highly sensitive paper-based sensors with diverse functionalities in 2007. In the meantime, paper-based technology used for developing low-cost and disposable devices has been studied extensively in the last few years.

Paper-based technology uses capillary action of fluid in fibrous substrate for fluid transport. In fact, the capillary action driven fluid resulted in simple, inexpensive operation technology. However, as the results of the research demonstrated, this technology can deliver high functionality and high precision while still preserving the simplicity and cost efficiency.

The micro fabricated paper-based devices are currently used for immunoassay, bio detection, environmental monitoring, glucose level measurement, cell culture substrate, bio fuel cells, and many other applications (Cate et al. 2015; Ellerbee et al. 2009; Lankelma et al. 2012; Martinez et al. 2010; Martinez, Phillips & Whitesides 2008; Martinez, Phillips, Wiley, et al. 2008; Nie et al. 2010; Zhang et al. 2015; La et al. 2015; Desmet et al. 2015).

In paper-based microfluidic devices, the most commonly used detection techniques are colorimetric detection, electrochemical detection, fluorescence, chemiluminescence, and electrochemiluminescence. However, the first two, colorimetric and electrochemical detection, are widely used while the other introduced techniques have limited applications.

The colorimetric detection works based on detection of color changes (intensity or wavelength) due to a reaction of reagents and samples. These changes are recorded with a camera, spectroscopy, and photodiodes or even with human eyes. This technique often generates qualitative or semi-quantitative [results based on detection instruments. Frequently, the detection instruments require complex optical setup or advanced signal-processing software , which limits the applicability of these techniques for portable and disposable devices.

The other issue with colorimetric detection is developing the pigment dyes for colorimetric detection which change color or intensity due to the reagent and sample reaction. Furthermore, bonding synthesized dyes to the reagents results in an extra complexity, which limits the stability of developed devices.

In the electrochemical detection technique, the conductivity change of the sample caused by the reaction is monitored and used to quantify the reaction. The readout of this technique is an electrical signal, which represents the electrical conductivity of the sample. Commercialized portable glucose meters use electrochemical detection to measure the blood glucose level. The electrochemical detection results are quantized values. Due to the simplicity of electrical measurement, it is very good candidate for portable measurements. However, the applications of electrochemical detection techniques are only limited to the reaction with electroactive byproducts.

Considering potential of thermal measurement methods, we proposed to use the thermal measurement method as a detection mechanism on paper-based devices. As the reagent and sample reaction causes the enthalpy change, the generated temperature can be used to quantify the progress of reaction and the concentration of substances with precise control on the volume. In next section, the proposed device structure and integrated temperature sensor is introduced.

3.3.2 Device Design

The proposed device for calorimetric detection on paper-based devices consists of three main parts: temperature sensor, substrate, and paper-based microfluidic channel. This section introduces the structure of the device and the principle of operation along with the characterization, which are covered more extensively in the next section.

Yeager group at The University of Washington intensively investigated the capillary action in paper fiber networks. They found that in 2D paper networks, fluid transport velocity can be controlled by changing the geometry of paper (Fu et al. 2011). Furthermore, they illustrated the capability of performing sophisticated chemical processes using paper-based microfluidic devices. In addition, the chemical signal amplification by changing the design of paper-based channel structure was investigated (Fu et al. 2010).

In general, the designed structure can be fabricated using a paper sheet with three major techniques; printing, lithography, and cutting(Cate et al. 2015). In printing techniques, hydrophobic polymer is printed to block the fluid flow paths in paper to construct a microchannel on paper. The common technique in the printing approach for paper microchannel fabrication is to use a wax printer and thermally anneal the printed wax to completely diffuse to the paper. In the lithography technique, a photo sensitive polymer is used to block the unwanted fluid paths on paper and only leave the channel structure by using photolithography techniques.

In both of these methods, the process channel can be exposed to undesirable contaminations like the polymer solvents. The printed polymers diffuse into the paper fibrous network and limit the resolution of fabrication where the thermal post processes can intensify this polymer redistribution.

To avoid the issues with the introduced methods, we proposed to make the channel structure using cutting techniques. The paper cutting technique offers great control on the resolution of channel by eliminating the polymer diffusion and the fabricated paper micro

channels do not suffer from contamination. The details of fabrication of paper using a desktop knife plotter is covered in Chapter 4.

The different designs for controlling the fluid transport velocity, reaction volume, and signal amplifications are considered. The different of the designed and cut geometries are demonstrated in Figure 3.8.

Figure 3-8 Knife plotter cut paper strips, ready for integrating with substrate and RTD temperature sensor.

3.3.3 Operation Principle

In the proposed design for the calorimetric paper-based microfluidic device, a reaction site is located on top of a temperature sensor to detect the reaction temperature. The reagent is immobilized on the reaction site and reacts when the sample is introduced to the paper-based microchannel. The reaction temperature is continually monitored by an integrated RTD sensor. Figure 3.9 illustrated the designed structure.

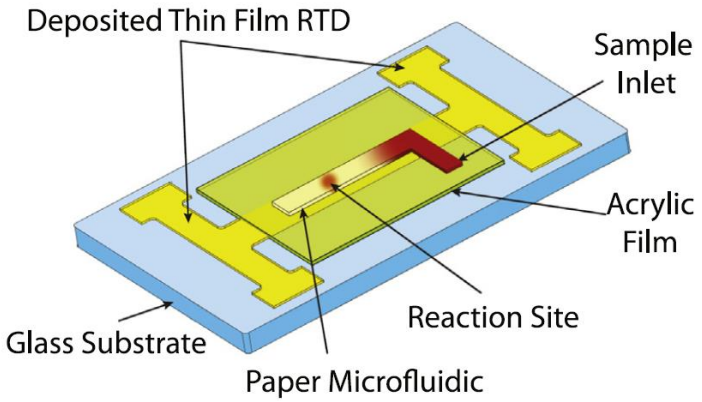

Figure 3-9 schematic of paper-based device with calorimetric detection.

The design of paper micro channels is specific to the volume of the sample and the reagent. To avoid mechanical disturbances, the entrance tail is added to the design of microchannel with L and F shapes. In the L shaped microchannel design, a small L-shaped tail is used to introduce samples. In F shape microchannel design, two tails are used for introducing the reagent and sample.

In this device, the RTD sensor is used for temperature measurements. As explained earlier, RTD sensors are linear in the range of our measurements (0 to 150 ^{o}C) and have larger sensitivity compared to thermocouples. The RTD is integrated into the metal substrate with the shadow masking technique and the thermal evaporation of nickel. The integrated RTD is illustrated in Figure 3.11. A thin (100μm) layer of polyimide film is added to protect the RTD from corrosive chemicals.

To explore the capabilities of the thermal measurement method as a functional analytical device, three different reactions are investigated in this study. The reactions selected are among the most commonly used reactions in analytical devices: enzyme based catalytic reaction, DNA cleavage reaction and protein binding reaction.

The first reaction is glucose reduction and oxidation reaction using the Glucose Oxidase (GOD) Enzyme. The catalytic reaction of GOD enzyme with glucose converts glucose to gluconic acid and hydrogen peroxide [ref]. The oxidation reaction of glucose results in an enthalpy change of $\Delta H = -80\left(kJ/mol\right)$. The catalytic reaction of glucose oxidation is exothermic (negative enthalpy change) and increases the surrounding temperature by releasing heat:

$$\beta DGlu\cos e + O_2 \xrightarrow{GOD} \beta DGlucono + \delta Lactone + H_2O_2 \tag{3.5}$$

From measuring the temperature change, the concentration of the reduced glucose can be quantified by following equation:

$$n_p = C_p \cdot \left(\frac{\Delta T}{\Delta H}\right) \tag{3.6}$$

where n_p is the number of moles of product, C_p is the heat capacity of system, ΔT is the measured temperature change caused by the reaction, and ΔH is the molar enthalpy change. Details of GOD enzyme activation, buffer preparation, and glucose sample handling and procedures are covered in the material section in Chapter 4, where the measurement results for blood glucose standards are presented.

The deoxyribonucleic acid (DNA) strand cleavage for DNA concentration detection is selected as the second case for implementation of calorimetric detection in paper-based microfluidic device. In this work, hydrogen peroxide (reagent), a good source of hydroxyl groups, is used to react with DNA. Intracellular iron from ferritin reacts and catalyzes the formation of hydroxyl groups in hydrogen peroxide, these hydroxyl groups cleaves DNA and breaks the DNA strands.

The cleavage of the strands is an exothermic reaction that releases heat to the surroundings. Concentration of the DNA is measured by recording the temperature change using the developed paper-based sensor. The sample and reagent preparation and experimental

procedure for measuring the concentration of DNA by the described method is presented in Chapter 4.

Finally, in the last experiment, the capabilities of the calorimetric detection technique in paper-based microfluidic devices are investigated for protein binding investigation. Protein binding investigation is an important field of biochemical research, which has many applications in disease detection, drug discovery, drug delivery, and biomarker research. The calorimetric microfluidic devices have3 been used for investigating protein binding in previous work. However, here we propose to use a paper-based device, which offers a simple and inexpensive method for portable and disposable applications. The measurement results are presented in the next chapter.

3.4 Single Cell Temperature Measurement

Living cells are building blocks of life and fundamental understanding of their behavior is critical to answer many biological questions. The biological function and malfunction of living cells are the origin of the health and illness. Biological and medical researchers are actively studying the responses of living cells to different stimuli for disease detection, drug discovery, and drug delivery research (Davaji et al. 2015).

In this section, we propose to use a thermal measurement method to develop a microfluidic platform for single cell behavior investigations. The presented devices, fabrication processes, and results are presented in Transducers 2015 (Davaji et al. 2015). This section introduces the advantage of single cell analysis, explains the disadvantages of studying cells in population, and reviews the single cell temperature measurement techniques. Afterwards, a microfluidic platform for capturing a single cell and measuring the temperature of a single cell is introduced.

3.4.1 Introduction

Historically, it is common to investigate a large population of cells together, when it was considered acceptable to use the average data. However, it was discovered that such analysis could result in misleading information. Recent work on gene expression, protein expression levels, and phenotypic outputs prove that single cell responses are different from the average response of a population, which shows the importance of single cell analytical techniques.

Single cell analysis requires developing special tools to precisely control the location of a single cell and changing the cell culture media continuously. Many devices are designed and developed using microfluidic technology for single cell detection and manipulation. Although many advanced designs with complicated structures are proposed for single cell biology and medical genomics, many of these devices are not practical. Most of these designs lack the ability to fully control the trapped cell and/or the flow of the media without disturbing the fluid.

It is scientifically proven that many intracellular processes such as cell division, metabolism, and gene expression result in heat exchange (Donner et al. 2012). In this work, we propose to develop a microfluidic platform to investigate the cell responses and intracellular processes by measuring the temperature of a single cell. The single cell calorimetry idea is a powerful tool for single cell metabolism analysis and cancer research (Lee et al. 2012), although the developed devices are not applicable for continuous temperature monitoring over time.

Currently, intracellular temperature mapping for single cells mostly uses indirect methods such as florescent thermometry, i.e. by dye coated nanoparticles or fluorescent proteins (Okabe et al. 2012; Gota et al. 2009; Donner et al. 2012; Hayashi et al. 2015). This technique requires the manipulation of cells and complex optical excitation and measurement instruments, where using the direct temperature measurement avoids such issues. The only reported method for direct temperature measurement of a single cell used a tiny thermocouple tip (Wang et al. 2011), where

the thermal contact area of the probe and the thermal mass of the probe limited the resolution of this technique.

3.4.2 Operation Principle

The proposed device structure is adopted from a planar patch clam device using the pressure difference. The microfluidic structure has a membrane with a tiny hole (3 – 5 μm diameter) at the center. There are two microfluidic channels at both sides of this membrane, where the hole (capturing cite) connects these two channels. The sectional view of the membrane with single cell capturing site is illustrated in Figure 3.10.

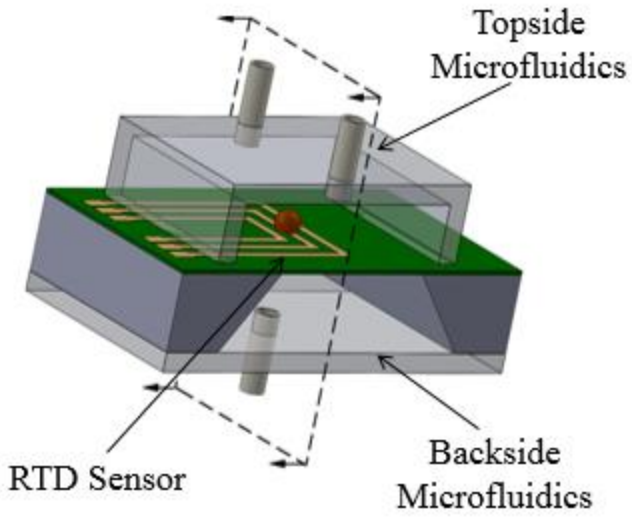

Figure 3-10 Microfluidic platform for temperature measurement of a single cell.

The pressure difference in two microfluidic channels results in a drag force across the membrane through the capturing site. The hole diameter is smaller than the cell diameter, so that the cell does not pass through. The drag force towards the negative pressure will immobilize a

single cell at the location of capturing site at center of membrane. The schematic of the proposed platform is demonstrated in Figure 3.11.

Controlling the pressure ratio in two channels immobilizes the captured cell over time, where the direction of flow and the flow rate can be adjusted. The proposed structure allows full control over flow after capturing a cell, which makes it possible to remove the excess cells form the channel (flushing the channel) and introduce the media to the cell.

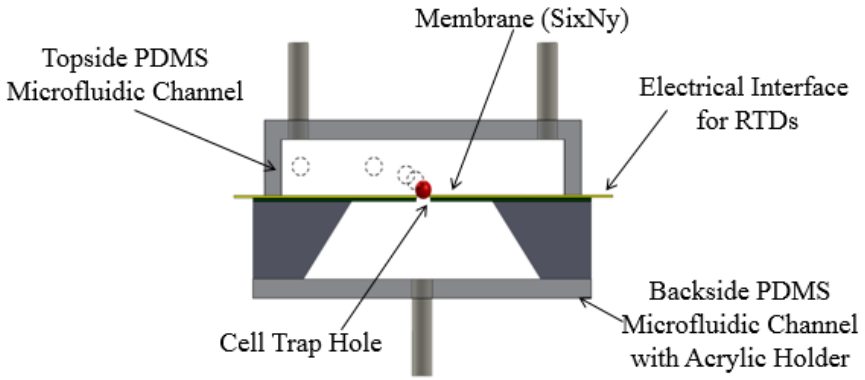

3-11 Figure 3-12 Sectional-view of fabricated platform shows the cell capturing and immobilization mechanism.

At the membrane, a thin film RTD sensor is integrated to measure the temperature change continuously. In addition, to reduce the ambient temperature noise, the temperature is measured differentially by integrating the second RTD from the capturing site in the microfluidic channel. Since most of the biological experiments are conducted using the inverted microscope with high magnification lenses, the device structure is modified to be compatible with the biological microscope. The schematic of the modified microfluidic platform is shown in Figure 3.12.

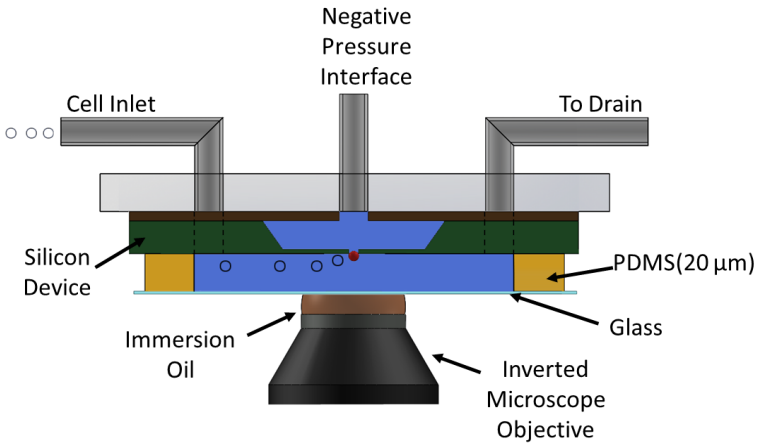

Figure 3-13 Sectional-view of converted platform to inverted configuration.

The fabrication process and the results of cell capturing, including the capturing pressure characteristics, are presented in chapter 4.

Chapter 4 Results and Discussions

In this chapter, the experimental results and discussions are independently presented for each application introduced in chapter 3. This chapter covers process development and device fabrication process for designed microfluidic devices with thermal measurements. Then, the experimental setup and measurement results are provided. At the end of each section, performance of the device is evaluated and verified in a discussion part, where the potential and capabilities of each device are highlighted.

4.1 Micro Calorimeter

The micro calorimeter device, introduced in chapter 3, consists of thermal components (heater and sensor), suspended chamber, and microfluidic channels. Next section will provide a detailed fabrication process for micro calorimeter device. Next section covers the characterization of fabricated micro calorimeter device. Then, the experimental setup and material preparation are presented with focus on electrical measurements. Finally, the measured results are analyzed and the performance of device are evaluated in last section.

4.1.1 Fabrication

In microfluidic devices, different types of heat source such as preheat liquid circulation [ref], Joule heating elements [ref], microwave heating sources [ref], and chemical reactions [ref] are reported. In this work, Joule heating generated by passing current through resistive element is used, which allows homogeneous heating over a wide temperature range of operation, precise control over heating [ref], and simplification of fabrication process by symmetry to the temperature sensor.

In fabrication of this device, Resistive Temperature Detector (RTD) sensors are used. RTD sensors offer high stability [ref], accuracy [ref] and linearity in operation range [ref], and can be integrated simply to the micro fabricated structures. The RTD sensors are resistive elements, commonly made with platinum, nickel, and nickel-iron alloys, where the resistance of RTD changes with temperature. In this work, evaporated nickel thin films are used as RTD devices.

The simplified form of Callendar-Van Dusen equation [Ref] provides the resistance relationship with temperature change in RTDs:

$$R = R_{Rm}\left(1+\alpha_{Ni}\cdot\Delta T\right) \tag{4.1}$$

where R_{Rm} is the resistance of RTD at room temperature, α_{Ni} is the temperature coefficient of resistance for deposited nickel thin film, and ΔT is the temperature change.

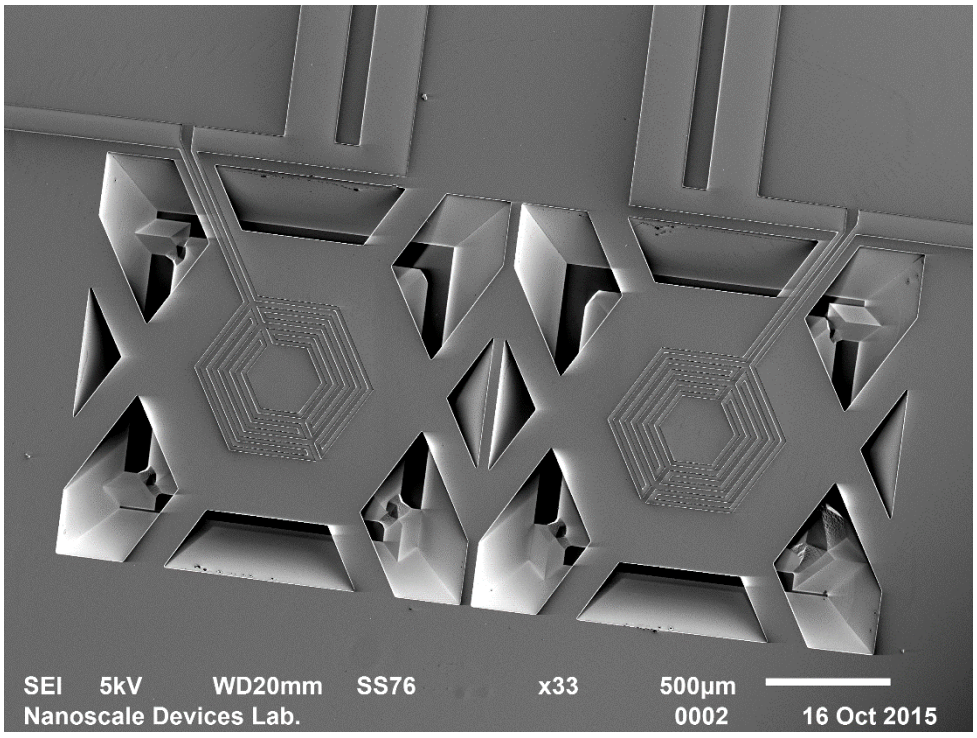

Figure 4-1 SEM image of completed suspended chamber fabrication.

The micro calorimeter device is fabricated by bulk micromaching of silicon wafer. The fabricated on-chip micro calorimeter device is shown in Figure 4.1. In this section, device fabrication processes are covered in details.

The fabrication process starts with thermally growing 250nm SiO_2 on a four-inch single crystal silicon wafer. Then, 0.5μm low stress SiN film is deposited by Low Pressure Chemical Vapor Deposition (LPCVD) process. The SiN layer in this device is used for fabricating suspended chamber structure and it acts as a chemical etching mask though the process.

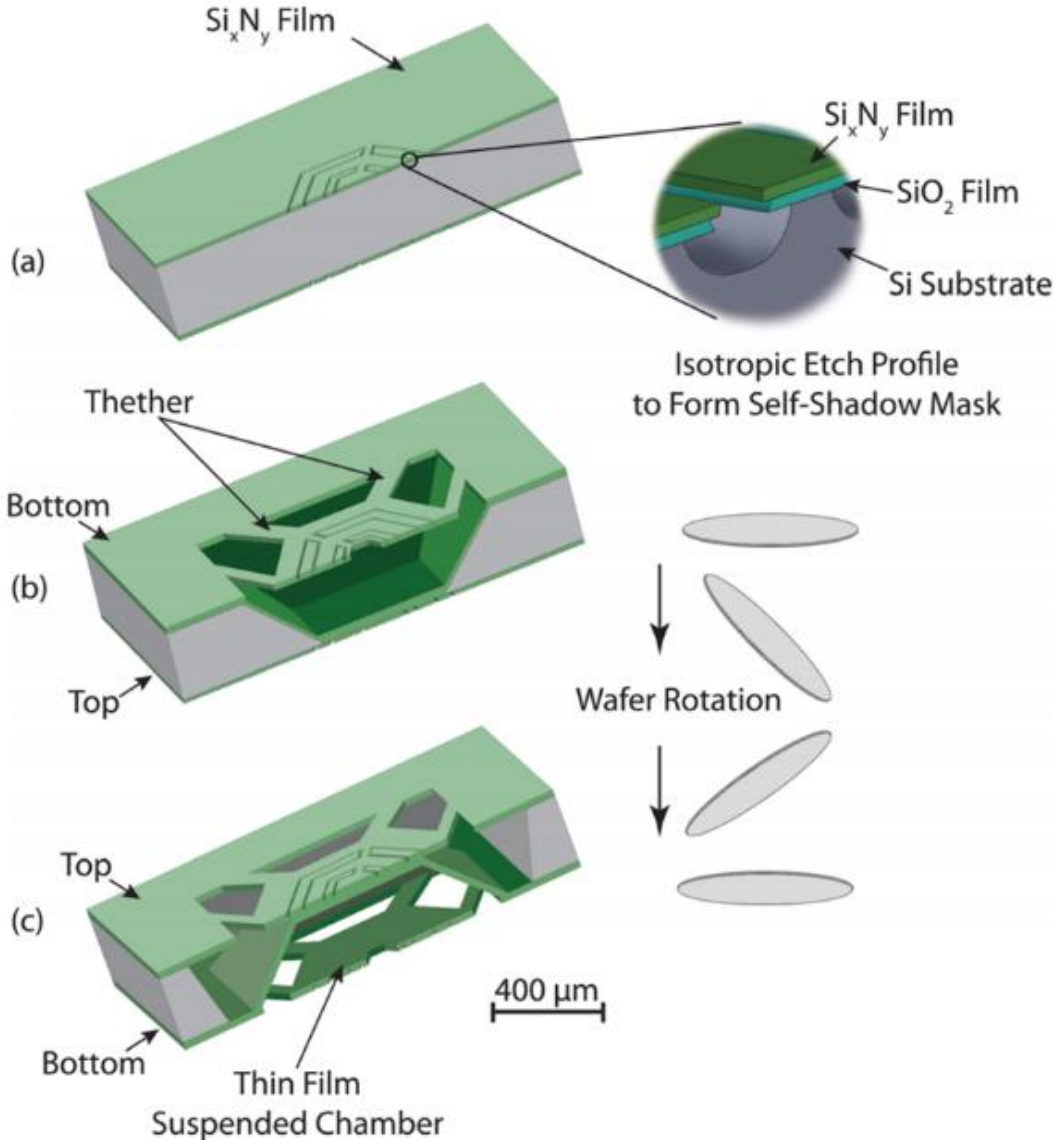

Figure 4-2 Fabrication process of micro calorimeter.

First, the thermal elements (resistive heater and RTD sensor) are patterned (Figure 4.2 (a)) on both sides of wafer (symmetric) using photolithography process and a double-sided contact mask aligner. Then, the SiN and SiO_2 layers are etched by Reactive Ion Etching (RIE) process (Figure 4.3(a)) and Buffered Oxide Etching (BOE) process (Figure 4.3(b)), respectively. Then, the exposed silicon in patterns are etched using isotropic wet silicon etching solution (Poly Etch) to form a 5μm undercuts. The undercut formed in this step is used in the last steps of fabrication as thermal elements. The formed overhung structure on top of etched silicon parts, as shown in Figure 4.3(C), acts as a self-shadow masking layer in metallization step.

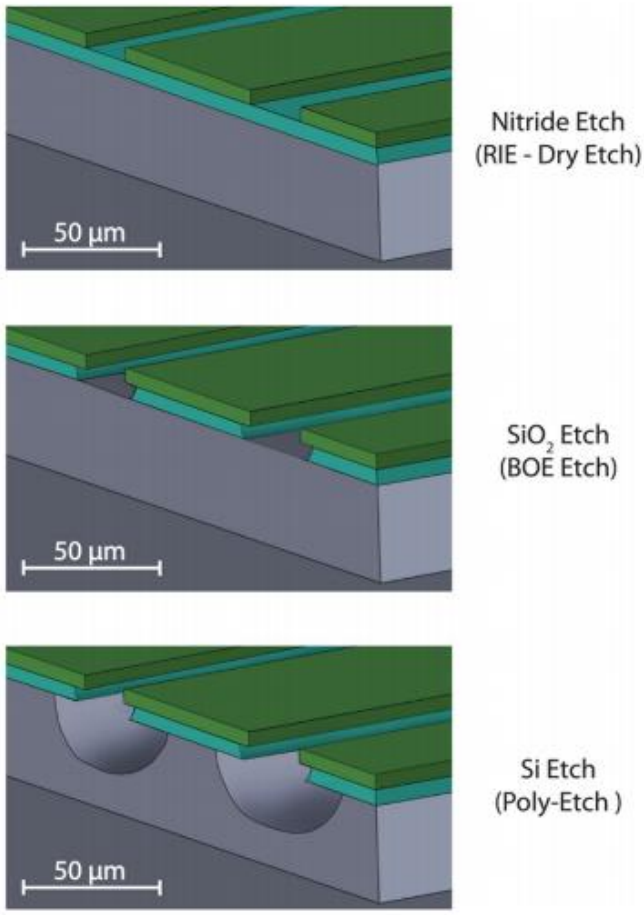

Figure 4-3 Fabrication process of RTDs where overhang structure is used for self-shadow masking in metallization step (nickel deposition.)

In the next step, second layer of SiN film (0.5µm) is deposited using LPCVD. The chamber patterns are printed on top of the wafer using photolithography process and a contact aligner. The SiN and SiO2 layers are removed using RIE and BOE, respectively to expose the silicon. Then, the silicon is etched using anisotropic wet chemical etching (KOH) process at 60^{o}C for 12hrs (the process is self-terminating). The KOH etching process forms the calorimeter chamber. The cross-sectional view of the chamber at this step is shown in Figure 4.2(b).

Then, the third layer of SiN film (LPCVD, 0.5µm) is deposited on the wafer. In this step, the microfluidic channel structures, microfluidic input and output interfaces, and chamber isolation area are fabricated all together. The patterns of microfluidics and chamber isolation area are printed using a lithography process on the backside of the wafer. Then, silicon at the printed pattern is exposed using etching of SiN and SiO2 layers by RIE and BOE, respectively. The second KOH process is used at 60^{o}C for 12hrs to remove the silicon all the way to the other side of the wafer. This process is self-terminating at this step.

After this step, the suspended SiN film chamber structure is formed with 200nL volume and chamber wall thickness is 0.5µm. The micro fabricated chambers are suspended using tether structures. The cross-sectional view of the chamber at this step is shown in Figure 4.2(c).

In next step, the 40nm of nickel film is deposited separately on each side of wafer using thermal evaporation process. The evaporated nickel formed the resistive heater and RTD temperature sensor. The close up image of the RTD sensor and the device after metallization are shown in Figure 4.4.

The last step in fabrication is thermally bonding thin polyimide layer (Kapton tape) to the backside of the devices after breaking the wafer into the dies at 70^{o}C for 2hrs on top of a hotplate. The polyimide film will close the exposed area at microfluidic and chamber and form a sealed structure.

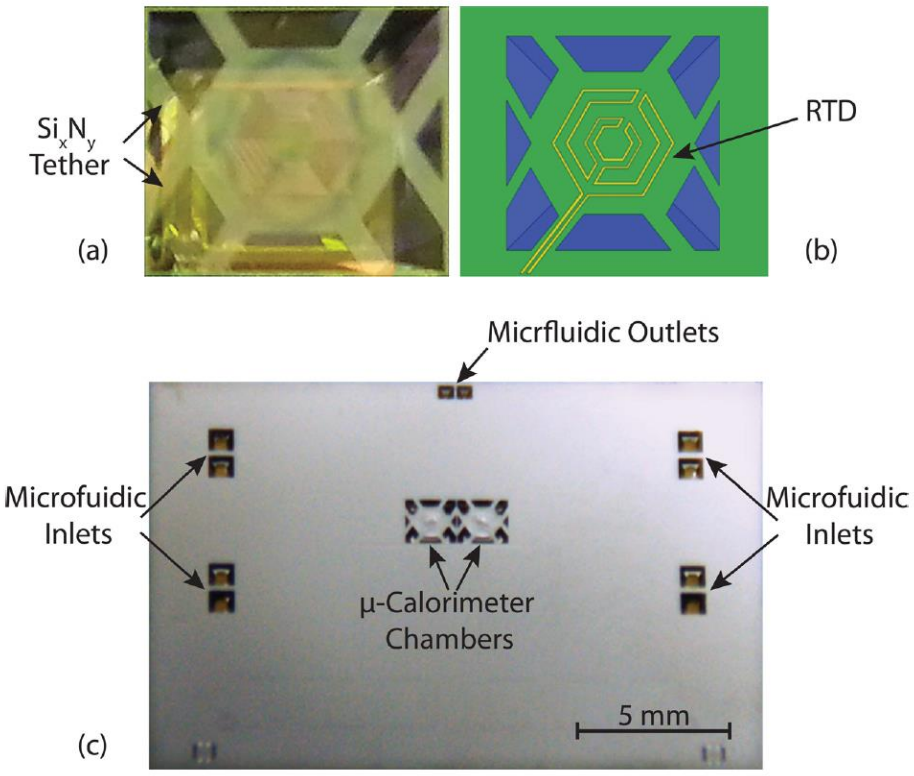

Figure 4-4 Micro Calorimeter device (a) optical image of suspended chamber with integrated RTD, (b) schematic of RTD integration to a suspended thin film structure, (c) top-view of completed micro calorimeter device.

4.1.2 Device Characterization

This section covers the characterization of fabricated micro calorimeter device. The characterization has two steps; RTD sensor calibration, and DC characterization of micro calorimeter for measuring thermal time constant of device.

The electrical resistance of fabricated thin film RTD is measured between $1-4k\Omega$ for 70-30nm thickness of deposited nickel film. In bulk, the TCR of nickel is reported $6\times10^{-3}/\,^{o}C$. However, in thin film metals, based on the thickness of the deposited film and grain size of the

metal, the mean free path of electrons are changing due to the scattering [ref]. Therefore, the TCR must be measured with lower values comparing to bulk.

In this work, a measurement setup is designed and assembled to measure the TCR of fabricated thin film RTD. The TCR of fabricated device is $2.58\times10^{-3}/{}^{o}C$ and has very high linearity $\left(R^2=0.9999\right)$ for calibrated $\left(10-50^{o}C\right)$ range.

In the second step, the step response of the fabricated calorimeter is used for measuring the thermal parameters of fabricated structure for calculating the thermal time constant of device. The micro calorimeter chamber is filled with DI water to perform the step response test. Then, a current pulse is applied to the heater by a source/meter (Keithley 2400) and the resistance change in sensor is measured by another source/meter by applying constant bias current (0.1mA). Both source/meters are computer controlled by a custom-made LabVIEW program.

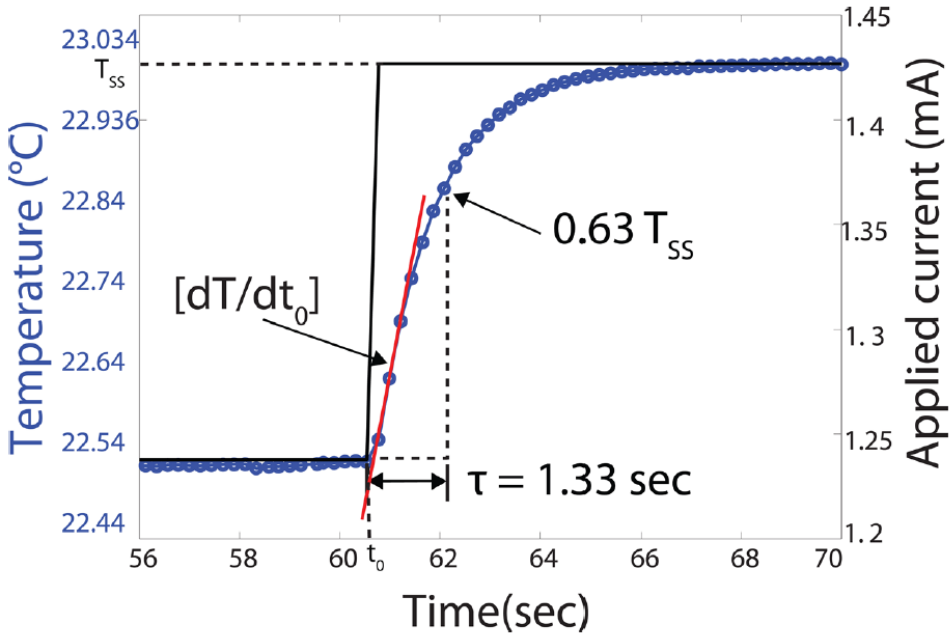

Figure 4-5 Step response test result from micro calorimeter device, where the chamber is filled with DI water.

From step response curve, thermal resistance and thermal mass and the time constant of micro calorimeter are $58.87\left(K/W\right)$, $6.63\times10^{-3}\left(J/K\right)$ and $1.33(s)$, respectively. Later in measurement section these thermal parameters are used for characterization of liquid samples. The step response curve of micro calorimeter is shown in Figure 4.5.

4.1.3 Experimental Results

As explained in chapter 3, developed micro calorimeter is capable of measuring thermal diffusivity of samples and specific heat of the sample. Heat penetration time measurement and TWA methods are used to measure thermal diffusivity and specific heat, respectively.

Thermal diffusivity of sample is quantified by measuring heat penetration time from heater to the sensor, when the heater is pulsed with a current pulse. In Figure 4.6(a), concept of heat penetration time measurement is illustrated. Since the measurement is time sensitive between input pulse at heater and measured temperature profile at sensor, a MATLAB code is used to extract the exact time (arrival time). The second derivative of the received signal is used for determining the exact location of the arrival pulse at sensor. The arrival time measurement of heat pulse to the sensor using second derivative method is shown in Figure 4.6 (b).

The thermal diffusivity of glycerol is measured using this technique and the measured value $9.94\times10^{-8}\left(m^2/s\right)$ is shown less than 8% error compared to the reported thermal diffusivity for glycerol [ref].

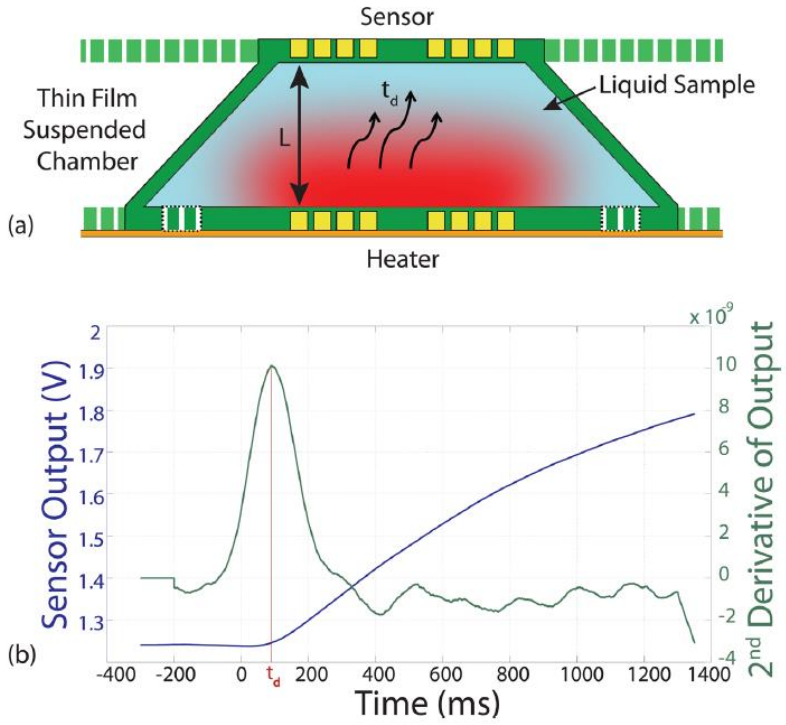

Figure 4-6 Penetration time measurement results and using the 2nd-derivative to measure the exact value of arrival time.

In specific heat measurement as described in chapter 3, TWA method is used, where an alternating heat is generated at the heater and travels through the sample. The detected temperature at the sensor is used to calculate the specific heat of the device.

The specific heat of DI-water is measured by the TWA method and using micro calorimeter device. The measured value is in good agreement (~5% error) with reported value (Table 4.1). Same technique is applied to measure specific heat of ionic liquids for the first time, where the specific heat of 1-ethyl-3-methylimidazolium bis(trifluoromethylsulfonyl)imide ([EMIM][Tf2N]), 1-buthyl-3-methylimidazolium hexafluorophosphate ([BMIM][PF6]), 1-hexyl-3-methylimidazolium hexafluorophosphate ([HMIM][PF6]), and 1-methyl-3-octylimidazolium hexafluorophosphate ([OMIM][PF6]), are measured and reported in Table 4.1.

Table 4-1 measured specific heat values

	Sample	Measured Specific Heat (J/g K)
1	[EMIM][Tf2N]	2.75
2	[BMIM][PF6]	2.83
3	[HMIM][PF6]	0.86
4	[OMIM][PF6]	2.55

4.1.4 Discussion

The micro calorimeter devices with 200nL volume chambers are fabricated and used to measure thermal diffusivity and thermal conductivity of liquid samples. The designed structure benefits from the symmetric design of the thermal elements where the structure provides homogenous heat transfer to reduce fringing effects.

Using thin film suspended structure leads to a reduction in thermal mass and an increase in the sensitivity of thermal measurements; however the structure is fragile to work with high viscosity samples. In addition, the difficulties in cleaning the chamber and microfluidics make it almost a single use device. The other point learned from the device is, the microfluidic interfacing and leak in the tubing need to be optimized in future work, where the first step will be moving them apart to enhance interfacing.

The advantages and disadvantages of fabricated on-chip micro calorimeter are presented. These characteristics define limitation for using this technology for real application mostly due to the cost of fabrication. This device is good for measuring very rare and costly samples.

4.2 Thermal Particle Detection Platform

The introduced microfluidic platform for thermal detection of suspended particles in chapter 3 consists of silicon substrate with a SiN membrane, a thin film RTD, and a PDMS microchannel. The first section provides a detailed fabrication process for silicon substrate and PDMS microchannel. The second section covers the experimental setup are for different sizes of suspended particles. Finally, the characteristics of output signals (resistance change) for different particle sizes are discussed in detail in the last section.

4.2.1 Device Fabrication

The silicon device (substrate and membrane) fabrication starts with growing SiO_2 (250nm) and depositing LPCVD SiN film (0.5μm) on both sides of a single crystal silicon wafer. Then, the membrane pattern is printed on the bottom of the wafer, using a photomask and optical contact lithography technique. In next step, the SiN and SiO_2 layers in printed patterns are removed by RIE and BOE etching, respectively.

In the next step, KOH process removed the silicon at patterned structure all the way to form SiN membranes at top of the wafer. To integrate RTD sensors, a 40 nm nickel film is deposited on top of the wafer and RTD structures are patterned on surface using the second photomask. Using the metal etchant ($HCl:HNO_3$:DI, 1:5:5) the excess metal parts are removed and RTD is formed on top of membrane. The RTD sensors on top of SiN membrane is shown in Figure 4.8.

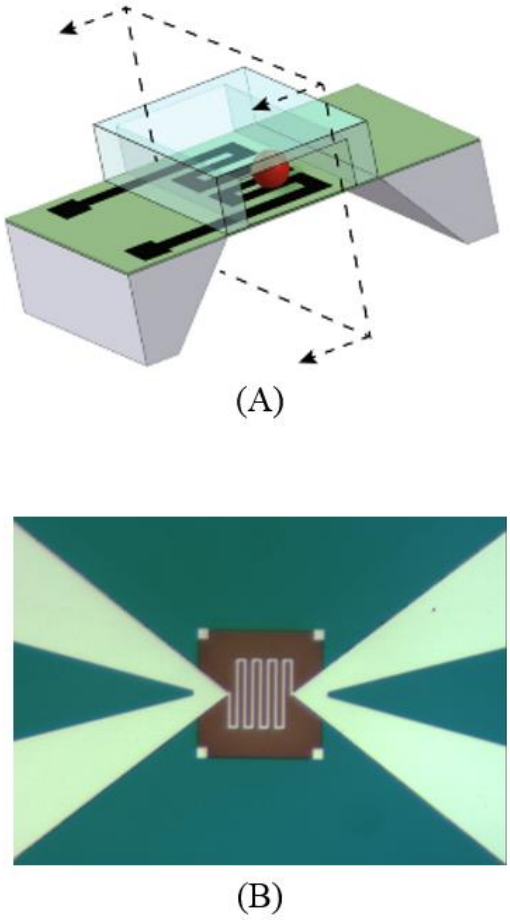

Figure 4-7 Fabricated device before microchannel binding, (A) the 3D view side view of fabricated platform, (B) completed silicon-based device with integrated RTD.

The PDMS microfluidic channels are fabricated with soft lithography technique by using an SU8 mold. The mold is fabricated using the lithography process and negative photoresist (SU8) is patterned and developed the mold for PDMS channels. This technique for fabricating SU8 mold is introduced earlier in chapter 2 (Figure 2.3).

The PDMS microfluidic channels are fabricated by pouring the mixed elastomer resin and hardener on top of the SU8 mold. Then, it is thermally cured at 70ºC for 2 hrs. The cured channels are peeled off from SU8 mold. The PDMS fabrication process is shown in Figure 2.4.

The fabricated channels are aligned with RTD sensors under optical microscope and bonded to the SiN surface. The completed device with bonded PDMS channel is illustrated in Figure 4.8.

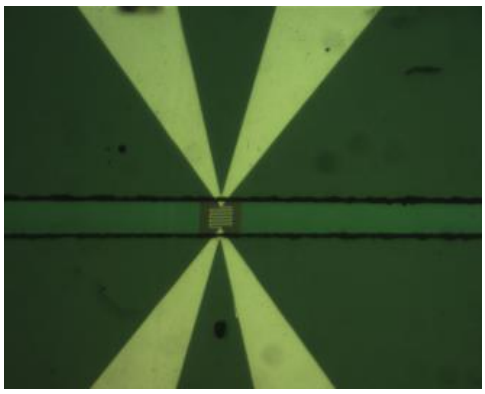

Figure 4-8 Thermal particle device platform after aligning and bonding of PDMS, microchannel to the membrane.

For connecting microfluidic tubes to channel inlet and outlet, and connecting RTD sensors to electrical measurement instruments, a measurement setup holder (jig) for interfacing is developed. The custom jig acts as a device holder to support the fabricated microfluidic device and provide electrical interfacing and improves the microfluidic connections to device. The designed jig is fabricated by 3D printing Acrylonitrile Butadiene Styrene (ABS) thermoplastic.

4.2.2 Experimental Results

In this experiment, two different sizes of polystyrene (PS) microspheres are used. The first is 90µm diameter PS beads and the second is 200µm dimeter PS beads. Since the PS has higher density (1.05 g/cm^3) than water, a mixture of water and glycerol is used as a buffer. The density of mixture is tuned to match the density of PS beads, which allows beads to stay suspended and prevent from settling.

Then, the 90μm PS beads are introduced to the microchannel while the resistance of RTD is continuously recoded by applying a constant DC bias current to the RTD. The resistance increased by about 0.5Ω, which is equivalent to 0.11K in temperature change. The results are shown in Figure 4.9.

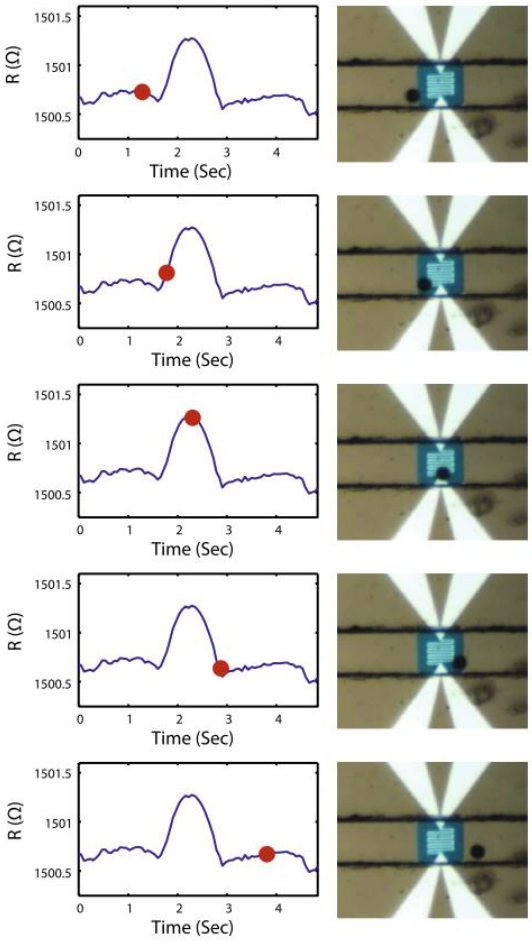

Figure 4-9 The measured signal due to passing of a 90um PS bead.

The same experiment is repeated for the 200µm diameter PS beads. As shown in Figure 4.10, the resistance decreased when 200um beads passed the RTD in microfluidic channel. The amplitude of peaks shows 2Ω resistance change, which corresponds to 0.44K drop in temperature.

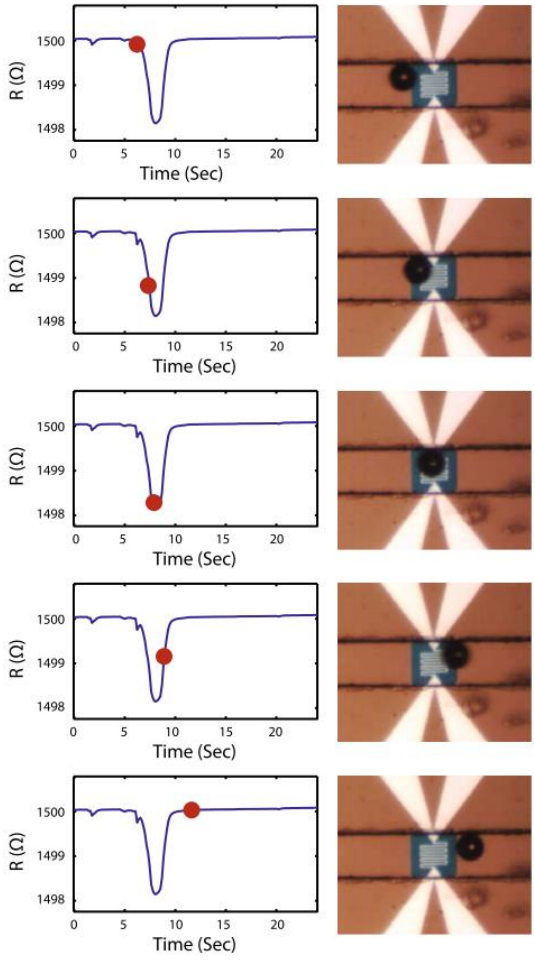

Figure 4-10 The measured signal due to passing of a 200um PS bead.

In this case, when the size of bead (200µm) is larger compared to the channel width (300µm), the local velocity change due to the passing beads is considerable. The local velocity change results in increasing convective heat transfer. Since the RTD is constantly biased, the area

over RTD is lightly experiencing higher temperature compared to other parts of microchannel. The induced change in local fluid velocity moves liquid faster and reduces the temperature.

The experiment is repeated with four 200µm PS beads and resulted in four peaks in detected resistance change, as shown in Figure 4.11. This result shows the capability of fabricated microfluidic platform in detecting and counting suspended particles.

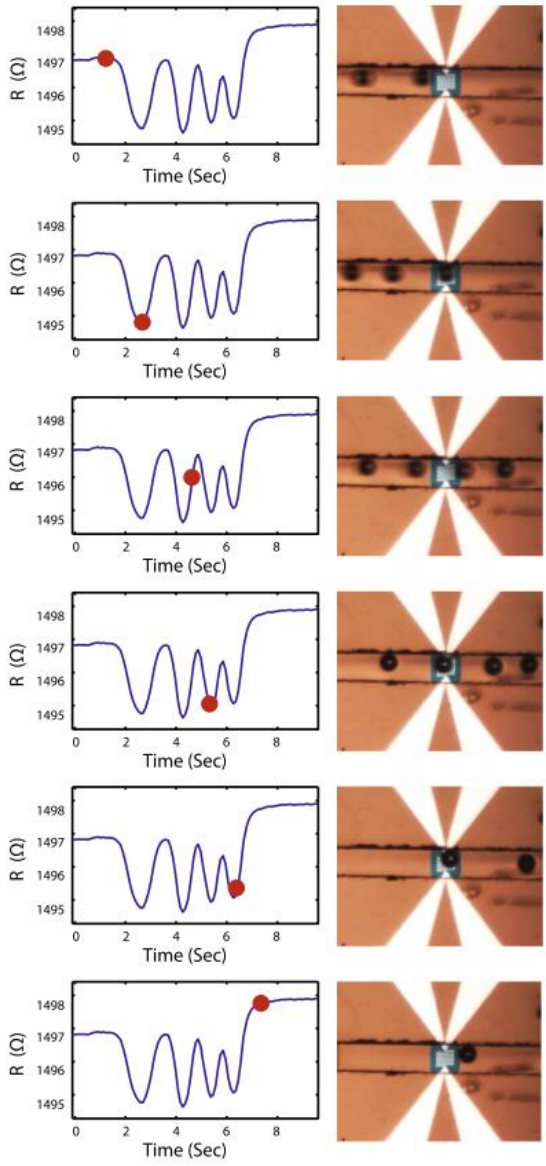

Figure 4-11 The measured signal due to passing of series of 200um PS beads.

4.2.3 Discussion

The results for detecting and counting micro particles suspended in water is presented in last section. To verify that the detected effect is caused solely by thermal conductivity change at the presence of the particle, the same experiment is repeated in buffers with different electrical conductivities (glycerol, DI water, and PBS). As it can be seen in Figure 4.12, the results are showing the same effects for 200µm PS beads. The electrical conductivity change only affects the base line of measured resistance.

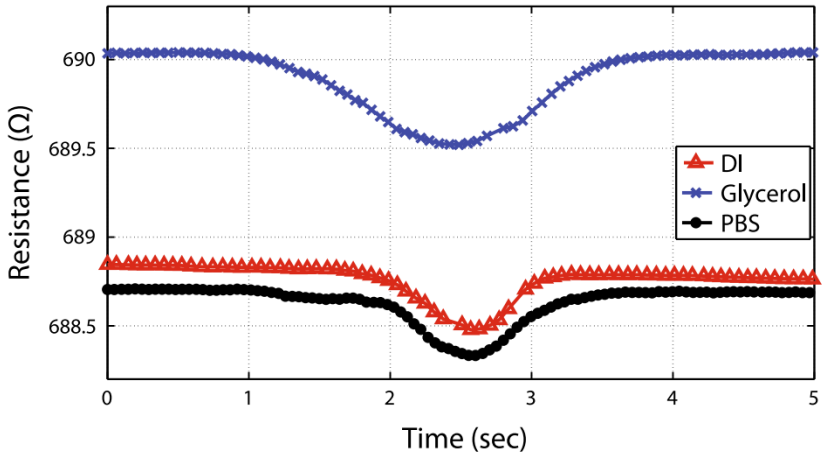

Figure 4-12 Thermal particle detection results in different buffers.

The presented results and analysis show the potential of the thermal measurement to analyze the suspended particles. The results are not limited to the detection and counting particles, and the microchannel width can be tuned to identify the size of passing particle.

4.3 Calorimetric Paper-Based Microfluidic Sensor

The third application, paper-based bio chemical sensor with calorimetric detection introduced in chapter 3, consists of three main elements: substrate (handle), paper-based microfluidic channel, and integrated RTD temperature sensor. This section starts by providing the details of paper-based channel fabrication and details of integrating thin film RTD on device using shadow masking technique.

Next section covers the experimental setup for glucose level measurements using developed microfluidic device. Then, DNA concentration detection and protein bonding analysis are provided and two additional examples to verify the applicability of this concept. Finally, last section provides a detailed dissolution on the advantages, disadvantages, and future applications of this technology.

4.3.1 Device Fabrication

Fabrication of a paper-based microfluidic device starts with designing and cutting paper microchannel. The geometry of the design provides a control parameter on the volumes of sample and required concentration of reagents. The paper microchannel with designed strips are cut using a desktop knife plotter.

In this project, a thin cover slide glass (150μm) is used as a substrate for the device and fixed on a laser cut acrylic holder. The metal RTD is patterned on top of the glass by using shadow mask technique and metal depositing. In this device, 40 nm nickel film is deposited on the device, where polyimide film shadow mask defines the structure of the RTD.

In next step, a protective layer is added on top of RTD to avoid chemical reaction of sample and metal RTD interferences in the measurement. The protection layer is a 100μm

polyimide layer and 5µm acrylic adhesive layer to improve the contact of paper-based micro channel and RTD sensor. Fabricated device is shown in Figure 4.13.

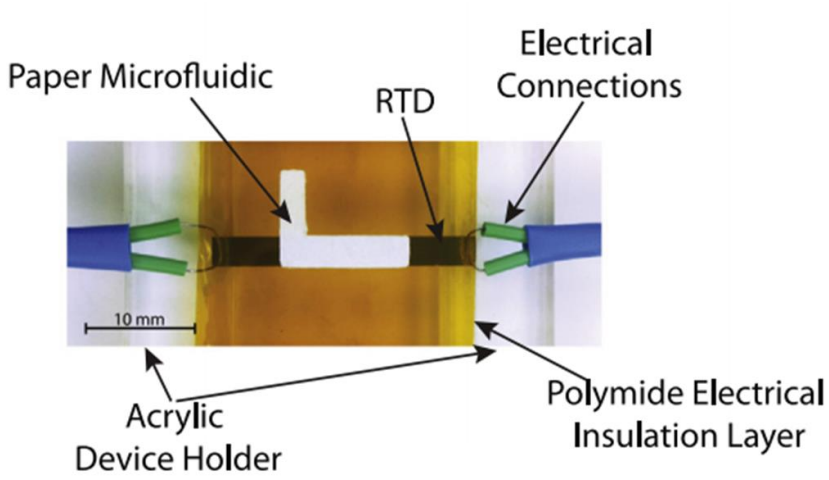

Figure 4-13 Fabricated paper-based microfluidic device with calorimetric detection.

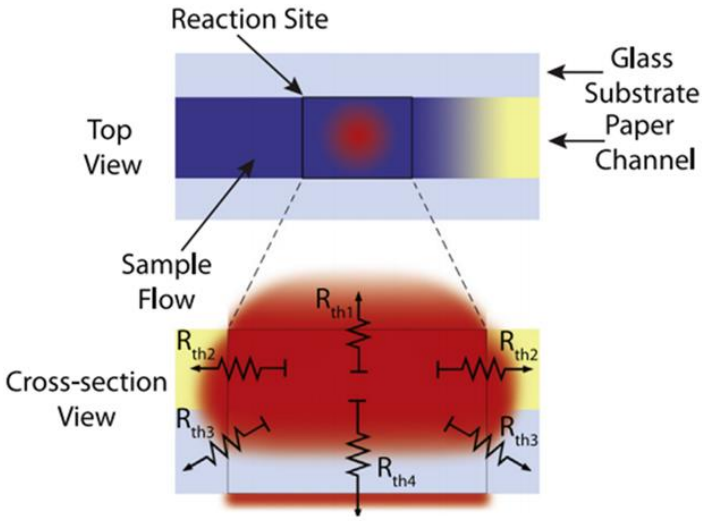

Figure 4-14 Equivalent thermal resistances for modeling heat transfer in sectional view of reaction site on paper-based microfluidic channel.

The fabricated device is analyzed using developed thermal equivalent circuit. Figure 4.14 illustrates the thermal resistances in the cross-sectional view of reaction site, where reaction of sample and reagents are causing a temperature change.

The thermal parameters of the system as the results of the thermal analysis are listed in Table 4.2, where the calculated values and measured values from step response test (same as micro calorimeter device) are compared.

Table 4-2 Thermal parameters of paper-based microfluidic device (Davaji & Lee 2014).

Symbol	Parameter	Unit	Value
R_{th1}	R_{th} of air boundary	K/W	6.17×10^{3}
R_{th2}	R_{th} of paper boundary	K/W	4.78×10^{3}
R_{th3}	R_{th} of glass boundary	K/W	4.76×10^{3}
R_{th4}	R_{th} of air through glass	K/W	6.17×10^{3}
$C_{P,Calc.}$	Calculated thermal mass	J/K	1.33×10^{-2}
$C_{P,M}$	Measured thermal mass	J/K	1.42×10^{-2}
$\tau_{Calc.}$	Calculated time constant	s	11.3
τ_{M}	Measured time constant	s	12.4

4.3.2 Experimental Results

In the first test as explained in chapter 3, catalytic reaction of glucose reduction and oxidation is used to detect the concentration of glucose in standard samples. In this measurement, the RTD temperature sensor measures the temperature continuously by a constant bias current. The constant bias current results in a higher operating temperature compare to room temperature due to Joule heating effect.

In the first step, activated GOD enzyme (2µL) is immobilized to the center of paper strip. Then, the glucose standard sample (8µL) is introduced to the inlet of the paper channel. The

glucose sample will transport into the paper toward the reagent (GOD) and the reduction and oxidation reaction will start. The heat generated by reaction is recorded and shown in Figure 4.15.

As it can be seen from the reaction signals, due to higher operating temperature of device, introducing samples with room temperature causes a decrease in the signal, once when the GOD enzyme is introduced and once when the glucose sample is introduced. However, the reaction (exothermic) peak is obvious in the close-up signal.

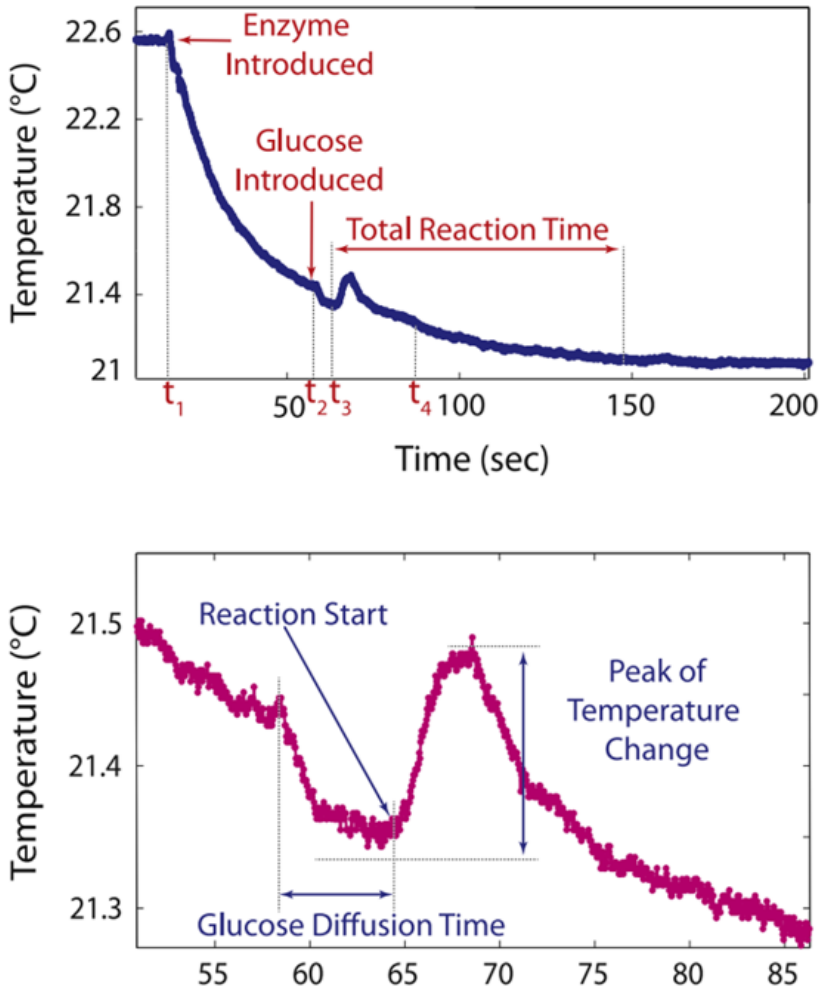

Figure 4-15 measured temperature due to reaction of oxidation reaction of glucose.

The experiment is repeated for three (low, medium, and high) glucose standard calibration sample and the measurements show the linear trend in the generated temperature. The results of generated temperature due to the concentration of the glucose in calibration sample is shown in Figure 4.16.

The measured results shown in Figure 4.17 are compared with the measurement results from commercially available glucose meter. The fabricated paper-based microfluidic with calorimetric detection has better resolution compared to the portable glucose meter. The errors in portable glucose meter can get as high as 30% from the actual concentration of glucose in standard sample.

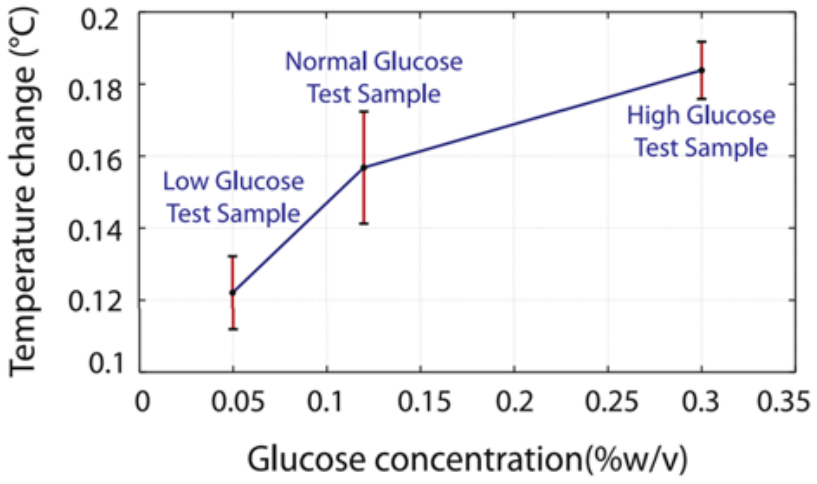

Figure 4-16 Measured temperature change caused by different concentrations of glucose sample.

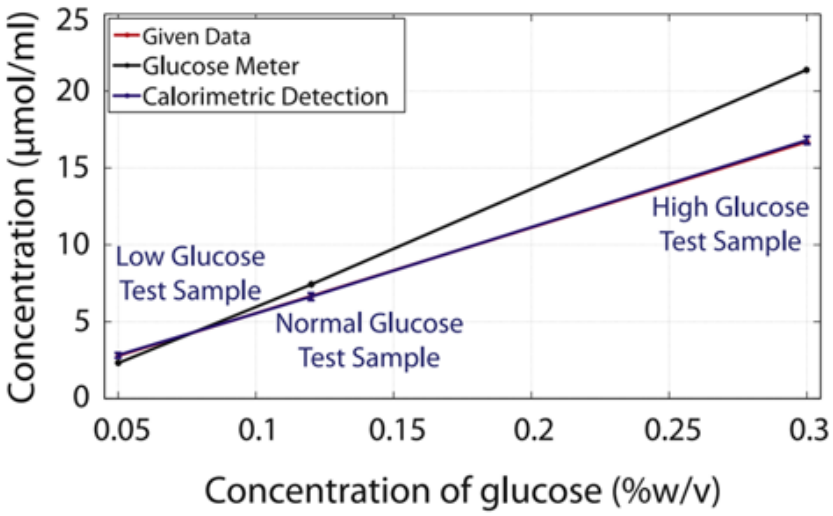

Figure 4-17 Result of glucose level measurement by a commercial glucose meter in comparison by measurement results from developed paper-based calorimeter.

After presenting the glucose level measurement using the calorimetric paper-cased sensor, same device is used for presenting feasibility of calorimetric detection in DNA concentration measurement and protein binding reaction detection. The details of the selected reaction for DNA cleavage and exothermic interactions are described elsewhere (Davaji & Lee 2014).

The experimental results for these reactions are shown in Figure 4.18. The measured temperatures for DNA cleavage reaction is used for quantizing the concentration of DNA and the measured binding temperature for proteins identifies the exothermic reaction.

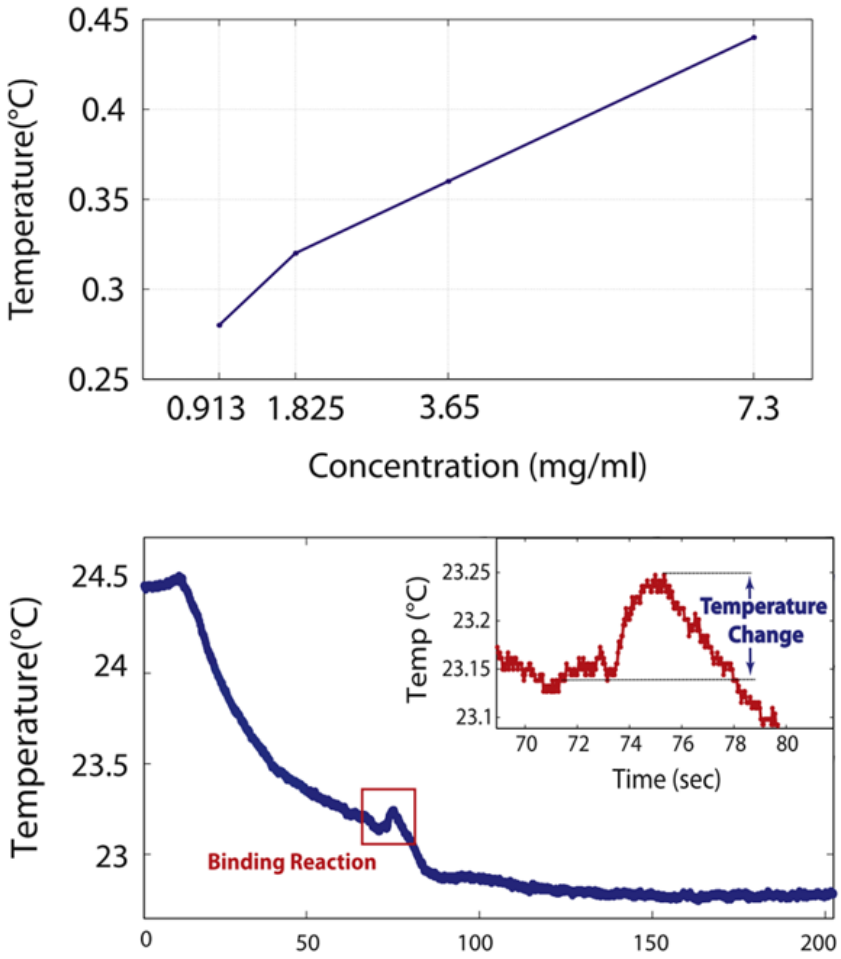

Figure 4-18 Temperature measurement result by paper-based calorimeter device, (A) the results of DNA concentration detection, (B) investigation results of exothermic protein binding reaction.

4.3.3 Discussions

The calorimetric detection results are presented for glucose level measurement, DNA concertation measurement, and protein binding identification using calorimetric detection method by the fabricated paper-based sensor. The paper-based devices are promising for low-cost portable applications due to several advantages of paper-based microfluidic compared to the conventional microfluidic channels.

As the results show, the thermal measurement methods will enhance the capability of paper-based devices and might broaden the applications of this device where the electrochemical and colorimetric detection techniques are not applicable.

However, in calorimetric detection technique, finding proper reagents for the detection reaction is critical. In selection of reagents, stability of reagents over time and room temperature, and reactions with detectable enthalpy changes must be considered. The proper detection reaction and reagents allow paper-based calorimetric detection to become a very good candidate to develop portable diagnostic device for low-income countries, where the cost of medical services are threatening many lives.

4.4 Microfluidic Platform for Temperature Measurement of a Single Cell

The microfluidic platform for single cell isolation and temperature measurement is introduced in chapter 3, where the details of operational principles of device based on differential pressure is presented. In this section, detailed fabrication process for silicon based microfluidic device and PDMS micro channel are presented. Next section covers cell-capturing results, where the temperature measurement experiments are still ongoing.

4.4.1 Device Fabrication and Primary Results

The microfluidic platform for single cell temperature measurement has two main parts: the silicon based micromachined device and microfluidic channel. The sectional-view of device fabrication process is shown in Figure 4.19.

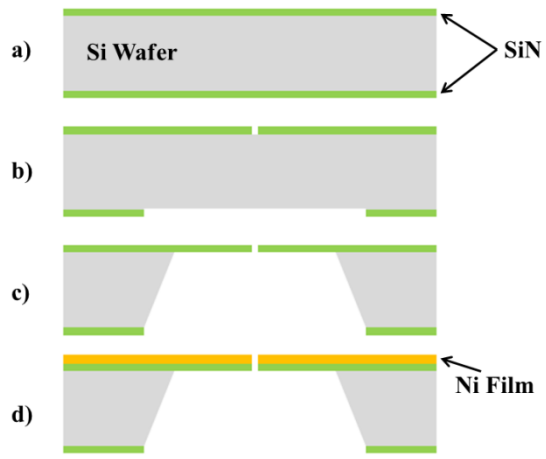

Figure 4-19 Fabrication process for the silicon-based substrate.

The fabrication process is very similar to that of the thermal particle detection platform presented in section 4.2, where the only difference is an additional lithography and RIE process to etch the cell capturing hole (Figure 4.20). The cell capturing hole is located at the center of membrane and very close to the location of the RTD temperature sensors.

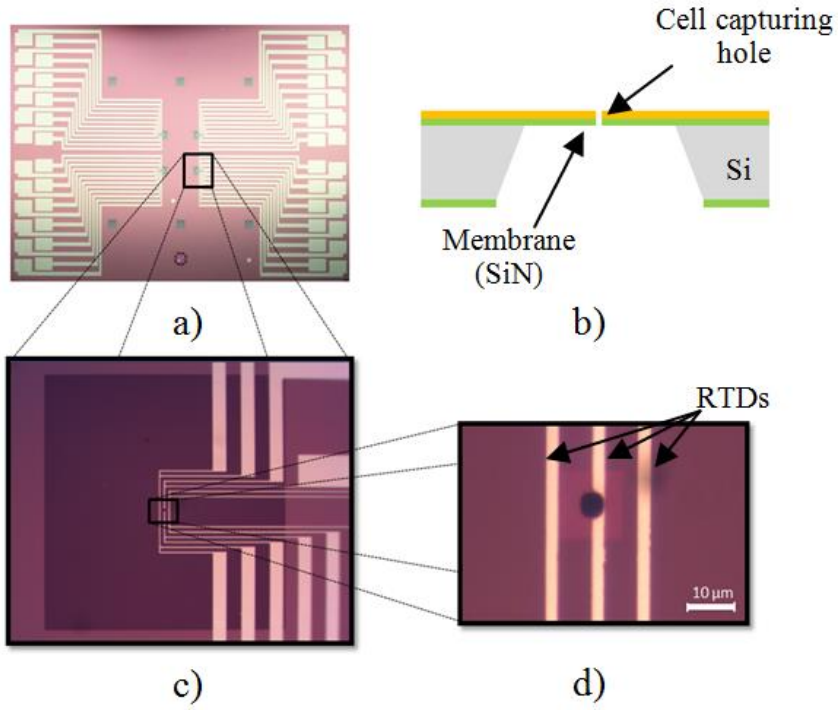

Figure 4-20Figure 4.20 Fabricated device for single cell capturing and thermal measurements, (a) completed device, (b) sectional-view of fabricated device, (c) close up image of SiN membrane and RTDs, (d) close-up image of RTDs and cell capturing hole.

The PDMS microfluidic channel is fabricated using soft lithography technique as explained in Section 4.2. However, the backing layer of the channel is a cover glass to reduce the thermal mass of the thick PDMS backing layer. The reduced thermal mass is required to increase the sensitivity of temperature measurement. The rigid glass backing layer makes it difficult to peel off PDMS after curing from mold. Therefore, a releasing agent (Polyvinyl Alcohol) is used to release the cured channels from mask by submerging in water.

Released channels are aligned and bonded to the fabricated silicon-based device under the microscope and RTD contact pads are wire bonded to the holding structure. The latest progresses on fabrication of interfaces allowed to develop a platform shown in Figure 4.21.

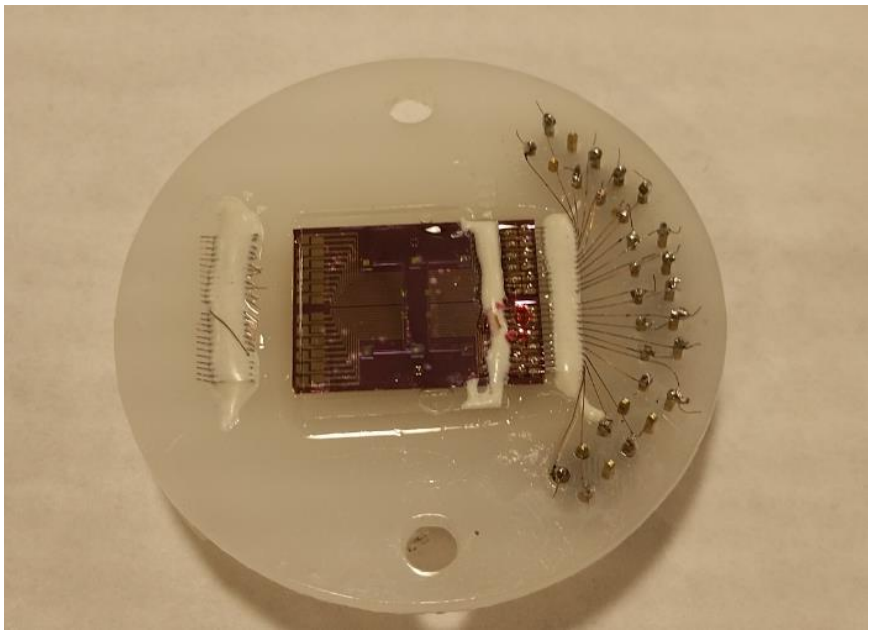

Figure 4-21 Completed microfluidic platform with integrated microchannel and completed wire bonding.

However, due to the practical difficulties in interfacing fluid and preventing leaks at the inputs and outputs, updated system is being developed. This project is being transferred to junior graduate student and he will carry out the rest of troubleshooting and updating process on the interfaces.

The 5µm glass microspheres are used as a cell to calibrate the flow rates in both channels. The suspended beads in water and glycerol solution (balanced density) are introduced to the top channel, when the bottom channel is filled with water. Then, the negative pressure is generated at the capturing hole by applying negative flow rate to the bottom channel while the top channel is experiencing constant flow rates. By varying the flow rates in both channels, the rate of success in capturing of beads are recorded. Figure 2.22 shows the results of this calibration experiment.

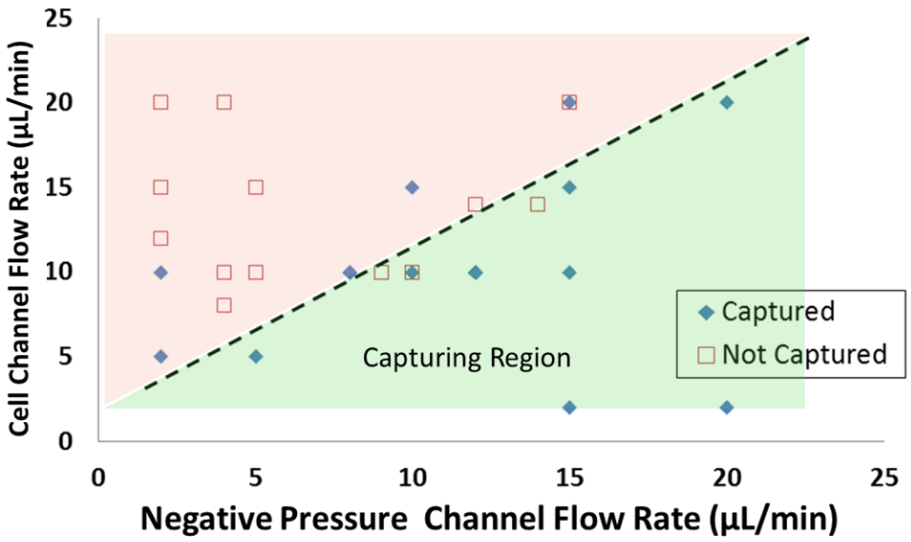

Figure 4-22 Cell capturing flow rate characterization. The 10 µm polystyrene beads suspended in buffer solution are used for characterization. The capturing region is illustrated in green.

Chapter 5 Conclusion and Future Work

5.1 Summary

In this dissertation, capabilities of thermal measurements on microscales are investigated. The main focus is the concept of using thermal measurement methods to detect and measure physical quantities. Thermal design considerations for microfluidic devices are modified to develop applicable and functional devices for thermal measurement. By implementing these considerations, microfluidic devices are designed and fabricated for four applications: micro calorimeter, thermal particle detection, calorimetric paper-based sensor, and a microfluidic platform for a single cell temperature measurement.

Thermal methods are a group of measurement techniques that study substance interactions with the ambient by investigating heat. Heat is not a measurable quantity; however, the generated temperature change due to heat transfer is a detectable quantity. Thermal measurement methods investigate both transient and steady state responses of a sample due to heating (thermal analysis), or measure the rate of heat transfer caused by a chemical or physical interaction (calorimetric techniques).

Thermal measurement techniques are applicable to vast range of measurements and offer many advantages such as producing quantitative results, simple measurement setup due to advancements in temperature sensor technology, and the label-free nature of such measurements. However developing thermal measurement techniques requires special design consideration. Therefore, in this work an equivalent circuit model is adopted to implement the thermal considerations in device design.

In order to validate the potential of thermal measurements in microfluidic devices, four applications are selected and a device is designed for each one. For each design, a microfluidic device is fabricated by implementing the identified thermal considerations in each design. An on-

chip calorimeter device is developed for thermal analysis of a liquid sample, a thermal technique is developed to detect particles suspended in a liquid buffer, a calorimetric paper-based enzymatic detection assay is fabricated, and a microfluidic platform for single cell capturing and temperature measurement is fabricated.

In the first application, a thin film, suspended chamber structure with 200nL volume is fabricated for micro calorimetry application. The RTD sensors are integrated on both sides of the chamber by our developed self-shadow masking technique. The fabricated device has two identical chambers that allow it to perform Differential Scanning Calorimetry (DSC). The fabricated nickel RTD sensors are calibrated for measuring the Temperature Coefficient of Resistance (TCR) and the micro calorimeter device is characterized for thermal parameters using a step test.

The fabricated micro calorimeter device is used for thermal diffusivity and specific heat measurement. To increase the speed of measurement, heat penetration time measurement is adopted for thermal diffusivity measurement. The thermal diffusivities of water and glycerol are measured and reported in Chapter 4. In addition, Thermal Wave Analysis (TWA) is applied to the same device without changing the sample, and specific heats of water and glycerol are again measured. Using the same setup, specific heat of ionic liquids are measured and reported for the first time.

In the second application, a novel technique is developed and introduced for particle detection using thermal measurement techniques. Detection of the change in thermal conductivity is used to detect and identify a suspended particle in a microfluidic channel. As presented in the results, the fabricated device is capable of detecting and counting suspended particles in a microfluidic chamber. Furthermore, the results describe the capability of detecting the particle properties such as size using the fabricated device. The 90µm and 200µm polystyrene spherical particles are detected and counted using the fabricated thermal particle detector device.

In the third application, thermal detection in paper-based microfluidic devices was utilized to enhance the capabilities of paper-based devices as low-cost analytical sensors for the first time. By introducing a micro fabricated thin film RTD temperature sensor to the paper-based device, the temperature change associated with the reaction of sample and reagent in the paper-based channel is measured. The detected temperature is used to quantify the concentration of reactive substances.

The measurement results for three samples are presented in chapter 4. The catalytic oxidation reaction of glucose in presence of a GOD enzyme shows 20 percent higher resolution compared to the commercially available portable glucose measuring device. Furthermore, DNA strand cleavage reaction by a hydrogen product is used for detecting salmon DNA on a paper-based channel using the thermal detection method. Similarly, protein bonding reactions of biotin and streptavidin are detected using the fabricated calorimetric, paper-based microfluidic device.

Finally, the last application is to develop a single cell, temperature measurement platform. A planar, patch clamp-like structure with two microfluidic channels is fabricated for capturing a single cell. The fabricated device is calibrated to find operational flow rates. The calibration data provides the required flow rates for capturing and fixing the captured cell at the microfluidic channel for measurements and releases the cell to capture another one for next experiment. As shown in chapter 4, the device successfully captured polystyrene microspheres and yeast cells.

Thin film metal RTD sensors are attached on platform near the capturing site to measure the cell temperature change over time. The silicon chip fabrication and micro channel fabrication processes are designed and developed, and the platform is fabricated in this work. The fabricated platform is even tested successfully for capturing multiple cells. However, as an ongoing project, efficient techniques for microfluidic interfacing are being developed for long time performance of the system. At this stage, some fluid leaks at interface are causing pressure drop issues where our group is actively working to overcome the problem.

The main subject of this work is to investigate thermal measurement capabilities in microscale devices by providing thermal consideration for device development processes. Details of device design and process development for fabrication along with test results of fabricated devices are presented in this work. The measurement results show the enormous capabilities of thermal measurement methods.

A few issues still remain in the implementation of these devices which require more research efforts. These limitations are developing and integrating the point temperature measurements, reducing the thermal mass of structures, three dimensional temperature profile measurements in microfluidic channels, and discovering new materials for RTD temperature sensor fabrication.

Since the demand of biological experiments over measurement sensitivity, and precise control and measurement are increasing, where developing the labels and tags for measurement are getting more complicated, label free thermal measurement methods will likely get more attention. Regenerative medicine already uses microfluidic technology for controlling culture of cells and tissues, and is moving toward growing organs using chip technology. This technology has potential to play a key role in future developments of regenerative medicine and three dimensional tissue engineering.

5.2 Ongoing Research

Since these works are considered among the first to look at thermal measurement in microfluidic device as a system concept rather than a focused application, there are many ongoing research studies being conducted at Marquette University's Nanoscale Devices Laboratory. The device for measuring response of a single cell to external stimuli is the major ongoing research. Additionally, a flowmeter development project is currently running, where thermal measurement technology is used to measure fluid velocity for industrial and utility applications.

Moreover, opportunities for using the thermal measurement to detect cell malfunction of high temperature stem cells are being investigated. Design and fabrication of a new type of open droplet micro calorimeter and measurement setup has been completed and measurements are being performed for future publications. Finally, new materials are being investigated to optimize the current thin film RTD temperature sensors.

During the rest of my appearance as an active research member, efforts will be directed towards the completion of the ongoing projects. However, chances of facing new issues with special care requirements are high. In this case, projects will be transferred to junior colleagues for further investigations.

5.3 Future Work

The ongoing research and uncompleted work at the end of a graduate program are commonly described as future works. However, as this work is structured differently, future work is not limited to unfinished projects. Implementation of thermal measurements in microfluidic devices is the expected direction of my future work.

Development of new materials for temperature sensing and new fabrication techniques will bring an opportunity to increase the sensitivity of thermal measurement techniques and allow the development of practical nano-calorimeter devices.

Intensity, power, and spot size controllability of optical excitation make it a great heat source in microfluidic devices. The light triggered calorimetry techniques, such as flash calorimetry can be miniaturized for more precise applications, where a small amount of sample is available or in single cell investigations.

Implementing IR lasers as a heat source allows targeted power delivery based on the absorption coefficient of a given substance. For instance, applications such as developing materials for hyperthermia targeted heating of cancer cells in tissue. Thermal microfluidic devices

will play a key role in measuring the delivered power to the targeted cells without affecting surrounding tissue. Thermal microfluidic technology also has great potential to contribute to regenerative medicine where 3D tissue culturing can benefit from having thermal stimuli and would allow for measuring the system behavior as feedback.

Applications of thermal actuation and measurements are not limited to light sources with larger wavelengths like RF waves, which can be used for enhancing the penetration. The recent research on developing Super Paramagnetic Iron Oxide Magnetic Nano Particles (SPIONs) allows this idea to become closer to reality, though more investigation is required. Perhaps genetic modifications to program cells to generate the SPIONs or targeted delivery of these particles soon will allow development of a practical method for treatment of cancer using the localized heating. The thermal microfluidic measurement device would be an essential tool to develop such treatments.

The recent developments of thermal imaging also will bring an opportunity to take thermal analysis in microfluidic devices to another level by direct integration of lens free optical temperature detectors to microfluidic devices.

Combining electromagnetic heat sources and contact free temperature measurement methods in the future might bring opportunities for 3D thermal analysis to solve complicated problems like brain signaling in neuroscience.

Bibliography

Barros, N. et al., 2011. Application of DSC–TG and NMR to study the soil organic matter. *Journal of Thermal Analysis and Calorimetry*, 104(1), pp.53–60.

Bech, N., Jensen, P.A. & Dam-Johansen, K., 2009. Determining the elemental composition of fuels by bomb calorimetry and the inverse correlation of HHV with elemental composition. *Biomass and Bioenergy*, 33(3), pp.534–537.

Becker, H. & Locascio, L.E., 2002. Polymer microfluidic devices. *Talanta*, 56(2), pp.267–287.

Blumm, J. & Kaisersberger, E., 2001. Accurate Measurement of Transformation Energetics and Specific Heat By Dsc in the High-Temperature Region. *Journal Of Thermal Analysis*, 64, pp.385–391.

Cate, D.M. et al., 2015. Recent developments in paper-based microfluidic devices. *Analytical chemistry*, 87(1), pp.19–41.

Chen, Q. et al., 2007. A rapid and low-cost procedure for fabrication of glass microfluidic devices. *Journal of Microelectromechanical Systems*, 16(5), pp.1193–1200.

Chin, C.D., Linder, V. & Sia, S.K., 2012. Commercialization of microfluidic point-of-care diagnostic devices. *Lab on a Chip*, 12(12), p.2118.

Davaji, B. et al., 2014. A novel on-chip three-dimensional micromachined calorimeter with fully enclosed and suspended thin-film chamber for thermal characterization of liquid samples. *Biomicrofluidics*, 8(3), p.34101.

Davaji, B. et al., 2015. In-Vivo single cell protein intraction investigation using microfluidic platform. In pp. 1541–1544.

Davaji, B. & Lee, C.H., 2014. A paper-based calorimetric microfluidics platform for bio-chemical sensing. *Biosensors and Bioelectronics*, 59, pp.120–126.

Davaji, B., Lee, C., 2015. Thermal Measurement Techniques in Analytical Microfluidic Devices. *J. Vis. Exp*, 100.

Desmet, C. et al., 2015. Paper electrodes for bioelectrochemistry: Biosensors and biofuel cells. *Biosensors and Bioelectronics*, pp.1–19.

Donner, J.S. et al., 2012. Mapping intracellular temperature using green fluorescent protein. *Nano Letters*, 12(4), pp.2107–2111.

Dyson, F., 1998. *Imagined Worlds* The Jerusa., Harvard University Press.

Dyson, F.J., 2012. Is Science Mostly Driven by Ideas or by Tools? *Science*, 338, pp.1426–1427.

E., C., H., P. & A., S.H., 1963. *Recent Progress in Microcalorimetry*, New York: The MACMILLAN Company.

Ellerbee, A.K. et al., 2009. Quantifying colorimetric assays in paper-based microfluidic devices by measuring the transmission of light through paper. *Analytical Chemistry*, 81(20), pp.8447–8452.

Erickson, D. & Li, D., 2004. Integrated microfluidic devices. *Analytica Chimica Acta*, 507(1), pp.11–26.

Fiorini, G.S. et al., 2004. Rapid prototyping of thermoset polyester microfluidic devices. *Analytical Chemistry*, 76(16), pp.4697–4704.

Fiorini, G.S. & Chiu, D.T., 2005. Disposable microfluidic devices: Fabrication, function, and application. *BioTechniques*, 38(3), pp.429–446.

Fu, E. et al., 2010. Chemical signal amplification in two-dimensional paper networks. *Sensors and Actuators B: Chemical*, 149, pp.325–328.

Fu, E. et al., 2011. Transport in two-dimensional paper networks. *Microfluidics and nanofluidics*, 10, pp.29–35.

Gota, C. et al., 2009. Hydrophilic fluorescent nanogel thermometer for intracellular thermometry. *Journal of the American Chemical Society*, 131(8), pp.2766–2767.

Hayashi, T. et al., 2015. A Cell-Permeable Fluorescent Polymeric Thermometer for Intracellular Temperature Mapping in Mammalian Cell Lines. *Plos One*, 10(2), p.e0117677.

Hemminger, W.H. & Hohne, G., 1984. *Calorimetry: Fundamentals and Practice*, Wrinheim: Verlag Chemie GmbH.

Iervolino, E., van Herwaarden, a. W. & Sarro, P.M., 2009. Calorimeter chip calibration for thermal characterization of liquid samples. *Thermochimica Acta*, 492(1-2), pp.95–100.

Iliescu, C. et al., 2012. A practical guide for the fabrication of microfluidic devices using glass and silicon. *Biomicrofluidics*, 6(1), pp.16505–1650516.

Incropera, F.P. et al., 2006. *Introduction to Heat Transfer* 5th editio., John Wiley & Sons, Inc.

Irving, R. & Wadsö, I., 1964. Use of tris (hydroxymethyl) aminomethane as a test substance in reaction calorimetry. *Acta Chemica Scandinavica*, 18, pp.195–201.

Is, I.T. et al., 2012. Rapid #: -9634145.

Jelesarov, I. & Bosshard, H.R., 1999. Isothermal titration calorimetry and differential scanning calorimetry as complementary tools to invesitigate the energetics of biomolecular recognition. *Journal of Molecular Recognition*, 12, pp.3–18.

Kotowski, J. et al., 2013. Fast and simple fabrication procedure of whole-glass microfluidic devices with metal electrodes. *Microelectronic Engineering*, 110, pp.441–445.

La, J.P. et al., 2015. Biosensors and Bioelectronics Recent advances in lab-on-a-chip for biosensing applications.

Ladbury, J.E. & Chowdhry, B.Z., 1996. Sensing the heat: the application of isothermal titration calorimetry to thermodynamic studies of biomolecular interactions. *Chemistry & biology*, 3(10), pp.791–801.

Lankelma, J. et al., 2012. Paper-based analytical device for electrochemical flow-injection analysis of glucose in urine. *Analytical Chemistry*, 84(9), pp.4147–4152.

Leavitt, S. & Freire, E., 2001. Direct measurement of protein binding energetics by isothermal titration calorimetry. *Current Opinion in Structural Biology*, 11(5), pp.560–566.

Lee, C.H. & Davaji, B., 2014. Calorimetric Microfluidic Sensor.

Lee, W., Lee, J. & Koh, J., 2012. Development and applications of chip calorimeters as novel biosensors. *Nanobiosensors in Disease Diagnosis*, 1, pp.17–29.

Magee, J.W., Deal, R.J. & Blanco, J.C., 1998. High-Temperature Adiabatic Calorimeter for

Constant-Volume Heat Capacity Measurements of Compressed Gases and Liquids. *Journal of Research of the National Institute of Standards and Technology*, 103(1), pp.63–75.

Marison, I. et al., 1998. Biological reaction calorimetry: Development of high sensitivity bio-calorimeters. *Thermochimica Acta*, 309(1-2), pp.157–173.

Martinez, A.W. et al., 2010. Diagnostics for the developing world: Microfluidic paper-based analytical devices. *Analytical Chemistry*, 82(1), pp.3–10.

Martinez, A.W., Phillips, S.T., Wiley, B.J., et al., 2008. FLASH: a rapid method for prototyping paper-based microfluidic devices. *Lab on a chip*, 8(12), pp.2146–2150.

Martinez, A.W., Phillips, S.T. & Whitesides, G.M., 2008. Three-dimensional microfluidic devices fabricated in layered paper and tape. *Proceedings of the National Academy of Sciences of the United States of America*, 105(50), pp.19606–19611.

McDonald, J.C. & Whitesides, G.M., 2002. Poly(dimethylsiloxane) as a material for fabricating microfluidic devices. *Accounts of Chemical Research*, 35(7), pp.491–499.

Miltenburg, J.C. va., Genderen, A.C.G. va. & den Berg, G.J.K. va., 1998. Design improvements in adiabatic calorimetry. *Thermochimica Acta*, 319(1-2), pp.151–162.

Mraw, S.C., 1984. Calvet-type calorimeter for the study processes I . Description appropriate of an apparatus for organic materials of. , pp.865–871.

Mucha, M. & Królikowski, Z., 2003. Application of dsc to study crystallization kinetics of polypropylene containing fillers. *Journal of Thermal Analysis and Calorimetry*, 74(2), pp.549–557.

Nassu, R.T. & Gonçalves, L. a. G., 1999. Determination of melting points of vegetable oil and fats by differential scanning calorimetry (DSC) technique. *Grasas y Aceites*, 50(1), pp.16–21.

Nie, Z. et al., 2010. Integration of paper-based microfluidic devices with commercial electrochemical readers. *Lab on a chip*, 10(22), pp.3163–3169.

Okabe, K. et al., 2012. Intracellular temperature mapping with a fluorescent polymeric thermometer and fluorescence lifetime imaging microscopy. *Nature Communications*, 3, p.705.

Ostmark, H. et al., 2002. N -guanylurea-dinitramide : a new energetic material with low sensitivity for propellants and explosives applications. *Thermochimica Acta*, 384(1), pp.253–9.

Pierce, M.M., Raman, C.S. & Nall, B.T., 1999. Isothermal Titration Calorimetry of Protein – Protein Interactions. , 221, pp.213–221.

Ren, K., Zhou, J. & Wu, H., 2013. Materials for microfluidic chip fabrication. *Accounts of Chemical Research*, 46(11), pp.2396–2406.

Roy, E. et al., 2011. Prototyping of microfluidic systems using a commercial thermoplastic elastomer. *Microfluidics and Nanofluidics*, 11(3), pp.235–244.

Rupp, J. & Birringer, R., 1987. Enhanced specific-heat-capacity (cp) measurements (150 300 K) of nanometer-sized crystalline materials. *Physical Review B*, 36(15), pp.7888–7890.

Sackmann, E.K., Fulton, A.L. & Beebe, D.J., 2014. The present and future role of microfluidics in biomedical research. *Nature*, 507(7491), pp.181–9.

Santos, L.M.N.B.F. et al., 2004. Measurement of enthalpies of sublimation by drop method in a Calvet type calorimeter: design and test of a new system. *Thermochimica Acta*, 415(1-2), pp.15–20.

Sato, H. et al., 2006. An all SU-8 microfluidic chip with built-in 3D fine microstructures. *Journal of Micromechanics and Microengineering*, 16(11), pp.2318–2322.

Schawe, J.E.K., 1995. Principles for the interpretation of modulated temperature DSC measurements. Part 1. Glass transition. *Thermochimica Acta*, 261, pp.183–194.

Stroock, a. D. & Whitesides, G.M., 2002. Components for integrated poly (dimethylsiloxane) microfluidic systems. *Electrophoresis*, 23(20), pp.3461–3473.

Tan, Z.-C. et al., 2000. An adiabatic calorimeter for heat capacity measurements of small samples. *Thermochimica Acta*, 352-353, pp.247–253.

Temiz, Y. et al., 2015. Microelectronic Engineering Lab-on-a-chip devices : How to close and plug the lab ? , 132, pp.156–175.

Thomas, S., 2008. Enhanced oil recovery-an overv

Thorsen, T., Maerkl, S.J. & Quake, S.R., 2002. Microfluidic large-scale integration. *Science (New York, N.Y.)*, 298(5593), pp.580–584.

Unger, M. a et al., 2000. Monolithic microfabricated valves and pumps by multilayer soft lithography. *Science (New York, N.Y.)*, 288(5463), pp.113–116.

Vutha, A.K. et al., 2014. A microfluidic device for thermal particle detection. *Microfluidics and Nanofluidics*, 17(5), pp.871–878.

Wang, C. et al., 2011. Determining intracellular temperature at single-cell level by a novel thermocouple method. *Cell Research*, 21(10), pp.1517–1519.

Whitesides, G.M., 2013. Cool, or simple and cheap? Why not both? *Lab Chip*, 13(1), pp.11–13.

Whitesides, G.M., 2006. The origins and the future of microfluidics. *Nature*, 442(7101), pp.368–373.

Yinping, Z., Yi, J. & Yi, J., 1999. A simple method, the -history method, of determining the heat of fusion, specific heat and thermal conductivity of phase-change materials. *Measurement Science and Technology*, 10(3), pp.201–205.

Zhang, Y., Zuo, P. & Ye, B.-C., 2015. A low-cost and simple paper-based microfluidic device for simultaneous multiplex determination of different types of chemical contaminants in food. *Biosensors and Bioelectronics*, 68, pp.14–19.

Zhuravlev, E. & Schick, C., 2010. Fast scanning power compensated differential scanning nano-calorimeter: 1. The device. *Thermochimica Acta*, 505(1-2), pp.1–13.

Appendix A: Published Journal Papers

BIOMICROFLUIDICS 8, 034101 (2014)

A novel on-chip three-dimensional micromachined calorimeter with fully enclosed and suspended thin-film chamber for thermal characterization of liquid samples

Benyamin Davaji,[1] Hye Jeong Bak,[1] Woo-Jin Chang,[2] and Chung Hoon Lee[1,a)]
[1]*Nanoscale Devices Laboratory, Marquette University, Milwaukee, Wisconsin 53233, USA*
[2]*University of Wisconsin-Milwaukee, Milwaukee, Wisconsin 53211, USA*

(Received 20 March 2014; accepted 29 April 2014; published online 8 May 2014)

A microfabricated calorimeter (μ-calorimeter) with an enclosed reaction chamber is presented. The 3D micromachined reaction chamber is capable of analyzing liquid samples with volume of 200 nl. The thin film low-stress silicon nitride membrane is used to reduce thermal mass of the calorimeter and increase the sensitivity of system. The μ-calorimeter has been designed to perform DC and AC calorimetry, thermal wave analysis, and differential scanning calorimetry. The μ-calorimeter fabricated with an integrated heater and a temperature sensor on opposite sides of the reaction chamber allows to perform thermal diffusivity and specific heat measurements on liquid samples with same device. Measurement results for diffusivity and heat capacitance using time delay method and thermal wave analysis are presented. [http://dx.doi.org/10.1063/1.4875656]

I. INTRODUCTION

Microfabricated calorimeters (μ-calorimeter) have been developed for "Lab-on-a-chip", medical and biochemical applications. The μ-calorimeter serves to characterize biochemical samples and interactions with high sensitivities while only using micro or nano-liter scale sample volumes.[1] The μ-calorimetry has been used to investigate DNA folding-unfolding processes, molecular recognition, isothermal titration, characterization of the thermal properties of liquid samples (heat capacity, diffusivity, and conductivity),[2] and for many other lab-on-a-chip applications.[3] A μ-calorimeter consists of three parts: A reaction chamber, a heater, and a temperature sensor. Based on the configuration of the reaction chamber, μ-calorimeters are classified into two categories: A closed reaction chamber configuration with a fully enclosed reaction/detection chamber[4] and an open reaction chamber configuration, in which the sample is placed on a membrane and partially exposed to the environment.[5] The open reaction chamber configuration, in contrast with the fact that it has an incomplex fabrication to achieve an excellent thermal resistance, suffers from the evaporation of volatile liquid samples and sample handling issues (manual spotting).[6] On the other hand, the closed reaction chamber configuration is more complex and typically suffers from a large thermal mass (heat capacity) owing to the use of bulky encapsulating materials such as Polydimethylsiloxane (PDMS) or glass covers,[7] resulting in reduced sensitivity in temperature measurement.

A typical μ-calorimeter uses an electrical heater to apply heat to a sample and a temperature sensor to measure resulting temperature changes. To accurately determine the thermal energy exchange of the reaction or interaction, the contact of the heater and the temperature sensor to the sample has to be thermally efficient. Integration of these thermal components using micromachined methods has advantages as they ensure intimate thermal contacts by design. However, conventional lithography-based methods are limited for use in substantially

a)Electronic mail: chunghoon.lee@marquette.edu

planar surfaces and are particularly difficult to use over 3-dimensional structures or cut-out surfaces.[8] Mostly, the heater and/or the temperature sensor are integrated on the same membrane-based planar surface,[9] or the heater and the sensor are fabricated on separate substrates with an off-chip bonding process to form the calorimeter chamber.[10] To simplify the integration of the heater and the temperature sensor, the 3ω (or AC mode) method uses a single metal strip as the heater and the temperature sensor. The 3ω has been extensively used for thermal conductivity measurements, which still requires a bulky material to encapsulate the reaction chamber and it yields to increase the thermal mass of the system and decreases the detection sensitivity.

In this paper, we present a μ-calorimeter with suspended three-dimensional (3D) closed reaction chambers with a heater and a temperature sensor integrated on the opposite sides of each reaction chamber. Figure 1 shows a fabricated calorimeter with two chambers for differential calorimetric measurements. The details of each reaction chamber are shown in the zoomed-in schematic in Figure 1. Each reaction chamber is suspended and fully enclosed by a low-stress silicon nitride (Si_xN_y) membrane and a polyimide thin film forming the opposite sides of the chamber. The thin film encapsulating structures, in contrast to other bulky closed chamber configuration μ-calorimeters, which are of the order of millimeters in thickness.[7,11,12] As a result, the thermal mass of the fabricated reaction chamber is about 3 orders of magnitude smaller compared to the conventional bulky chambers, directly resulting in a corresponding increase in temperature detection sensitivity. In this device, the heater and the temperature sensor are integrated on different sides of the reaction chamber such that the sample can be placed between the heater and the sensor. Configuration of heater and sensor on fabricated device creates the capability of performing different calorimetric measurements such as differential scanning calorimetry (DSC),[9] thermal wave analysis (TWA),[13,14] 3-ω technique,[15] and titration[16] without any change in measurement setup. In addition, the heat flux directly travels through the sample inside the chamber and with minimal fringing effects of heat flux. This enables

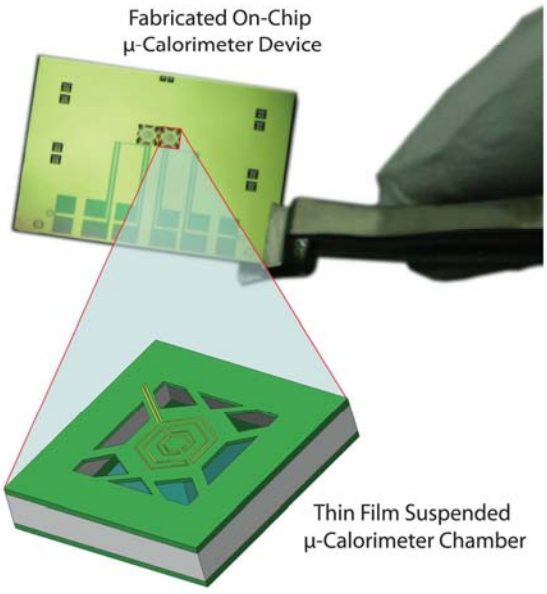

FIG. 1. A 3D micromachined on-chip calorimeter with suspended reaction chambers is shown. Each calorimeter has two identical chambers for differential measurements, and each chamber has two microfluidic inlets and one outlet.

excellent fit with a 1-D heat model used to extract thermal properties of the samples, as the boundary conditions used to drive the relations for thermal properties.[17] In contrast, calorimeters that have a heater and a temperature sensor on the same side have non-negligible fringe effects and have to employ 3D models specific to device configuration to accurately extract thermal properties. These also result in lower detection sensitivity since heat fluxes diffuse radially. The measurement results for thermal properties (thermal diffusivity and specific heat) of liquid samples using fabricated μ-calorimeter are demonstrated.

II. MATERIALS AND METHODS

A. Reaction chamber design

A wide range of materials and designs have been used for the fabrication of on-chip μ-calorimeter chambers. The μ-calorimeters with closed reaction chambers are made for the characterization of liquid samples of volumes ranging from a few microliters to few nanoliters, where evaporation of any of the sample is resulting in considerable measurement errors.[7] Previously reported methods for fabricating closed reaction chambers for μ-calorimeters have used soft lithography techniques, isotropic etching of micro cavities,[12] off-chip wafer bonding processes[10] or made using polymer thin films.[7] Effective use of calorimetric techniques requires quasi adiabatic conditions in the μ-calorimeter, which requires good thermal isolation of the reaction chamber from the ambient and substrate. Another desirable aspect of a μ-calorimeter is the negligible thermal mass of the reaction chamber compared to that of the sample to enable calibration-free characterization.[18]

Aiming to reduce the thermal mass, the reaction chambers in this work have been designed and fabricated using a Si_xN_y thin film and a thin polyimide film. The reaction chamber is also fully suspended from silicon handle to minimize the thermal loss to the substrate by thermal conduction. The reaction chamber has been 3D-micromachined using an anisotropic wet chemical etching process. The reported fabrication method eliminates the off-chip wafer bonding processes and keeps the device fabrication robust and simple, while achieves the low thermal mass and high thermal insulation result in high sensitivity of detection.

B. Device fabrication

Micromachining of 3D structures using conventional photolithographic methods and the integration of thermal components (heater and sensor) on thin film suspended structures are yet challenges. In this work, we used a self-shadow masking process to form the reaction chamber using a combination of isotropic and anisotropic wet etching techniques of silicon. The main objectives for the process design are direct integration of the thermal components to the reaction chambers and wafer scale fabrication of 3D thin film chambers. Our μ-calorimeter device was fabricated on a 300 μm thick silicon (100) wafer with thermally grown silicon dioxide layers and low-stress Si_xN_y thin films deposited by low-pressure chemical vapor deposition (LPCVD) at both sides of wafer. The process flow for device fabrication is outlined in Figure 2, shows the various fabrication processes in three major steps, which are described in Subsections II B 1–II B 3 in details.

1. Design and fabrication of the thermal components

In thermal microfluidics systems, different heat sources such as preheated liquids,[19,20] Joule heating,[21–25] microwave heating,[26–28] and chemical reactions[29] have been used. Resistive heating (Joule heating) is selected as a heat source in this work to achieve homogeneous heating with a wide operational temperature range, better heat control compared to other methods[30] and for ease of integration onto thin film substrates.[31]

An integrated resistive temperature detector (RTD) is used for the temperature sensor in this work. The RTD temperature sensor has a number of advantages such as stability,[32,33] high accuracy,[32] linearity,[32] reproducibility,[34] and ease of fabrication. The RTD works on the

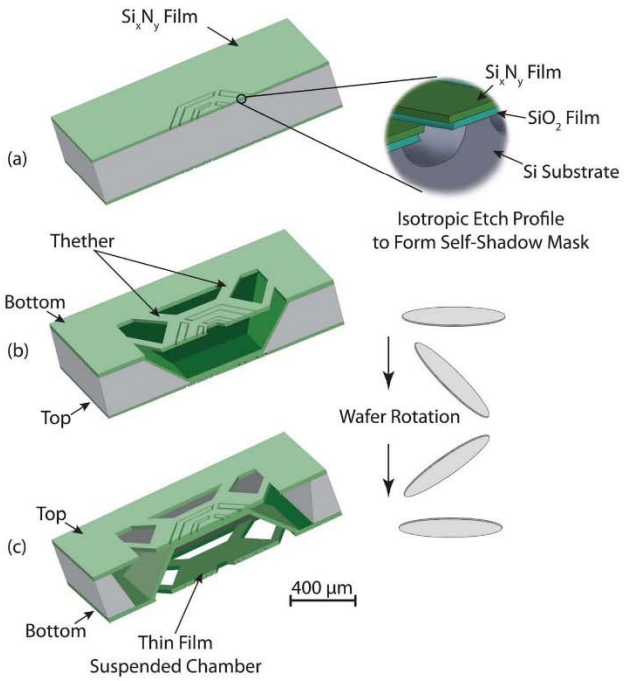

FIG. 2. The process flow for 3D microfabrication of the calorimeter device. (a) Electrode patterns are printed symmetrically on both sides of the wafer and isotropically etched to form self-shadow masks, (b) a first anisotropic wet chemical (KOH) etching on the bottom surface of the wafer defines the reaction chambers, and (c) second KOH etch to define suspended tethers of Si_xN_y on the top surface.

principle that the resistance of the RTD changes in relation to the RTD temperature. Platinum, nickel, copper, and nickel-iron are common materials used in the RTD sensors. Platinum has a linear resistance-to-temperature response over a wide range of temperature (−50 to 250 °C) and long term stability. The linear regime of nickel is less (0–150 °C)[35] but adequate for most biochemical reactions. In this work, the nickel thin film is deposited using an evaporation process. Nickel has a higher temperature coefficient of resistance (TCR) and low evaporation temperature is required to deposit using an evaporation process compared to platinum.

The heater is designed with a serpentine structure to achieve a uniform planar heat source to satisfy the constant heat flux boundary conditions, which are used to drive the heat transfer equation through the liquid sample in the chamber.[17] The RTD sensor is also designed symmetrically and aligned with the heater to detect the heat at the other side of the chamber. The process to form the heater and RTD patterns in both sides of the wafer is shown as the first step in the fabrication process flow in Figure 2(a). We developed a novel metal patterning process to place the thermal components on the reaction chamber to resolve the difficulties of lithographic patterning over 3D structures of the microfabricated Si_xN_y chamber. We first print serpentine grooves symmetrically on both sides of the wafer using a double-sided mask aligner. After patterning serpentine structures, the silicon nitride and silicon dioxide layers are etched by reactive ion etching (RIE) (Figure 3(a)) and buffered oxide etching (BOE 6:1) (Figure 3(b), respectively. The exposed silicon is undercut using an isotropic wet silicon etch process (Poly Etch 95%, KMG Chemicals) to form the Si_xN_y overhangs. The cross-sectional view of the isotropic silicon etch is shown in Figure 3(c). The Si_xN_y overhang is used as an integrated self-shadow mask in

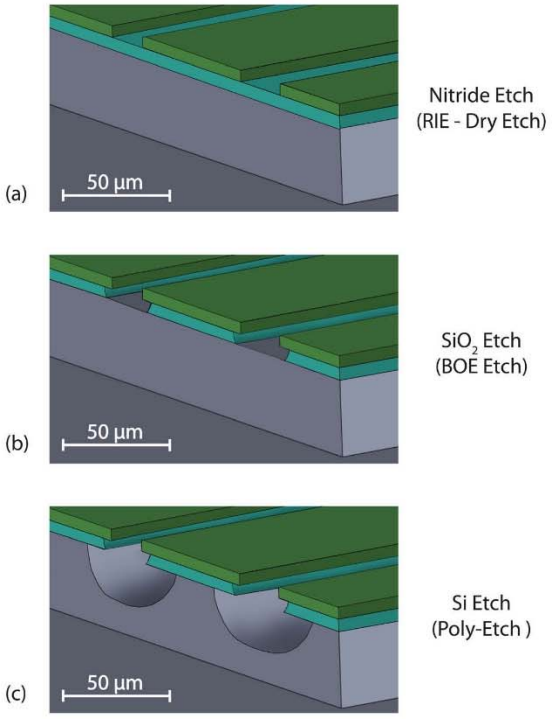

FIG. 3. The process flow for the integration of the heater and the temperature sensor on the thin film chamber. (a) The Si_xN_y film is etched by reactive ion etching, (b) the silicon dioxide is etched with BOE isotropic wet etching, and (c) the poly etch is used to isotropically undercut the silicon.

a blanket metal evaporation process (last step) to isolate thermal components from the substrate.

2. Chamber and microfluidic channels fabrication

After the isotropic silicon etch on the both sides of the silicon wafer, a 0.5 μm thick low-stress LPCVD Si_xN_y film is deposited to protect the exposed silicon. The reaction chamber and microfluidic channels are patterned on the bottom surface (heater side) of the wafer as shown in Figure 2(b). An anisotropic silicon wet etch (potassium hydroxide, KOH, 30% w/w) is used to etch the silicon. After the first KOH etch process. Subsequently, another LPCVD process is used to deposit 0.5 μm thick low-stress Si_xN_y. The deposited Si_xN_y film at this step is used to form side walls of the reaction chambers. To suspend and thermally isolate the reaction chambers from the silicon substrate, the top surface (sensor side) of the wafer is patterned and etched with another anisotropic KOH silicon wet chemical etching process as is shown in Figure 2(c).

The resulting suspended thin film chamber configuration allows maximum thermal insulation from the surrounding environment. The thin film Si_xN_y walls reduce the thermal mass of the chamber and increases the sensitivity of the sensor. The entire micromachining process is fabricated monolithically from a silicon substrate avoiding any wafer bonding processes. The μ-calorimeter chip is designed with two identical chambers next to each other to be able to perform differential scanning calorimetry. Each chamber has two microfluidic inlets and one outlet, which will be used in future work to study heat exchanges in mixing and reactions.

3. Metallization and polyimide bonding

At the final step of the microfabrication process, the thermal components are integrated on the device by a blanket deposition of nickel on both sides of the wafer. A 30–70 nm thick film of nickel is thermally evaporated on each sides of the wafer to achieve the designed heater/RTD resistance of 1-4 kΩ. Figure 4 shows the fabricated chamber before and after metal deposition. After metallization for the thermal components, a 25 μm polyimide film is used to seal the bottom of the wafer using a silicone adhesive (70 μm total), forming a fully enclosed reaction chamber, as shown in Figure 4. The total volume of the reaction chamber to contain a liquid sample is designed to be 200 nl.

C. Device characterization

1. RTD sensor characterization

The electrical resistance value of a 30–70 nm thick nickel film on the wafer is 1–4 kΩ, respectively. The resistance change of a RTD is a function of temperature given by the simplified Callendar–Van Dusen equation[36]

$$R = R_{rm}(1 + \alpha_r \Delta T), \tag{1}$$

where the R_{rm} is the RTD resistance at room temperature, α_r is the TCR of the nickel RTD, and ΔT is temperature change.

The TCR for the nickel RTD is measured using a HAAKE thermal bath by sweeping the bath temperature range from 10 to 50 °C. The measured resistance of the nickel film as a function of temperature shows excellent linearity ($R^2 = 0.9999$) within the calibration range. From the slope of the measured values, the measured α_r of the sensor is 2.58×10^{-3}/°C. The α_r for bulk nickel has been reported to be 6×10^{-3}/°C.[37] The α_r is a function of the film thickness to the mean free path of electrons in the film[38] and the scattering at the film surface and the grain

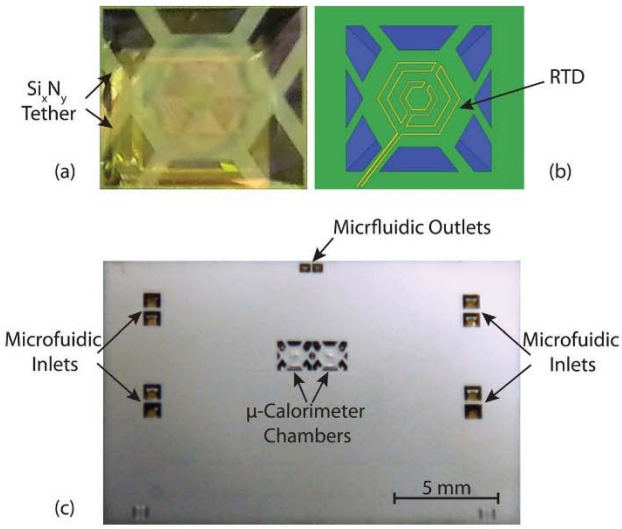

FIG. 4. The fabricated chamber and the final device after metallization are illustrated. (a) shows the optical image of the fabricated chamber after anisotropic wet chemical etching, (b) shows the top view of the fabricated chamber, and (c) shows the final calorimeter chip after metallization.

boundaries of deposited metal.[39] The α_r is changing based on different deposition parameters and film thinness.

Increasing the thickness and thermal annealing of the nickel film may increase the α_r.

Using a commercial RTD sensor (Pt-100) at the same time as the calibration test, the accuracy of the RTD over the measured temperature range was calculated to be 2.36%. The resolution of temperature measurement with RTD is limited by the Johnson–Nyquist thermal noise.[40,41] From calculated thermal noise, 8.17×10^{-6} °C resolution for the temperature measurement with bandwidth of 28.5 Hz for fabricated device is expected. However, the measurement noise of the preamplifier and source meter far exceeds this noise floor and results in a measurement temperature resolution of 2×10^{-3} °C. An 1 mA DC is used as excitation current of the sensor with a 4-wire measurement configuration to minimize the effects of contacts and connecting wires on temperature measurements.

2. μ-calorimeter DC characterization

A first-order lumped element model is used to model the μ-calorimeter and the loaded sample, as shown in Figure 5. A step function response is used to extract thermal parameters such as the thermal resistance, the thermal mass, and the equilibrium time constant of the system. A heat pulse is generated at the heater by applying a 1 mA current, and travels through the liquid sample. The temperature response (step response) as well as measured DC parameters of the calorimeter is shown in Figure 6. Two Keithley 2400 source/meters are used as a current source and a 4-wire resistance measurement unit for the heater and the sensor, respectively.

The step response of the temperature change can be expressed as

$$\Delta T = a[1 - e^{(-t/b)}], \tag{2}$$

where ΔT is the temperature change, a and b are fitting parameters obtained from the measured data, and t is time.

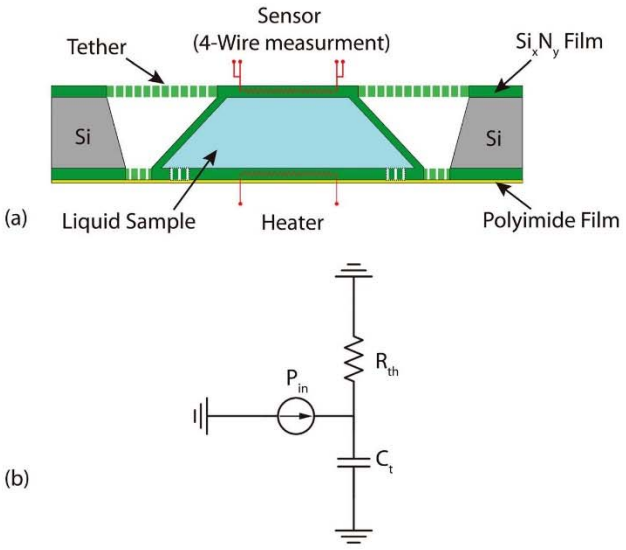

FIG. 5. (a) Shows the calorimeter reaction chamber cross sectional view and (b) shows the lumped parameter circuit model where the P_{in} is the input power, the R_{th} is the total thermal resistance of the fabricated calorimeter, and the C_t is the thermal mass of the system.

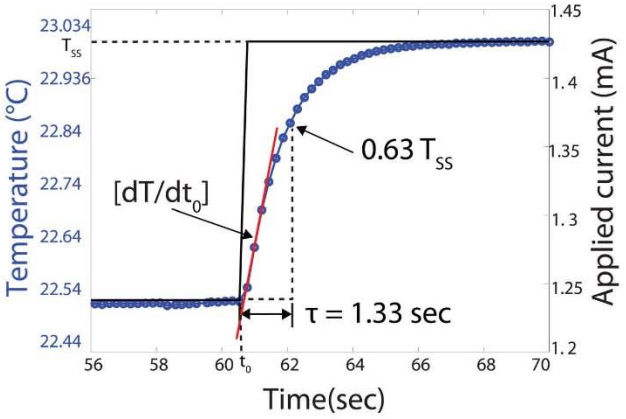

FIG. 6. Shows the DC step response of the μ-calorimeter and the calculation of the DC parameters of the calorimeter from the output data. T_{ss} is the steady state temperature response, to the input DC step, measured at the sensor. The $R_{th} = 58.87$ K/W is calculated from ΔT_{ss} over input power, thermal time constant ($\tau = 1.33$ s) based on the Eq. (2) is the time it takes the temperature rises to 0.63 T_{ss} and the thermal mass ($C_p = 6.63 \times 10^{-3}$ J/K) is the input power times the inverse of the slope at $t = 0$.

From the step response, the thermal resistance, thermal mass, and the time constant of our μ-calorimeter are 58.87 K/W, 6.63×10^{-3} J/K, and 1.33 s, respectively. These DC parameters are used for the DC thermal characterization of samples such as water, glycerol, and ionic liquids.

III. EXPERIMENTAL RESULTS AND DISCUSSIONS

Our μ-calorimeter is designed to integrate different calorimetry methods capabilities in a single device using 3D micromachining of a suspended chamber on a silicon wafer. The fabricated calorimeter is designed to perform DC calorimetry, AC calorimetry (transient), and TWA. The fabricated μ-calorimeter has two identical chambers with separate microfluidic channels, one as the calorimeter chamber and other as the reference chamber, which makes it possible to perform differential calorimetry (e.g., DSC) as well. The methods and the experimental setup to measure different thermal properties of liquid samples are described in this section using different calorimetric methods. The thermal properties of Deionized (DI)-water, glycerol, ionic liquid samples are measured and compared with literature values. The measurements are all performed in stationary condition to avoid any external flow and its impact on the measurement.

A. Thermal diffusivity measurement

The 3ω method using the phase change measurement for liquid samples has been commonly used for the thermal diffusivity measurement.[42] However, this method requires calibration of the device with various samples of known thermal diffusivity to fit the two unknown parameters. In this paper, the non-steady-state (transient) method is used to measure the thermal diffusivity of liquid samples. The laser flash method developed by Parker *et al.*[43] is a commonly used non-steady-state method. Although this method has been used to measure the diffusivity of both solid and liquid samples, the experiment requires no heat loss to surroundings (adiabatic condition). Other researchers have further developed the method for non-adiabatic conditions due to radiation[44,45] and a heat pulse width effects on the measurements.[46] In our case, the heat loss mechanism is more complex than the laser flash method. To avoid the complex analysis for the thermal diffusivity measurement, we adapted the heat penetration time measurement method.[17] The principle of the heat penetration time measurement is to apply a

constant continuous heat flux to the one side of the sample, and to measure the time delay to reach the other side, where the sensor is located. The time delay can be expressed as[17]

$$t_0 = \left[\frac{L^2}{(\frac{16}{\pi})\alpha}\right], \tag{3}$$

where L is the length of the sample in the direction of the heat flux and α is the thermal diffusivity.

The time delay for the heat to travel across the reaction chamber in this work is typically a few hundred milliseconds. Since the time constant for our μ-calorimeter is 1.33 s, the measurement satisfies the requirement of quasi-adiabatic condition.

In the time delay thermal diffusivity measurement method, the μ-calorimeter and microfluidic pumps are placed in an enclosure to reduce the ambient effects. The DC source (Keithley source/meter) is used to apply a current pulse to the heater. At the sensor side, the other DC source (a second Keithley source/meter) is used to apply constant excitation current to the RTD sensor and measure the temperature change by monitoring the resistance change. To amplify the signal and increase the detection limit and resolution, a low noise current preamplifier (Stanford SR570) was used to amplify the current signal and convert it to a voltage signal. The output signal is monitored and recorded by a LabView program controlling an oscilloscope (Agilent DSOX2024A). The program ensures the synchronization between the input pulse to the heater and data acquisition at the sensor side. Figure 7 shows the measurement setup for the time delay method.

The typical time delay measurement is shown in Figure 8(a). To determine the time the temperature changes arrives at the sensor, the maximum of the second derivative of the temperature profile is used as shown in Figure 8(b). Although the thickness of the sample is approximately the thickness of the wafer, which is $300 \pm 5\,\mu$m, we used DI-water with a known diffusivity[47] at 25 °C to calibrate the thickness of our device. The time delay, t_0, can be expressed as

$$t_0 = \left[\frac{(L \times p)^2}{(\frac{16}{\pi})\alpha}\right], \tag{4}$$

where p is a correction parameter for the chamber thickness.

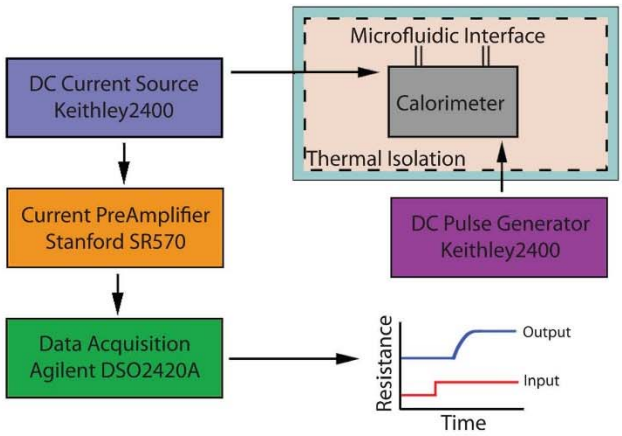

FIG. 7. The experimental setup for the time delay method to measure the thermal diffusivity of liquid samples with the on-chip μ-fabricated calorimeter.

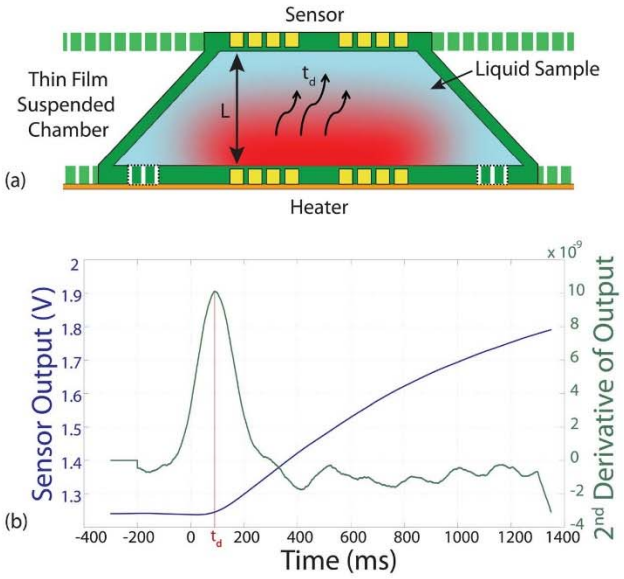

FIG. 8. The results of the time delay method to measure thermal diffusivity are presented. (a) The cross-sectional view illustrating the heat flux from the heater to the sensor across the liquid sample and (b) time-signal of temperature recorded at the temperature sensor and its second derivative to calculate exact time of arrival of the heat pulses at the sensor.

With the DI-water sample, p is found to be 0.89, which means the effective distance between the heater and sensor is 270 μm. Using this correction factor, the thermal diffusivity of glycerol is measured (9.94×10^{-8} m^2/s). The measured values of thermal diffusivity show good agreement (<8% error) with values reported in literature.[48]

B. Specific heat measurement

TWA was first introduced by Garden *et al.*[1] to measure the specific heat of a material. When an AC voltage with an angular frequency ω is applied to a heater, the power from the Joule heating results in 2ω frequency, which can be expressed as

$$P_{in} = \frac{A^2 R}{2}[1 + \cos(2\omega t)], \tag{5}$$

where A is the amplitude of the current, R is the resistance of the heater, and ω is angular frequency of the applied AC voltage to the heater.

When the alternating power is applied to the heater, the temperature of the sample is raised and this changes the resistance of the heater, which generates the 3ω component of temperature at the heater. This 3ω component is measured in the typical single-strip heater and the sensor configuration. In this work, the 2ω component of the heat is measured at the sensor for measuring the heat capacitance of the sample. The measurement setup for performing TWA using the fabricated μ-calorimeter is shown in Figure 9.

An AC source voltage 3 V_{pp} with frequency from 0.01 Hz to 0.1 Hz is applied to the heater using a function generator (HP 3324A) with a frequency increment of 0.005 Hz between each measurement. To measure the temperature change at the sensor, a DC source (0.1 mA sources current) is used with a source/meter (Keithley 2400 source/meter). The output voltage from the

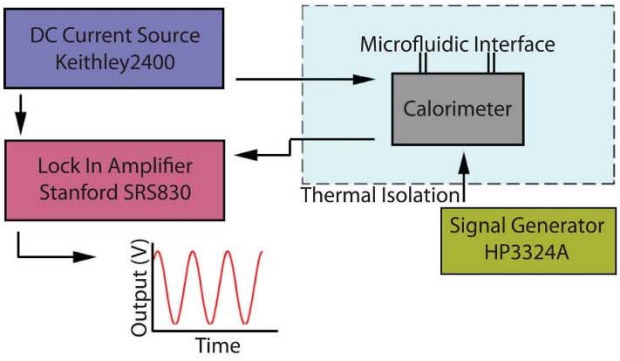

FIG. 9. The experimental setup for thermal wave analysis to measure the specific heat of liquid samples with the μ-calorimeter.

sensor is measured using a lock-in amplifier (Stanford Research Systems SRS830). A LabView program was used for data acquisition and to synchronize all sources and measurement units.

Two conditions have to be satisfied for TWA. First, the temperature within the sample has to be homogenous and second, the system has to maintain the quasi-adiabatic condition.[1] The quasi-adiabatic condition is satisfied if

$$\tau_{int} \ll \frac{1}{\omega} \ll \tau, \tag{6}$$

where τ_{int} is diffusion time of the heat into the sample, ω is excitation frequency in the heater, and τ is the thermal relaxation time of the sample to the environment.

The specific heat of a sample is determined from the frequency at which the normalized value, $\omega \cdot T_{ac}$, is maximum to satisfy the required condition (Eq. (6)), where T_{ac} is the amplitude of temperature oscillation.[1] Figure 10 shows the normalized T_{ac} graph for different measured samples. A 1% error line is used to detect the thermal bandwidth of the system and determine the working frequency of the TWA method for each sample.

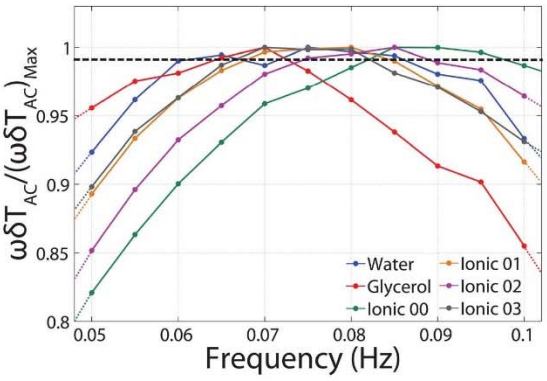

FIG. 10. The normalized values of the measured T_{ac} for different samples are illustrated. The dotted line represents the 1% error line and the selected frequency within this range that satisfies the TWA condition.

The specific heat, c_p can be expressed with measured AC temperature at the sensor

$$c_p = \frac{C_0 P_{in}}{2\,\omega\, m\, \partial T_{AC}}, \tag{7}$$

where the C_0 is the input power calibration factor, P_{in} is the input power, ω is the frequency of input thermal wave, m is the mass of the sample, and ∂T_{AC} is the amplitude of oscillating temperature. The input power calibration factor is used to reduce the measurement error by calibration of effective input power to the chamber excluding the heat loss. DI-water sample is used to calculate the calibration factor for input power.

The specific heat of DI-water is measured (3.93 J/g K) by the described method and the measured value is in good agreement(~5% error) with reported value.[49] The heat capacity for different Ionic liquids is measured for the first time. For the Ionic liquids, 1-ethyl-3-methylimidazolium bis(trifluoromethylsulfonyl)imide ([EMIM][Tf2N]), 1-buthyl-3-methylimidazolium hexafluorophosphate ([BMIM][PF6]), 1-hexyl-3-methylimidazolium hexafluorophosphate ([HMIM][PF6]), and 1-methyl-3-octylimidazolium hexafluorophosphate ([OMIM][PF6]), the measured specific heats are 2.75, 2.83, 0.86, 2.55 J/g K, respectively. The specific heat measurement results, using the TWA method is presented to demonstrate the feasibility of performing specific heat measurement with the fabricated μ-calorimeter for different liquid samples. The measured errors in the thermal parameters are always less than 10%, and it might be caused by two reasons: The high surface area of the chamber, which cases heat loss to the environment and the small volume (200 nl) of samples where in all of measured parameters the bulk samples with large volume is being used.

IV. CONCLUSION

We demonstrate a novel on-chip μ-calorimeter fabricated using wafer-scale 3D micromachining processes to measure the thermal properties of liquid samples. Our fabrication method of μ-calorimeter allows the integration of heaters and temperature sensors on the 3-dimensional chambers for the efficient coupling and detection of heat from the thermal elements for accurate characterization. The reaction chambers of the μ-calorimeter are fully enclosed using thin film materials to reduce the thermal mass of the system and are suspended by narrow tethers to increase the thermal resistance without any bonding process. The incorporation of the heater and the sensor on opposite sides of the reaction chamber allows for the measurement of both the thermal diffusivity and specific heat without changing or re-configuring the measurement setup. Two methods, the time delay and thermal wave analysis, are used to determine the thermal diffusivity and capacitance showing repeatable measured performance and good agreement (within 8%) with previously reported results. The μ-calorimeter can characterize liquid samples using only a small volume of sample (200 nl) and can be used to perform various measurements with the same sample and the same setup.

ACKNOWLEDGMENTS

Partial financial support for this work was provided by the U.S. National Science Foundation through the Industry/University Cooperative Research Center on Water Equipment & Policy located at the University of Wisconsin-Milwaukee (IIP-0968887) and Marquette University (IIP-0968844).

[1]J.-L. Garden, E. Chteau, and J. Chaussy, Appl. Phys. Lett. **84**, 3597 (2004).
[2]I. Jelesarov and H. R. Bosshard, J. Mol. Recognit. **12**, 3 (1999).
[3]J. Khler and T. Henkel, Appl. Microbiol. Biotechnol. **69**, 113 (2005).
[4]Y. Zhang and S. Tadigadapa, Appl. Phys. Lett. **86**, 034101 (2005).
[5]J. Xu, R. Reiserer, J. Tellinghuisen, J. P. Wikswo, and F. J. Baudenbacher, Anal. Chem. **80**, 2728 (2008).
[6]J. L. Wonhee Lee and J. Koh, Nanobiosens. Dis. Diagn. **2012**(1), 17.
[7]W. Lee, W. Fon, B. W. Axelrod, and M. L. Roukes, Proc. Natl. Acad. Sci. U. S. A. **106**, 15225 (2009).
[8]K. Ariga, J. P. Hill, M. V. Lee, A. Vinu, R. Charvet, and S. Acharya, Sci. Technol. Adv. Mater. **9**, 014109 (2008).
[9]E. Zhuravlev and C. Schick, Thermochim. Acta **505**, 1 (2010).

[10]E. Iervolino, A. van Herwaarden, and P. Sarro, Thermochim. Acta **492**, 95 (2009).
[11]J. Lerchner, A. Wolf, G. Wolf, V. Baier, E. Kessler, M. Nietzsch, and M. Krgel, Thermochim. Acta **445**, 144 (2006).
[12]Y. Zhang and S. Tadigadapa, Biosens. Bioelectron. **19**, 1733 (2004).
[13]T. Hashimoto, J. Morikawa, T. Kurihara, and T. Tsuji, Thermochim. Acta **304–305**, 151 (1997).
[14]J. Morikawa, C. Leong, T. Hashimoto, T. Ogawa, Y. Urata, S. Wada, M. Higuchi, and J.-I. Takahashi, J. Appl. Phys. **103**, 063522 (2008).
[15]D. G. Cahill, Rev. Sci. Instrum. **61**, 802 (1990).
[16]H. Huth, A. A. Minakov, and C. Schick, J. Polym. Sci., Part B: Polym. Phys. **44**, 2996 (2006).
[17]V. S. Arpaci, *Conduction Heat Transfer* (Addison-Wesley Pub. Co., 1966).
[18]W. Winter and G. W. Hhne, Thermochim. Acta **403**, 43 (2003).
[19]G. Maltezos, A. Gomez, J. Zhong, F. A. Gomez, and A. Scherer, Appl. Phys. Lett. **93**, 243901 (2008).
[20]G. Velve Casquillas, C. Fu, M. Le Berre, J. Cramer, S. Meance, A. Plecis, D. Baigl, J.-J. Greffet, Y. Chen, M. Piel, and P. T. Tran, Lab Chip **11**, 484 (2011).
[21]T.-M. Hsieh, C.-H. Luo, F.-C. Huang, J.-H. Wang, L.-J. Chien, and G.-B. Lee, Sens. Actuators, B **130**, 848 (2008).
[22]J.-H. Wang, L.-J. Chien, T.-M. Hsieh, C.-H. Luo, W.-P. Chou, P.-H. Chen, P.-J. Chen, D.-S. Lee, and G.-B. Lee, Sens. Actuators, B **141**, 329 (2009).
[23]B. Selva, J. Marchalot, and M.-C. Jullien, J. Micromech. Microeng. **19**, 065002 (2009).
[24]A. J. de Mello, M. Habgood, N. L. Lancaster, T. Welton, and R. C. R. Wootton, Lab Chip **4**, 417 (2004).
[25]J. Wu, W. Cao, W. Wen, D. C. Chang, and P. Sheng, Biomicrofluidics **3**, 012005 (2009).
[26]J. J. Shah, J. Geist, and M. Gaitan, J. Micromech. Microeng. **20**, 105025 (2010).
[27]A. Kempitiya, D. A. Borca-Tasciuc, H. S. Mohamed, and M. M. Hella, Appl. Phys. Lett. **94**, 064106 (2009).
[28]K. J. Shaw, P. T. Docker, J. V. Yelland, C. E. Dyer, J. Greenman, G. M. Greenway, and S. J. Haswell, Lab Chip **10**, 1725 (2010).
[29]R. M. Guijt, A. Dodge, G. W. K. van Dedem, N. F. de Rooij, and E. Verpoorte, Lab Chip **3**, 1 (2003).
[30]V. Miralles, A. Huerre, F. Malloggi, and M.-C. Jullien, Diagnostics **3**, 33 (2013).
[31]C.-Y. Lee and G.-B. Lee, J. Micromech. Microeng. **13**, 620 (2003).
[32]A. Tong, Sens. Rev. **21**, 193 (2001).
[33]P. R. N. Childs, J. R. Greenwood, and C. A. Long, Rev. Sci. Instrum. **71**, 2959 (2000).
[34]A. Dziedzic, L. J. Golonka, J. Kozlowski, B. W. Licznerski, and K. Nitsch, Meas. Sci. Technol. **8**, 78 (1997).
[35]E. J. P. Santos and I. Vasconcelos, in *Proceedings of the 26th International Conference on Microelectronics* (2008), pp. 333–336.
[36]M. S. V. Dusen, J. Am. Chem. Soc. **47**, 326 (1925).
[37]F. Lacy, IEEE Sens. J. **11**, 1208 (2011).
[38]J. S. Jin, J. S. Lee, and O. Kwon, Appl. Phys. Lett. **92**, 171910 (2008).
[39]Q. Zhang, X. Zhang, B. Cao, M. Fujii, K. Takahashi, and T. Ikuta, Appl. Phys. Lett. **89**, 114102 (2006).
[40]L. B. Kish, Phys. Lett. A **305**, 144 (2002).
[41]D. R. White, R. Galleano, A. Actis, H. Brixy, M. D. Groot, J. Dubbeldam, A. L. Reesink, F. Edler, H. Sakurai, R. L. Shepard, and J. C. Gallop, Metrologia **33**, 325 (1996).
[42]T. Adrega and A. van Herwaarden, Sens. Actuators, A **167**, 354 (2011).
[43]W. J. Parker, R. J. Jenkins, C. P. Butler, and G. L. Abbott, J. Appl. Phys. **32**, 1679 (1961).
[44]A. R. Mendelsohn, Appl. Phys. Lett. **2**, 19 (1963).
[45]L. Chen and D. R. Clarke, Comput. Mater. Sci. **45**, 342 (2009).
[46]R. E. Taylor and J. A. Cape, Appl. Phys. Lett. **5**, 212 (1964).
[47]A. Matvienko and A. Mandelis, Int. J. Thermophys. **26**, 837 (2005).
[48]J. A. Balderas-Lopez, A. Mandelis, and J. A. Garcia, Rev. Sci. Instrum. **117**, 2933 (2000).
[49]G. Meng, A. J. Jaworski, and N. M. White, Chem. Eng. Process. **45**, 383 (2006).

Microfluid Nanofluid (2014) 17:871–878
DOI 10.1007/s10404-014-1369-z

RESEARCH PAPER

A microfluidic device for thermal particle detection

Ashwin Kumar Vutha · Benyamin Davaji · Chung Hoon Lee · Glenn M. Walker

Received: 27 August 2013 / Accepted: 17 February 2014 / Published online: 7 March 2014

Abstract We demonstrate the use of heat to count microscopic particles. A thermal particle detector (TPD) was fabricated by combining a 500-nm-thick silicon nitride membrane containing a thin-film resistive temperature detector with a silicone elastomer microchannel. Particles with diameters of 90 and 200 μm created relative temperature changes of 0.11 and −0.44 K, respectively, as they flowed by the sensor. A first-order lumped thermal model was developed to predict the temperature changes. Multiple particles were counted in series to demonstrate the utility of the TPD as a particle counter.

Keywords Microfluidics · Particle counting · Thermal

1 Introduction

Particle counters have been an active area of research in the microfluidics community for over a decade (Zhang et al. 2009). During this time, many particle counting strategies have been explored, but the vast majority use either electrical or optical methods for detection. Electrical, or coulter, particle counters are relatively inexpensive to fabricate and can be miniaturized, but they cannot provide detailed information about particle subpopulations and are sensitive to the working fluids that carry the particles. For example, a conventional coulter counter that measures only resistance cannot enumerate metallic particles suspended in an insulating fluid such as oil (Murali et al. 2009). Instead, changes in capacitance must be measured. In contrast, optical counters, based on the detection of fluorescently labeled tags or light scattering, can identify cell subpopulations and are exquisitely fast, but they require expensive optical components to function and are not easily miniaturized. In addition, fluorescent flow cytometers are fundamentally limited to measuring 6–10 colors, or parameters, because the optical spectra of dyes begin to overlap if more colors are used (Janes and Rommel 2011). There is a need for new particle counting approaches that are both low cost and that can identify subpopulations of particles in a heterogeneous mixture.

Of all the particle counting methods explored so far, heat remains uninvestigated. Microfabrication allows the creation of inexpensive yet sensitive thermometers that can detect minute changes in the thermal properties of a liquid within a microchannel. Since particles suspended in a fluid alter the thermal properties of that fluid, a sensitive thermometer becomes a de facto particle counter. In addition to counting, a microscale thermometer could measure the thermal properties of cells and other particles or droplets to identify and characterize them. For example, Yi et al. (2011) generated DI water droplets containing bovine serum albumin (BSA) and measured the thermal conductivity of the droplets within a microchannel. However, the

A. Vutha
Department of Mechanical, Aerospace, and Nuclear Engineering, Rensselaer Polytechnic Institute, 2112 Jonsson Engineering Center, Troy, NY 12180, USA

B. Davaji · C. H. Lee
Department of Electrical and Computer Engineering, Marquette University, 1515 W Wisconsin Ave., Milwaukee, WI 53233, USA
e-mail: chunghoon.lee@marquette.edu

G. M. Walker (✉)
Joint Department of Biomedical Engineering, UNC Chapel Hill and NC State University, 911 Oval Drive, Raleigh, NC 27695, USA
e-mail: gmwalker@ncsu.edu

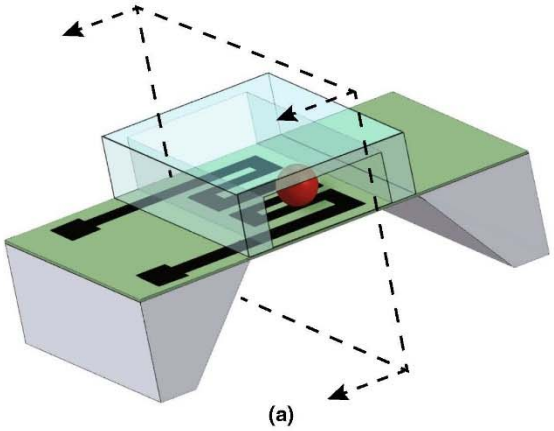

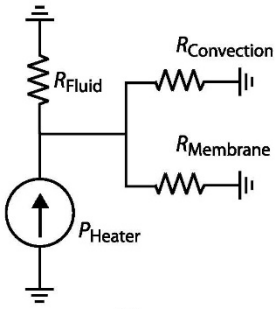

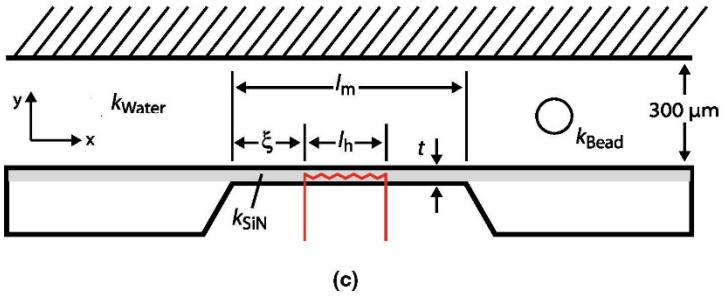

Fig. 1 **a** Three-dimensional rendering of the device showing a bead passing over the sensor. **b** Heat enters the system through Joule heating of the RTD and leaves through convection and conduction through the membrane and fluid. **c** Cross-section of the device showing relevant dimensions: $l_m = 300$ μm, $l_h = 200$ μm, $\xi = 50$ μm, $t = 0.5$ μm

focus of their work was on characterizing the contents of liquid droplets which occupied the entire width of the channel, and not on counting particles.

In this paper, we demonstrate a thermal particle detector (TPD) that can count and quantify solid particles suspended in a liquid using only heat. A lumped thermal model explains the observed results and predicts the effect of particle size and thermal conductivity on the detected temperature change. To demonstrate proof-of-concept, we used a microfabricated resistance temperature detector (RTD) within a microchannel to detect polystyrene microspheres.

2 Theory

The heat flux through a material is described by Fourier's law of heat conduction: $q = -k\partial T/\partial y$, where q is heat flux $(\mathrm{W/m^2})$, k is the thermal conductivity of the material $(\mathrm{W/m\,K})$, and $\partial T/\partial y$ is the temperature gradient (K/m) along the y direction. For a heater producing a constant heat flux, an increase in the thermal conductivity of the material will decrease ΔT, and vice versa. Therefore, Fourier's law can be used to detect particles flowing in a microchannel if they have a different thermal conductivity than the fluid. Consider a constant heat flux from the floor of a microchannel. Even with fluid flow, the heat flux will eventually generate a steady-state temperature gradient within the microchannel. If a particle with a different thermal conductivity than the fluid passes over the heat source, as illustrated in Fig. 1a, the temperature gradient will either increase or decrease depending on the thermal conductivity of the particle. If the heater is also used as a thermometer, the heater temperature can be used to detect particles. This general principle forms the basis of the TPD.

The heat flow within the TPD can be modeled using a first-order electrical circuit analogy, as illustrated in Fig. 1b. In the circuit, the RTD generates a small amount of heat via Joule heating and is analogous to a current source, and the thermal resistances within the TPD are analogous to electrical resistances. The voltage at the node above the current source is analogous to the temperature of the heat source. Heat enters into the TPD through the RTD and exits through three routes: (1) conduction through the membrane, (2) conduction through the fluid directly above the RTD, and (3) convection within the microchannel (van der Wiel et al. 1993). Each of these routes has a thermal resistance associated with it. Using the system diagram in Fig. 1c, the thermal resistances can be calculated. The thermal resistance of the membrane is

$$R_{\mathrm{Membrane}} = \frac{\ln(r_{\mathrm{m}}/r_{\mathrm{h}})}{2\pi k_{\mathrm{SiN}} t} \tag{1}$$

where r_{m} is the membrane radius ($r_{\mathrm{m}} = \sqrt{l_{\mathrm{m}}^2/\pi}$), r_{h} is the heater radius ($r_{\mathrm{h}} = \sqrt{l_{\mathrm{h}}^2/\pi}$), k_{SiN} is the thermal conductivity of the silicon nitride (SiN) membrane (16 $\mathrm{W/m\,K}$), and t is the membrane thickness (Lee et al. 2008).

The thermal resistance of the hemispherical volume of fluid directly above the RTD can be calculated with

$$R_{\mathrm{Fluid}} = \frac{1/r_{\mathrm{i}} - 1/r_{\mathrm{o}}}{2\pi k_{\mathrm{Water}}} \tag{2}$$

where $r_{\mathrm{i}} = \sqrt{l_{\mathrm{h}}^2/2\pi}$ is the inner hemisphere radius, $r_{\mathrm{o}} = \sqrt{3l_{\mathrm{m}}^2/2\pi}$ is the radius of the outer hemisphere, and k_{Water} is the thermal conductivity of water (0.6 $\mathrm{W/m\,K}$) (Incropera and DeWitt 1996).

The thermal resistance due to convection from fluid moving within the microchannel must also be calculated. Determining the thermal resistance of convection first requires calculating a convection coefficient, h_x, that represents the local environment. The coefficient h_x depends on multiple factors and can be calculated by

$$h_x = \frac{0.453 k_{\mathrm{Water}} Re^{1/2} Pr^{1/3}}{x\left[1 - \left(\frac{\xi}{x}\right)^{3/4}\right]^{1/3}} \tag{3}$$

where Re is the Reynolds number, Pr is the Prandtl number, and ξ is the distance between the edge of the membrane and the heater (van der Wiel et al. 1993; Incropera and DeWitt 1996). The thermal resistance can then be found by integrating h_x over the membrane length using the formula

$$R_{\mathrm{Convection}} = \frac{1}{l_{\mathrm{h}} \int_{\xi}^{\xi + l_{\mathrm{h}}} h_x \mathrm{d}x} \tag{4}$$

To calculate the overall thermal resistance of the TPD, all three resistances are added in parallel:

$$R_{\mathrm{Total}} = \frac{1}{\frac{1}{R_{\mathrm{Fluid}}} + \frac{1}{R_{\mathrm{Membrane}}} + \frac{1}{R_{\mathrm{Convection}}}} \tag{5}$$

When a bead flows past the RTD, it changes R_{Fluid} and $R_{\mathrm{Convection}}$ because its thermal conductivity and specific heat are different from the fluid. The thermal conductivity of the bead, k_{Bead}, combines with the thermal conductivity of the water, k_{Water}, to form a composite thermal conductivity, k_{c}. We used effective medium theory (EMT) to model the change in average thermal conductivity caused by a bead suspended in a volume of fluid (Karayacoubian et al. 2005). The composite thermal conductivity, k_{c}, of the volume directly above the RTD can be calculated with

$$k_{\mathrm{c}} = k_{\mathrm{Water}} \frac{k_{\mathrm{Bead}}(1 + 2\phi_{\mathrm{Bead}}) - k_{\mathrm{Water}}(2\phi_{\mathrm{Bead}} - 2)}{k_{\mathrm{Water}}(2 + \phi_{\mathrm{Bead}}) + k_{\mathrm{Bead}}(1 - 2\phi_{\mathrm{Bead}})} \tag{6}$$

where k_{Water} is the thermal conductivity of water, k_{Bead} is the thermal conductivity of the bead, and ϕ_{Bead} is the volume fraction of the bead within the heated volume.

The composite specific heat of the fluid volume, $C_{\mathrm{p,c}}$, above the RTD can be calculated with

$$C_{\mathrm{p,c}} = C_{\mathrm{p,Water}}(1 - \phi_{\mathrm{Bead}}) + C_{\mathrm{p,Bead}}\phi_{\mathrm{Bead}} \tag{7}$$

where $C_{\mathrm{p,Water}} = 4.184\,\mathrm{J/g\,K}$ is the specific heat of water and $C_{\mathrm{p,Bead}}$ is the specific heat of the polystyrene bead. Neither supplier of the beads could provide thermal data so we assumed $k_{\mathrm{Bead}} = 0.168\,\mathrm{W/m\,K}$ and $C_{\mathrm{p,Bead}} = 1.9\,\mathrm{J/g\,K}$ for the model.

After k_{c} is calculated, it replaces the k_{Water} value in Eqs. 2 and 3. The composite specific heat $C_{\mathrm{p,c}}$ is used to recalculate the Pr number, which is used in Eq. 3. A new R_{Total} is calculated with these substituted values using

Eq. 5, which represents the new thermal resistance due to the bead.

The temperature change caused by the passing bead is calculated using an energy balance that equates the energy entering the system from Joule heating to the heat flow out of the system via conduction and convection. The equation for the energy balance is (Lee et al. 2008)

$$\frac{\Delta T}{R_{\text{Total}}} = I^2 Z(1 + \alpha \Delta T) \tag{8}$$

where ΔT is the change in temperature within the system, Z is the electrical RTD resistance at room temperature, I is the current supplied to the RTD by the multimeter, and α is the temperature coefficient of resistance. A ΔT value is calculated with and without a bead present, using the appropriate R_{Total} values as described previously. The difference between these two ΔT values gives the predicted temperature change as a bead passes.

The lumped model neglects thermal capacitance effects for simplicity. Thermal response times for the components of the TPD are on the order of 20 ms, so it is reasonable to assume that the system is at steady state. As discussed later, this assumption is valid except at high flow rates.

3 Materials and methods

3.1 Device fabrication

The experimental setup is illustrated in Fig. 2. Microchannels were made out of the elastomer polydimethylsiloxane (PDMS) using standard micromolding procedures (Duffy et al. 1998). Briefly, SU8-2100 photoresist was spin-coated on a silicon wafer to a height of 250–300 μm and then soft-baked. A high-resolution film mask was used to pattern microchannels in the SU8-2100. After a hard bake, the master was developed to reveal a positive relief of the microchannels. PDMS was mixed in a 10:1 elastomer-to-crosslinker ratio, degassed, and poured over the master and cured at 80 °C for 2.5 h. After curing the PDMS, it was carefully peeled from the waferand diced, and ports were cored using a blunt 17-gauge syringe needle on one end of the microchannel and a 3-mm-diameter cork borer on the other end. The larger hole was used as a reservoir for depositing samples. Tubing was inserted into the smaller hole and connected to a syringe pump which was used to withdraw the fluid. The PDMS was then placed on the silicon substrate containing the RTD to form a watertight reversible seal. Typical microchannel dimensions were 300 μm (W) × 300 μm (H) × 8 mm (L).

The RTD was fabricated using traditional silicon microfabrication procedures. A silicon wafer was coated with a low-stress SiN film using low-pressure chemical vapor deposition (LPCVD). The SiN was then patterned with AZ5214 and etched by a reactive ion etch (RIE). The exposed backside of the silicon was etched in a 30 % KOH bath at 60 °C. The KOH etch is an anisotropic and self-terminating etch and resulted in a well-defined 300 μm^2 SiN membrane that was 500 nm thick. A liftoff process was then used to pattern the Ni RTD and contact pads on the SiN membrane. The RTD and contact pads were patterned using AZ5214 image reversible photoresist followed by thermal evaporation of Ni metal film (30 nm thick) on the SiN membrane. The RTD was completed after liftoff of the metal in MicroChem 1,165 solvent. The resistance of the RTD was always about 1,500 Ω.

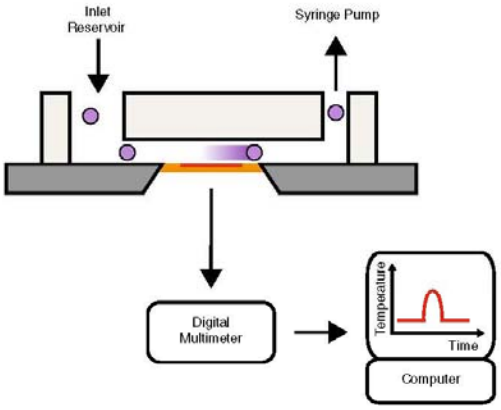

Fig. 2 Overview of the experimental setup. Beads that flow past the RTD cause small changes in temperature, which are recorded via a LabView program

3.2 Temperature measurement

The temperature of the Ni RTD was calculated using the equation

$$\Delta Z = Z_o(1 + \alpha \Delta T) \tag{9}$$

where ΔZ is the measured change in resistance, Z_o is the resistance at room temperature, α is the temperature coefficient of resistance for Ni, and ΔT is the change in temperature. A HAAKE thermal bath was used to calibrate the RTD and calculate α. To prevent self-heating of the RTD during calibration, a 0.1 mA current was applied to the RTD. Typical RTD linearity was excellent ($R^2 = 0.9999$). However, the temperature coefficient of resistance, α, was consistently about 3×10^{-3} K^{-1}, which is lower than values reported in the literature (6×10^{-3} K^{-1}) (Lacy 2011). Because α is a function of the ratio of film thickness to the mean free path of electrons in metals, the lower α value is likely due to the graininess of the evaporated thin

(30 nm) Ni film, which is comparable to the mean free path of electrons in typical metals (Jin et al. 2008; Leonard and Ramey 1966). Increasing the thickness of the Ni film should increase α.

Temperature measurements were made in the TPD by mounting it in a custom jig that contained pogo pins to make contact with the Ni pads on the Si substrate. The pogo pins were then connected to a Keithly 2400 SourceMeter, which measured the RTD resistance using a 4-point measurement. Resistance values were recorded to a computer via GPIB and a custom LabView program. The 1 mA sourcing current from the SourceMeter through the RTD resulted in 1.5 mW of Joule heating. The steady-state temperature within the TPD at room temperature showed excellent stability.

The predicted Johnson noise of the resistor was 20 μΩ for the measurement bandwidth, but the lower limit of detection was determined by the SourceMeter which had a resolution of 10 mΩ (2 mK). Experiments showed that the system was capable of reliably measuring changes in resistance as low as 8 mΩ (1.8 mK) on a RTD with a nominal resistance of 1,500 Ω.

3.3 Sample preparation

Polystyrene beads 90 μm (Polysciences) and 200 μm (Corpuscular) in diameter were used to validate the TPD device. Since polystyrene has a density slightly higher than water ($\approx$1.04 g/cm^3), we suspended beads in a mixture of DI water and glycerol to match the bead density. This mixture prevented beads from settling quickly and made it easer to flow multiple beads into the microchannel.

4 Results and discussion

Figure 3 shows the predicted temperature change as a function of bead diameter and thermal conductivity. A bead creates a temperature difference proportional to its diameter assuming it has a thermal conductivity different from the carrier fluid. The white dashed lines show the theoretical detection limit for the Keithly SourceMeter. For a polystyrene bead, the minimum detectable diameter is about 25 μm. Our experiments support this prediction as we were not able to detect beads with diameters of 5, 10, and 15 μm. A TPD with smaller membrane and microchannel dimensions would be able to detect these smaller beads because the device sensitivity depends on the ratio of the bead size to the heated fluid volume within the channel.

The thermal conductivity of the bead determines the magnitude of the temperature change. In the device we tested, the thermal conductivity threshold was

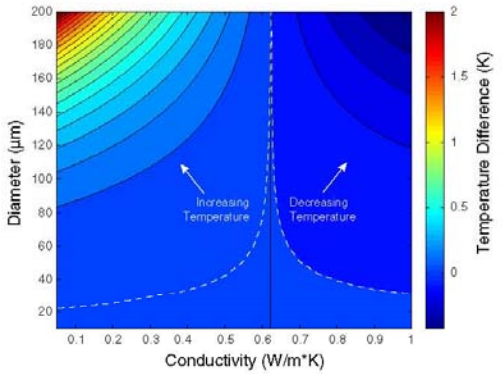

Fig. 3 Contour plot of the lumped model showing the effect of bead diameter and thermal conductivity on the predicted temperature difference. The model assumes a volumetric flow rate of 5 μl/min in a channel with a cross-section of 300 μm^2. The *dashed lines* show the theoretical limit of detection for the device (2 mK). *Black contour lines* are drawn for each 0.1 K change

approximately 0.62 W/m K. This threshold is a function of both the thermal conductivity of water and the convective heat transport within the device. A bead with a thermal conductivity higher than the threshold will generate negative temperature changes regardless of its size, while a bead with a thermal conductivity below the threshold will generate positive temperature changes. Thermally insulating beads like polystyrene generate a positive temperature change because they cause heat to build up near the RTD as they flow by. In contrast, thermally conductive beads such as those made from metal generate negative temperature changes because they rapidly conduct heat away from the RTD, resulting in a temperature drop.

The lumped thermal model predicts increases in RTD resistance (i.e., temperature) as polystyrene beads flow at a flow rate of 5 μl/min: 0.09 K for a 90-μm bead and 1.34 K for a 200-μm bead. Figures. 4 and 5 show representative traces for 90- and 200-μm beads, respectively. The predicted temperature shift for the 90-μm beads agrees well with the observed value of 0.5 Ω, or 0.11 K. Assumptions made about model parameters can explain the minor difference. For example, neither supplier of the beads could provide thermal conductivity data, so we used the thermal conductivity and heat capacity of regular polystyrene. The assumed thermal conductivity of SiN (16 W/m K), which influences heat flow into the membrane, may also contribute to the difference between model and experimental results.

In contrast to the 90-μm bead, the 200-μm bead produces a 2 Ω decrease in resistance, or an equivalent change in temperature of −0.44 K. The most likely explanation for this

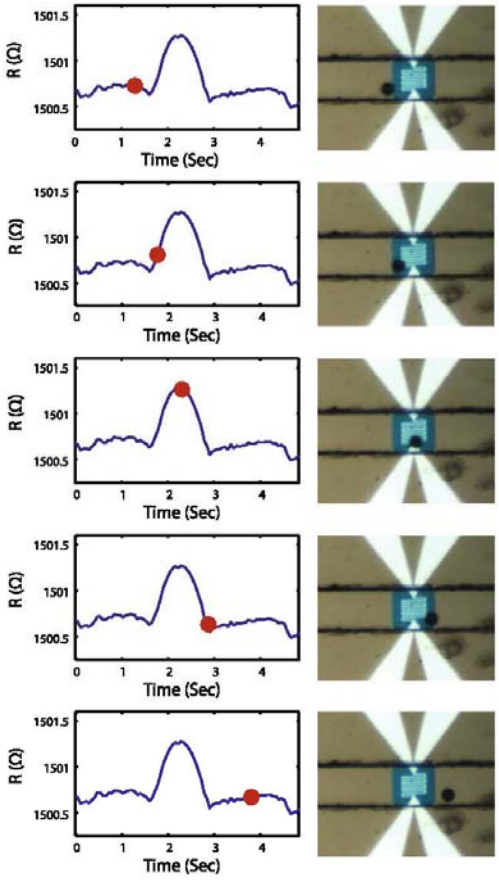

Fig. 4 A *representative plot* showing the signal generated by a 90-μm-diameter bead. Signals were consistently about 0.5 Ω (0.11 K) in amplitude

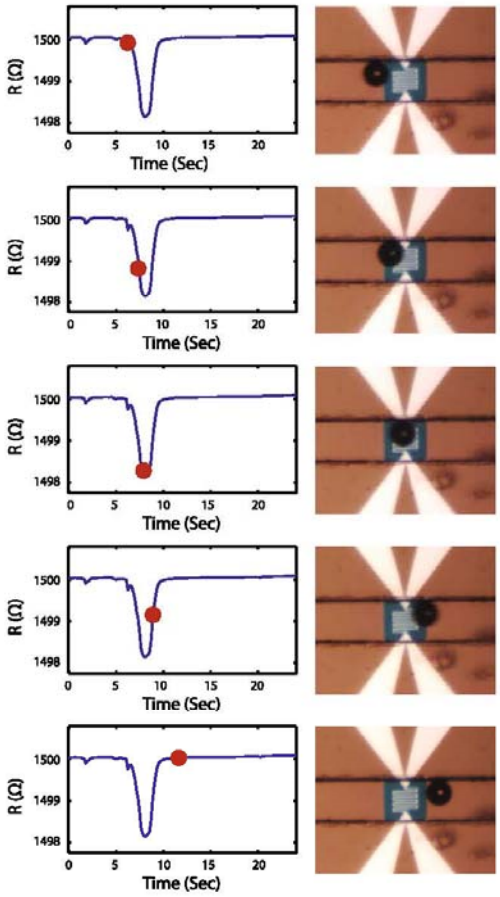

Fig. 5 A *representative plot* showing the signal generated by a 200-μm-diameter bead. Single beads of this size consistently generated negative peaks with amplitudes of about −2 Ω (−0.44 K)

result is that the bead is altering the fluid velocity near the sensor. The membrane resistance cannot decrease nor can the resistance of the heated fluid volume directly above the sensor. The only remaining thermal resistance that can decrease is $R_{\text{Convection}}$. The model predicts that a velocity of 10 mm/s reduces the RTD temperature by 2 K compared to a velocity of 0.01 mm/s because of the increased heat transfer via convection. Therefore, velocity changes on the order of 1 mm/s, or less, will result in measurable decreases in RTD temperature. The velocity field around a sphere flowing a microchannel is known to be complex (Shardt et al. 2012). For example, it is likely that the bead is rotating due to the non-uniform flow field within the microchannel, which would enhance the cooling effect by increasing the local velocity over the RTD. Thus, it is reasonable to assume that local velocity changes caused by the bead can yield negative temperature changes, even though the bead has a thermal conductivity lower than water. In contrast, the 90-μm-diameter bead is smaller and perturbs the local flow field less than the 200-μm bead, minimizing the velocity cooling effect, and yielding the expected increase in temperature.

Another prediction from the model is that the measured change in temperature is not affected by the distance of the bead from the sensor, assuming the bead is small enough to not significantly perturb the flow field. The thermal resistance of the water volume and bead are lumped together—the precise location of the bead does not impact the contribution of the bead to the overall thermal resistance. The

net result is the same: the temperature near the current source will increase if the thermal resistance of the fluid volume increases. However, the distance of the bead from the sensor will affect the thermal time constant of the system. The further away a bead is from the RTD, the larger the time constant is of the water between the RTD and bead. In practice, a longer time constant would increase the amount of time for the system to reach steady state, which would in turn limit how fast measurements can be made. Thus, the further the beads are away from the sensor, the slower the throughput. However, a key advantage of the TPD is that it can be made massively parallel because no cross talk exists between sensing channels.

As a proof-of-concept for particle counting, multiple beads were sequentially detected in the TPD using a flow rate of 2 μl/min. Representative results are shown in Fig. 6. The beads all produced negative peaks of about 2 Ω, similar to the experimental results shown in Fig. 5. The beads are spaced about one sensor width (300 μm) apart except for the last two, which are closer together. The results from this recording highlight the effect thermal capacitance has on throughput, namely that as beads become closer together there is less time for the system to reach steady state between beads resulting in peaks with reduced amplitude. The last two peaks have changes in resistance closer to 1.5 Ω. These results suggest that the TPD can count beads in two different ways. The first approach would be to simply count the number of passing particles. In this case, the relative amplitudes of the peaks are not important and the rate of counting can be high. However, accurate amplitudes might be needed to distinguish among multiple cell types or particles made of different materials. If these accurate measurements are needed, a second counting approach can be used. In this approach, a slower flow rate is used so that the system can reach steady state between peaks. The microscale dimensions and material properties of most particles mean that time constants are on the order of 100 ms, so counting rates would be limited to a few Hz per channel.

Lastly, we tested the effect of the carrier fluid on particle detection. We detected 200-μm-diameter particles in glycerol, de-ionized (DI) water, and phosphate buffered saline (PBS), and the results are summarized in Fig. 7. Glycerol is an electrical insulator and was used to confirm that particle detection is due to thermal and not electrical sensing. The thermal and electrical conductivities of glycerol are lower than water which yields a higher baseline RTD resistance. Electrically conductive PBS is often used to suspend cells and other biological particles during counting. As shown by the representative trace in Fig. 7, a high salt concentration does not degrade the signal, but it

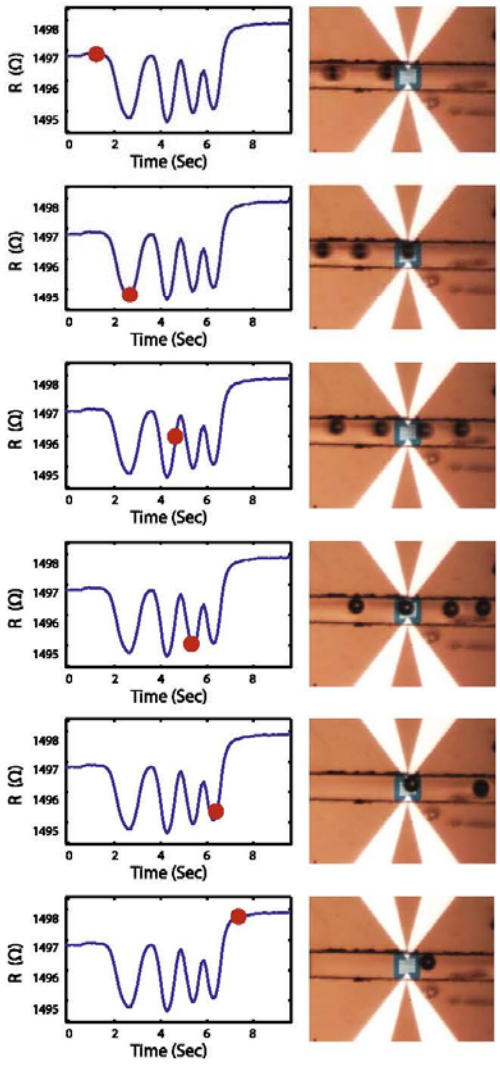

Fig. 6 Multiple beads about 300 μm apart were detected with the TPD. The amplitude of the last two beads is attenuated because they are closer together than the first two

does result in a slightly lower baseline RTD resistance. Even though saline is a good conductor of electricity, there is a negligible electrical potential within the device since only a single wire is used for sensing temperature. Furthermore, the RTD resistivity is orders of magnitude less than the resistivity of the fluids, so the geometric and material properties of the RTD will be the main

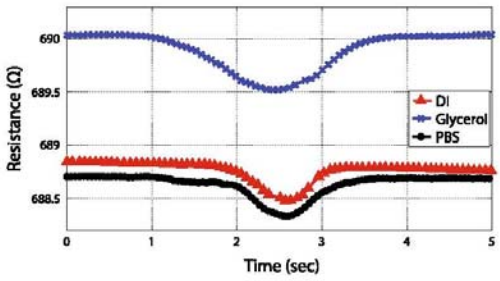

Fig. 7 Beads 200 μm in diameter were detected while suspended in glycerol, DI water, and PBS. A slower flowrate was used for glycerol, resulting in a broader peak as the bead flowed past the sensor

determinant of the baseline RTD resistance. The TPD works with fluids that possess a variety of thermal and electrical conductivities, which broadens its range of possible applications.

5 Conclusions

In summary, we have demonstrated a new device for detecting and counting particles based on thermal measurements. We have developed a first-order lumped model to explain the measured results. The size of the particles detected was roughly one-third of the sensor, but the principle can be used to detect particles of other sizes. We anticipate using this device to count other particles of interest, most notably biological cells, where it could be used in conjunction with, or a replacement for, flow cytometers. We also envision that the TPD can be used to thermally characterize particles as they flow by, opening up a new dimension in the high-throughput characterization of single cells.

Acknowledgments We thank Clement Kleinstreuer and John Sader for helpful discussions.

References

Duffy DC, McDonald JC, Schueller OJA, Whitesides GM (1998) Rapid prototyping of microfluidic systems in poly(dimethylsiloxane). Anal Chem 70(23):4974–4984

Incropera FP, DeWitt DP (1996) Fundamentals of heat and mass transfer, 4th edn. Wiley, New York

Janes MR, Rommel C (2011) Next-generation flow cytometry. Nat Biotechnol 29(7):602–604

Jin JS, Lee JS, Kwon O (2008) Electron effective mean free path and thermal conductivity predictions of metallic thin films. Appl Phys Lett 92(17):171910

Karayacoubian P, Bahrami M, Culham JR (2005) Asymptotic solutions of effective thermal conductivity. In: Proceedings of IMECE 2005. ASME international mechanical engineering congress and exposition. Orlando, Florida, USA, IMECE2005-82734

Lacy F (2011) Evaluating the resistivity-temperature relationship for RTDs and other conductors. IEEE Sens J 11(5):1208–1213

Lee J, Spadaccini C, Mukerjee E, King W (2008) Differential scanning calorimeter based on suspended membrane single crystal silicon microhotplate. J Microelectromech Syst 17(6):1513–1525

Leonard WF, Ramey RL (1966) Temperature coefficient of resistance in thin metal films. J Appl Phys 37(9):3634–3635

Murali S, Jagtiani AV, Xia X, Carletta J, Zhe J (2009) A microfluidic coulter counting device for metal wear detection in lubrication oil. Rev Sci Instrum 80(1):016105

Shardt O, Mitra SK, Derksen J (2012) Lattice boltzmann simulations of pinched flow fractionation. Chem Eng Sci 75(0):106–119

van der Wiel A, Linder C, de Rooij N, Bezinge A (1993) A liquid velocity sensor based on the hot-wire principle. Sens Actuators A Phys 37(38(0):693–697

Yi N, Park BK, Kim D, Park J (2011) Micro-droplet detection and characterization using thermal responses. Lab Chip 11:2378–2384

Zhang H, Chon C, Pan X, Li D (2009) Methods for counting particles in microfluidic applications. Microfluid Nanofluid 7(6):739–749

Biosensors and Bioelectronics 59 (2014) 120–126

Contents lists available at ScienceDirect

Biosensors and Bioelectronics

journal homepage: www.elsevier.com/locate/bios

A paper-based calorimetric microfluidics platform for bio-chemical sensing

Benyamin Davaji, Chung Hoon Lee *

Nanoscale Devices Laboratory, Marquette University, Milwaukee, WI 53233, United States

ARTICLE INFO

Article history:
Received 10 December 2013
Received in revised form
3 March 2014
Accepted 11 March 2014
Available online 27 March 2014

Keywords:
Micro-calorimetry
Thermal bio-sensor
Label-free detection
Paper-based sensor

ABSTRACT

In this report, a paper-based micro-calorimetric biochemical detection method is presented. Calorimetric detection of biochemical reactions is demonstrated as an extension of current colorimetric and electrochemical detection mechanisms of paper-based biochemical analytical systems. Reaction and/or binding temperature of glucose/glucose oxidase, DNA/hydrogen peroxide, and biotin/streptavidin, are measured by the paper-based micro-calorimeter. Commercially available glucose calibration samples of 0.05, 0.15 and 0.3% wt/vol concentration are used for comparing the device performance with a commercially available glucose meter (electrochemical detection). The calorimetric glucose detection demonstrates a measurement error less than 2%. The calorimetric detection results of DNA concentrations from 0.9 to 7.3 mg/mL and temperature changes in biotin and streptavidin reaction are presented to demonstrate the feasibility of integrating the calorimetric detection method with paper based microfluidic devices.

1. Introduction

The first paper-based chemical analytical technique was chromatography and was developed by Martin and Synge (Martin, 1952) in 1943. The first immunoassay using paper as a fluidic channel was reported by Muller (Muller and Clegg, 1949). More recently, paper-based microfluidics were re-introduced by Martinez et al. (2007) for low-cost disposable bio-chemical sensing applications. Further development and extension of this technique for higher accuracy and extended functionality were demonstrated recently using microfabricated devices (Liana et al., 2012; Martinez et al., 2008b). Inexpensive paper-based microfluidic systems have also been expanded to other applications such as environmental monitoring (Liana et al., 2012; Li et al., 2012). Paper-based microfluidic devices exploit capillary action in porous paper to transport and manipulate liquid samples. This extremely simple and robust liquid transport mechanism is well-suited for the development of assays, particularly in applications where portability and/or disposability are important. As a result, paper-based analytical techniques are used in several commercially available products such as glucose-meter strips, pregnancy test strips, and pH strips.

Biochemical assays have been developed and commercialized based on several different types of detection methods. The most popular detection methods are colorimetric (Ellerbee et al., 2009; Martinez et al., 2008a) and electrochemical (Nie et al., 2010; Dungchai et al., 2011). Colorimetric detection is based on changes in intensity of colors due to the reaction of a reagent and a sample. The changes in color (wavelength) and intensity can be detected using a camera, spectroscopy, or in some applications, even by the unaided human eye. Electrochemical detection is based on changing electroinactive substrates to electroactive products (Wang, 2008). In the electrochemical detection readout is an electrical signal representing the change in electrical conductivity or electrical potential providing a quantification of the chemical reaction. Colorimetric detection has been widely used for inexpensive semi-quantitative assays to indicate the presence or absence of targeted molecules. However, precise quantification of the chemical reaction typically requires complex optical detection instrumentation (Ellerbee et al., 2009) or image processing software (Martinez et al., 2008a), which is not suitable for the development of inexpensive portable devices. An added difficulty is the requirement to develop dyes that change color or intensity via a reaction with the molecule being measured. Electrochemical detection systems are easier to miniaturize because they only need to quantify electrical conductivity or changes in potential. However, this technique requires reactions that produce electroactive molecules.

In this paper, a calorimetric paper-based microfluidic system for bio-chemical sensing is presented for the first time. Since most bio-chemical reactions or interactions are accompanied by a change in heat, this label free calorimetric detection method extends and enhances the capabilities of existing paper-based microfluidic systems to include a wide range of bio-chemical sensing and diagnostic applications.

* Corresponding author.
E-mail address: chunghoon.lee@marquette.edu (C.H. Lee).

http://dx.doi.org/10.1016/j.bios.2014.03.022
0956-5663/

2. Materials and methods

2.1. Micro-calorimetric detection

Thermal detection methods have been used by others to explore bio-chemical interactions (Allen and Lai, 1998; Abramson and Tien, 1999; Yi et al., 2014; Kwak et al., 2008). In this method, the temperature changes resulting from endothermic or exothermic reactions are used to detect and/or quantify the concentrations of targeted molecules. However, it is impractical to use a traditional macro-scale calorimeter for disposable and inexpensive sensing applications. A paper-based microcalorimetric device, as shown in Fig. 1(a), offers a number of advantages: small volume of required sample, ease of sample handling, increased sensitivity at micro-scale, and low-cost manufacturing.

The heat generated or absorbed from a bio-chemical reaction causes a temperature change, which depends on the concentration of the reagent and the samples and the enthalpy of the reaction. It can be readily shown that the sensitivity of the temperature detection of a calorimeter is inversely proportional to its heat capacity (Barnes et al., 1994; Lai et al., 1995).

From generated heat in reaction the temperature change can be expressed by

$$\Delta T = (1/C_p)\Delta Q \tag{1}$$

where T is the temperature, Q is the heat, and C_p is the heat capacity.

A paper-based microfluidic system has the inherent advantage of a low thermal mass due to the thin and porous nature of the paper and thin glass substrate configuration as shown in Fig. 1(a). In order to measure the temperature changes from the reaction, the measurement system is ideally required to be in the adiabatic condition. The adiabatic condition ensures that all of the heat released or absorbed from the reaction is used to affect a temperature change, rather than lost to the surroundings before the temperature change is measured. However, with practical calorimeters it is only possible to achieve a quasi-adiabatic condition. The amount of heat lost to the surroundings can be characterized by a thermal time constant, which is a function of the heat capacity of the calorimeter and the thermal resistance between the calorimeter and its surroundings (i.e., its thermal isolation). Fig. 1(b) shows a schematic cross-sectional view of the sensor where the chemical reaction occurs in the spot indicated in the figure. Fig. 1(b) shows the lumped equivalent circuit model representing the thermal conductivity from the reaction area. Using a first order approximation, the thermal time constant of the system can be expressed as

$$\tau = R_{th}C_p \tag{2}$$

where R_{th} is the thermal resistance and C_p is the thermal capacity of the system, respectively.

The R_{th} can be calculated as

$$R_{th} = L/(kA) \tag{3}$$

for a material bounded surface and

$$R_{th} = 1/(4kr) \tag{4}$$

for an air bounded surface (Carslaw and Jaeger, 1986), where L is the length along the heat flow direction, k is the thermal conductivity of material, A is the area perpendicular to the heat flow, and r is the radius of area. The total thermal resistance of our system can be expressed as

$$R_{th} = R_{th1} \| R_{th2} \| R_{th2} \| R_{th3} \| R_{th3} \| R_{th4} \tag{5}$$

where the R_{th1} to R_{th4} are the thermal resistances for each of the components indicated in Fig. 1(b).

The total heat capacity can be expressed as

$$C_p = C_{pg} + C_{ppl} \tag{6}$$

where C_{pg} is the heat capacity of the glass substrate and C_{ppl} is the heat capacity of the paper and liquid. The heat capacity can be

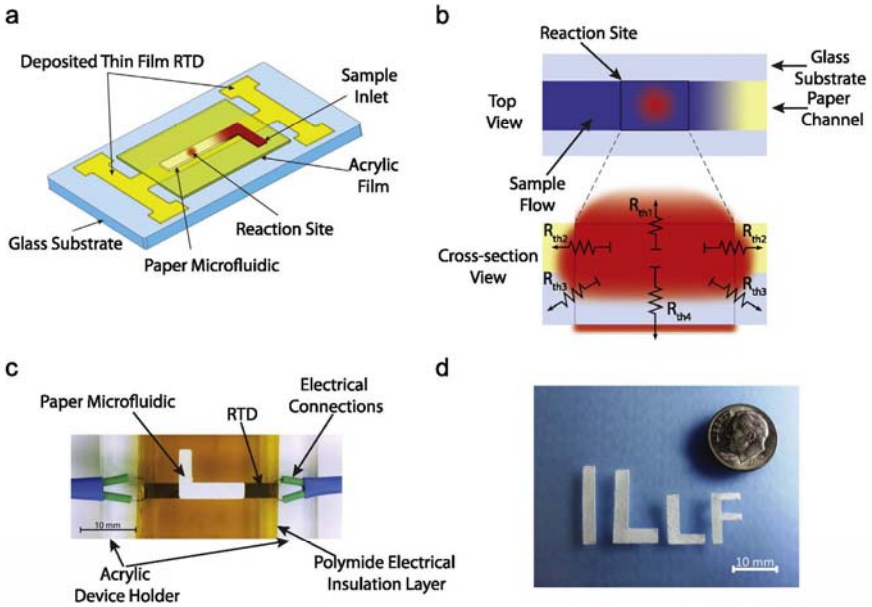

Fig. 1. (a) Overview of the paper-based device, (b) top view and cross-sectional view of the reaction site and heat transfer with the thermal resistance equivalent model, (c) fabricated paper-based microfluidic device with calorimetric detection, (d) knife plotter cut paper strips as a reaction substrate and a microfluidic channel.

Table 1
Thermal parameters of the device.

Symbol	Parameter	Unit	Value
R_{th1}	R_{th} of air boundary	K/W	6.17×10^3
R_{th2}	R_{th} of paper boundary	K/W	4.78×10^3
R_{th3}	R_{th} of glass boundary	K/W	4.76×10^3
R_{th4}	R_{th} of air through glass	K/W	6.17×10^3
$C_{P,Calc}$	Calculated thermal mass	J/K	1.33×10^{-2}
$C_{P,M}$	Measured thermal mass	J/K	1.42×10^{-2}
τ_{Calc}	Calculated time constant	s	11.3
τ_M	Measured time constant	s	12.4

expressed as

$$C_p = \rho V c_p \tag{7}$$

where ρ is the mass density of the material, V is the volume and c_p is the constant volume specific heat of the material.

Table 1 lists the thermal parameters of a micro-calorimeter of typical dimensions used in this work. In this case, the micro-calorimeter was made of a 100 μm thick glass substrate and a 180 μm thick paper microfluidic channel. The reagent was immobilized within a 3×4 mm area of the channel, called the reaction site. It was assumed that the reaction within the reaction site is homogeneous and that the reaction is not diffusion-limited. Thus the reaction site in this device was considered to be isothermal. In Table 1, $C_{p,Calc}$ is the calculated thermal mass of the system, $C_{p,M}$ is the measured thermal mass of device, τ_{Calc} and τ_M are the calculated and measured time constants, respectively. The calculated heat capacity is in close agreement with the measured heat capacity as discussed later.

The paper-based microcalorimeter presented here is bounded by air on the top of the device, which has a high thermal resistivity. However, convection of air can be a significant thermal path for most thermal measurements. To suppress the convection of air, an enclosure can be used. Radiation is also a thermal loss pathway, but it is significant only at high temperature differences between the system and its surroundings (Bergman et al., 2011). Radiation losses in paper-based microfluidic systems are neglected because most bio-chemical reactions result in lower temperature differences than those required for significant radiation loss.

2.2. Paper-based thermal calorimeter platform

The paper-based device consisted of a microfluidic channel made of a chromatography-grade filter paper placed directly on top of a resistive temperature detector (RTD), as shown in Fig. 1(c). A 100 μm thick cover glass (VWR 48393-106) was used as a substrate for the paper and RTD. A thin layer of 5 μm acrylic film (Nitto Denko 5600) was used for electrical isolation and also served as the adhesion layer between the paper microfluidic channel and the glass substrate.

2.2.1. Microfluidic channel design

The mechanism of liquid transport by capillary action simplifies microfluidic systems by eliminating the need for actuation (pumping) and valves to control the flow. An important advantage of this technique is bubble-free operation. Suppressing or preventing bubble formation in microfluidic devices has long been a challenge during sample introduction and operation (Cho et al., 2007; Sung and Shuler, 2009), but is necessary to produce reliable and repeatable results.

The material of the reaction site (paper microfluidic channel) plays a key role in enzyme-based detection of bio-chemical reactions. Various reaction substrates (e.g. cellulose, solid glass particles, porous glass particles, and nickel screen) have been used for immobilizing glucose oxidase (GOD) enzyme. Among these, porous glass and cellulose fiber networks are the most common materials due to their high surface area (Bankar et al., 2009).

In our design chromatography filter paper (Whatman3001-845) was used as a microfluidic channel and a reagent substrate. Laser cutting has been used to cut paper strips to make the microfluidic channel (Fu et al., 2011) but the residue of burned paper along the cutting line will remain on the paper which may interfere with the reaction. Our paper fluidic channel was patterned and cut using a knife plotter (from Silhouette, Inc.). The patterns were designed to guide the sample flows in the paper strip. The paper strip was affixed on top of the RTD, which was integrated on the glass substrate. In order to minimize the mechanical stress caused by introducing liquids to the RTD, L- and Γ-shaped designs were used instead of a straight strips. Examples of the paper fluidic channels cut by the knife plotter are shown in Fig. 1(d). The tails of the L-shape and Γ-shape papers were positioned outside the RTD, where the samples were introduced. In this paper, the L-shape design was used to obtain a simpler geometry (increasing uniformity of enzyme distribution on paper) for an enzyme immobilization site. In each measurement, a known amount of reagent was placed at the center of the channel. The introduced sample was transported by capillary action towards the reagent. Once the sample came in contact with the reagent, the reaction started.

In previous works, paper-based fluidic channels were fabricated by using wax printing (Carrilho et al., 2009; Martinez et al., 2008b) and photolithography (Martinez et al., 2007). In this work, a knife plotter tool was used to cut out precise paper microchannels. The knife plotter method also results in minimal chemical contamination of the paper and requires no heat treatment, which prevents the cellulose network from developing defects and eliminates solvent diffusion into the paper. Paper strips defined by the knife plotter also provide a higher integration capability for 3D microfluidics to define more complex shapes (Liu and Crooks, 2011).

2.2.2. RTD design, fabrication and measurement

A resistive temperature detector (RTD) was used to detect the temperature change in the reaction and is preferred over other temperature sensors due to its excellent linearity, high sensitivity, low fabrication cost, easy integration, and simple readout and interfacing. Typically, platinum is used for commercial RTD sensors due to its chemical inertness and linearity of resistance change over wide temperature ranges (−50 to 250 °C).

The thin film RTD sensor used in this work was made of nickel due to its high thermal coefficient and excellent resistance linearity in the range of bio-chemical reactions (−10 to 150 °C). Shadow masking was used to pattern a 35 nm thick nickel film by thermal evaporation. The nickel evaporation process is also simple and inexpensive. To increase the device sensitivity to temperature changes from the reaction, the RTD surface area was larger than the chemical reaction area to ensure all the heat generated or absorbed was received by the RTD. A Keithley 2600 source/meter with 4-point configuration was used to measure the resistance change of the RTD caused by the temperature change from the bio-chemical reactions. The 4-point measurement setup was used to eliminate the effect of junction resistance and thermal fluctuations of electrical leads on the resistance measurement of the RTD sensor. The measurements, data acquisition and data-preprocessing were automated and controlled by a LabView™ program.

A bias current of 1 mA was applied using the Keithley 2600 source/meter to the RTD (1.1 kΩ) and the voltage drop across the RTD was measured to monitor the resistance change of the RTD. For the design shown in Fig. 1, the 1 mA sourcing current through the RTD resulted in 0.11 mW of Joule heating, which elevated the

RTD temperature approximately 1–2 °C above the room temperature. The resistance value of the RTD can be written as

$$R = R_0(1+\alpha\Delta T) \quad (8)$$

where R_0 is the resistance of the RTD at room temperature, α is the temperature coefficient of resistance and ΔT is the temperature change.

The thin film nickel RTD was calibrated using a thermal bath (HAAKE) to get the thermal coefficient of resistance (TCR). The nickel RTD showed a linear response between 10 °C and 50 °C (R^2=0.9999). The TCR of the nickel RTD was measured to be 0.0011/K, which was lower than values reported for bulk nickel (6.14×10^{-3}/K) (Lacy, 2011). Since α is a function of the ratio of film thickness to the mean free path of electrons in metals (Jin et al., 2008; Leonard and Ramey, 1966), the difference is likely due to the film thickness (35 nm) and grain size of the thermally evaporated thin nickel film. Increasing the film thickness and a post-annealing process would likely improve the TCR.

3. Results

In order to demonstrate that the paper-based microcalorimetric detection method works, three applications were investigated: detection of glucose, detection of DNA, and the detection of streptavidin and biotin binding.

3.1. Glucose detection

The concentration of glucose was measured using the heat generated by the glucose oxidase (GOD) enzyme, which was used to convert glucose to gluconic acid and hydrogen peroxide. Due to its low pH sensitivity, GOD from *Aspergillus niger* (SigmaAldrich-G7141) was used to prepare a 1.0 mg/ml reagent in a 50 mM sodium acetate buffer. Sodium acetate buffer, as well as sodium phosphate buffer, is commonly used to activate GOD enzymes (Gibson et al., 1964). The buffer was made from anhydrous sodium acetate (Fisher Scientific-S210-2) and diluted with acetic acid to maintain the pH of the buffer constantly at 5.1. The activated GOD enzyme in the buffer was used to react with different concentrations of glucose. The GOD enzyme catalyzes the oxidation reaction of glucose (Bankar et al., 2009),

$$\beta D\ Glucose + O_2 \xrightarrow{GOD} \beta D\ Glucono - \delta\ lactone + H_2O_2 \quad (9)$$

This reaction causes an enthalpy change of $\Delta H = -80$ kJ/mol (Scheper, 1999). Two microliters of active GOD enzyme were placed and immobilized at the reagent introduction site of the paper strip as shown in Fig. 1(a) and (b). The heat generated by the oxidation of glucose was recorded for different concentrations of glucose samples introduced to the immobilized GOD. Measurements for each concentration were repeated 10 times to calculate the measurement error. The measurement for each sample concentration was a temperature–time plot which was post-processed to extract the temperature change for each sample concentration. Commercially available glucose solutions were used to test three different concentrations of glucose which were representative of low, normal and high glucose levels in the blood (0.05, 0.12 and 0.3% wt/vol of glucose, respectively) (Bayer Contour Control Solution) (Frank et al., 2011; Kilo et al., 2005). Fig. 2 shows a typical temperature profile from the reaction.

When the 2 μL volume of GOD enzyme was first placed at t_1 (in Fig. 2) at the center of the paper strip, the temperature of the RTD dropped due to the temperature difference between the RTD and GOD enzyme and evaporative cooling of the enzyme buffer. The time between t_1 and t_2 shows the aforementioned temperature drop. The temperature of the RTD and the enzyme reached a stable temperature,

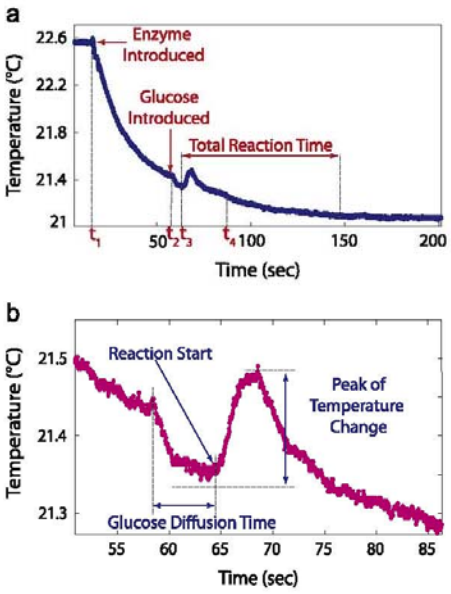

Fig. 2. Measured temperature change for reaction of glucose oxidase enzyme and glucose sample is illustrated. (a) Measured reaction data, (b) close-up reaction data from t_1 to t_4.

which was still higher than room temperature because the RTD Joule heating. After the temperature was stabilized, an 8 μL glucose sample at room temperature was placed to the tail of the L-shaped paper strip (sample inlet shown in Fig. 1), and traveled along the strip toward the GOD enzyme. During the time period between t_2 and t_3, the glucose continued to travel along the paper strip before it reached the enzyme site. The temperature drop during this period is again due to a temperature difference between the RTD and the glucose, and the evaporation of the sample. At time t_3, before the reaction, the glucose sample reached the enzyme and the oxidation reaction of glucose commenced. Due to the exothermic nature of the glucose oxidation process, the temperature rises. As the reaction completed, the temperature decreased, and reached equilibrium with surroundings.

The following equation is used to correlate the peak of temperature change, ΔT, to the concentration of glucose (Scheper, 1999)

$$n_p = C_p\frac{\Delta T}{\Delta H} \quad (10)$$

where ΔH is molar enthalpy change, n_p is moles of product, and C_p is the heat capacity of the system.

The heat capacity (or thermal mass) of the system is calculated by calibrating with a low concentration of the glucose test sample. Knowing the exact concentration of glucose, enthalpy change, and temperature change, the thermal mass of our system can be determined. The effect of sample evaporation is also taken into account in the calibration.

The detected temperature for different concentrations of glucose shows an upward trend with increasing concentration as shown in Fig. 3. In order to convert the detected temperature to concentration data using Eq. (10), two additional terms must be considered: the reaction rate of GOD and glucose, and the ratio of reaction area to the total RTD area. For the reaction rate of GOD and glucose, the catalytic reaction of the enzyme can be saturated and shows a nonlinear behavior as the concentration of the glucose increases because the finite reaction rate is limited by

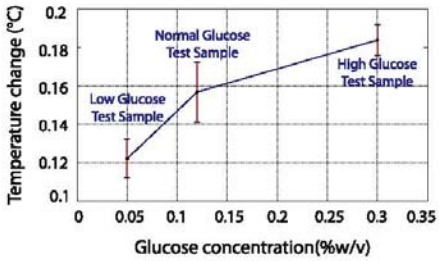

Fig. 3. Measured temperature change for different concentrations of glucose. Error bars are standard deviation of the samples where 10 different measurements for each concentration are performed.

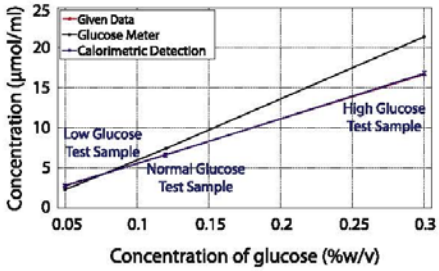

Fig. 4. The results of glucose with the paper-based calorimetric device and commercialized glucose meter for different concentrations.

the number of available GOD oxidation sites for glucose molecules (the Michaelis–Menten model for enzyme kinetics Murugan, 2002). In this experiment the number of moles of glucose is calculated by the concentration and the volume size of the samples. In the 8 μL droplets of the low, normal, and high concentrations of the glucose test sample, a total number of 1.34×10^{16}, 3.21×10^{16} and 8.02×10^{16} molecules of glucose are available to react with the GOD, respectively. The calculated number of molecules of glucose in the sample is higher than the number of the molecules of the GOD, which is 7.53×10^{15} molecules in 2 μL of enzyme. Therefore, the reaction is in the saturated region of the reaction rate. However, at high concentrations the reaction rate can be modeled as linear (Pant et al., 2008). For the ratio of reaction area to the total RTD area, the reaction area is designed to be 45% of the whole channel area. Therefore only 4 μL of glucose is reacting with GOD.

Fig. 4 shows the measured glucose concentrations of the glucose test solution, taking the reaction rate factor and the ratio of reaction area into account. The results are also affected by the diffusion time of glucose into the GOD reaction site and the error may be resolved with optimizing the paper channel design. Results show good linearity and agreement with the solution concentrations from the manufacturer in the micro-molar range of glucose concentration. While a commercial glucose meter shows as high as 30% error in the glucose concentration measurement, the calorimetric paper-based microfluidic device shows less than 2% error as shown in Fig. 4.

Enzyme-based sensors have shown their expanding capabilities to improve health care quality. The integration of the paper-based technology and enzyme-based sensors may replace expensive and time consuming portions of clinical monitoring used by patient bedsides and home testing (Ispas et al., 2012). From Eq. (10), the detectable concentration is directly proportional to the temperature change, given the device heat capacity and enthalpy. Therefore, the concentration detection limit is determined by the minimum detectable temperature. With our measurement setup, the Kiethley 2600 source/meter, noise in the resistance is 0.004 Ω. The signal-to-noise ratio of 1:1 corresponds to 26 mK. With the signal-to-noise ratio, the measurable minimum concentration is 1.51 μmole/mL.

3.2. DNA concentration detection

In biological systems, intracellular iron from ferritin reacts with hydrogen peroxide and catalyzes the formation of hydroxyl groups, which cleaves deoxyribonucleic acid (DNA) (Arosio and Levi, 2002). The reaction of the hydroxyl group and DNA causes DNA strand breakage (Mello-Filho et al., 1984). Hydrogen peroxide is a good source of hydroxyl groups, and is used in this work to react with salmon DNA in a buffer solution. The heat generated by the reaction was detected for different concentrations of salmon DNA (without the use of any catalyst). Deoxyribonucleic acid sodium salt from salmon testes (Sigma D1626) was used as the test DNA sample. DNA samples were diluted in IDTE DNA buffer (1xTE-pH8) to maintain the pH, and 30% wt/wt hydrogen peroxide solution (Fisher Scientific H325) was used for DNA detection experiments. The different concentrations of DNA reagents were placed to the reagent site on the paper microfluidic device, and then the hydrogen peroxide solution was introduced to the sample inlet on the channel. The hydrogen peroxide solution traveled along the paper and the reaction started when it reached the DNA sample location. The generated heat, proportional to the DNA concentration, was detected by the thin film RTD under the paper microfluidic device. To compare the results for different concentrations, four different reagents with different DNA concentrations were prepared (0.91 mg/ml, 1.83 mg/ml, 3.65 mg/ml, and 7.30 mg/ml). The generated heat by DNA experiments has the same pattern as the glucose detection experiment. The detected temperature change for different concentrations of DNA shows a rising trend as the concentration goes up. As shown in Fig. 5, a higher concentration caused a higher temperature change. Differential measurement (Fig. 5(a) and (b)) was used to minimize the effect of buffer on temperature measurement.

The main point of this experiment is to demonstrate low-cost DNA concentration detection. The purification of DNA after extraction is necessary for many sequencing approaches. Therefore, this method provides a low cost and simple way to monitor the concentration of DNA.

3.3. Protein binding detection

Protein–protein binding is used to identify or isolate different kinds of cells with related biomarkers, as well as in disease detection by studying the reaction of antibodies and antigens. Microfluidic devices have been developed for the detection of the protein binding via calorimetry (Torres et al., 2004). Biotin and streptavidin binding was selected to demonstrate the paper-based calorimeter device for an enthalpy assay. The biotin was placed at the reagent introduction site of the paper strip and the streptavidin was introduced to the sample inlet. The streptavidin travels along the paper to the biotin while the temperature was continuously recorded. Biotin (Sigma B4501) and streptavidin (Sigma S4762) are both diluted in DI water to prepare 1 mg/ml and 0.1 mg/ml solutions, respectively. Detection of protein binding is identified by the temperature spike in the temperature–time recording, resulting in a label-free detection mechanism (Ray et al., 2010).

For the binding of the proteins, the 2 μL of diluted biotin is placed first on the strip. Again as in the glucose and DNA cases, this causes the temperature drops due to the temperature difference and evaporative cooling. By introducing the 5 μL of streptavidin to the sample inlet, streptavidin is transported to the reagent and as soon as it gets to

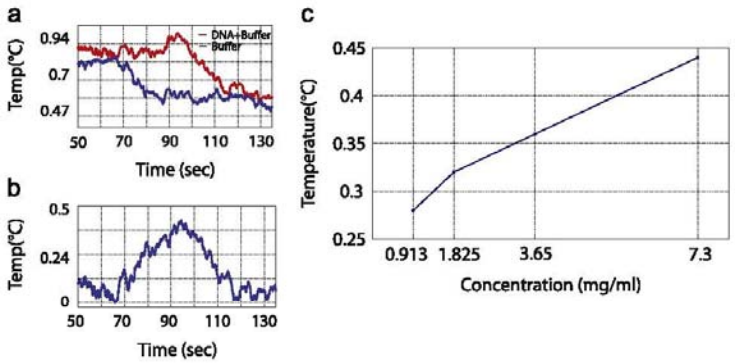

Fig. 5. The DNA concentration detection experiment results. (a) Signals from control experiments, a peak in temperature at the presence of DNA shows the oxidation reaction, (b) differential signal which shows the temperature change only from DNA reaction, (c) measured temperature change from the reaction of different DNA concentrations and hydrogen peroxide.

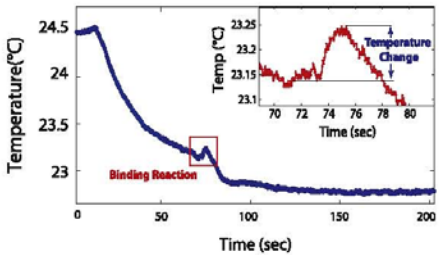

Fig. 6. Measured temperature change for binding reaction of biotin and streptavidin.

the biotin, a temperature change is detected. The temperature signal has the same pattern as previous experiments, which makes it possible to extract sample concentration by applying the same approaches. Fig. 6 illustrates the binding detection based on the enthalpy change with the paper-based microfluidic device. This result shows the feasibility of the device for thermal detection of protein binding events.

4. Discussion

The ultimate detection limit of the paper-based calorimetric device will be determined by the noise of the detection system. The calculated Johnson noise floor of the sensor RTD is 40 μΩ with a measurement bandwidth of 100 Hz. However, the lower limit of detection was determined by the Source/Meter, which had a resolution of 1 mΩ. Experiments showed that the system was capable of reliably measuring changes in resistance as low as 4 mΩ (26 mK) of 1.1 kΩ. Because the temperature of the RTD is a function of the TCR (α), improving purity (in our evaporated nickel film case) or using a material with higher α will directly improve the measurement sensitivity.

The knife plotter cut paper strips used in this work can be further optimized to effectively guide the reactants (reagent and sample). The paper microfluidic channel design with only the knife plotter cut induces the flow of reactants when mixed, which contributed to the measurement of errors in Fig. 3. Also, the glucose diffusion time to reach the GOD is solely limited by the length of the strip. Combining techniques such as wax patterning and surface treatments along with improved cutting can significantly improve the reactant transport stability resulting in better measurement repeatability. In Fig. 6, the temperature profiles before and after the reaction varied due to evaporation of liquid to surroundings. In the ideal case, the temperature profile should follow a monotonic decrease. The deviation prevents accurate calculation of the area under the reaction, which may be used for calculation of total enthalpy of the reaction. This deviation can be minimized by optimizing the paper strips.

The calorimetric detection mechanism is a label-free method that allows the expansion of applications of enzyme-based sensors to a wide range of enzymatic reactions. The application of this type of portable device has been limited due to the complexity of detection methods. The calorimetric method overcomes these limitations and could result in new devices with applications in portable healthcare diagnostics. Calorimetric DNA concentration detection is a method in which thermal information from the reaction can be used to obtain useful information about DNA. Calorimetric protein binding detection using the paper-based micro-calorimetric device has the ability to expand the applications of current disposable disease detection devices. The calorimetric detection demonstrated in this paper can expand the functionality of microanalytical devices by adding a thermal detection scheme for bio-chemical materials based on the enthalpy changes.

5. Conclusion

A framework for using calorimetric detection with paper-based analytical devices is presented. The calorimetric detection method of the reaction on a paper network is a novel technique that expands the detection capabilities of paper-based sensors. The paper-based calorimetric method is capable of detecting various enzymatic and biological reactions with an electronic readout. Calorimetric detection for three different bio-chemical samples is demonstrated. The results demonstrate the feasibility of the calorimetric paper-based device to detect various bio-chemical reactions without having any embedded markers or complex measurements. The thermal detection paper-based analytical device will help realize future low-cost, portable, and non-complex point-of-care devices.

Acknowledgments

We thank Glenn M. Walker and Shankar Radhakrishnan for helpful discussions.

References

Abramson, A.R., Tien, C.L., 1999. Microscale Thermophys. Eng. 3 (4), 229–244.
Allen, L.H., Lai, S.L., 1998. Microscale Thermophys. Eng. 2 (1), 11–19.
Arosio, P., Levi, S., 2002. Free Radic. Biol. Med. 33 (4), 457–463.
Bankar, S.B., Bule, M.V., Singhal, R.S., Ananthanarayan, L., 2009. Biotechnol. Adv. 27 (4), 489–501.
Barnes, J.R., Stephenson, R.J., Woodburn, C.N., O'Shea, S.J., Welland, M.E., Rayment, T., Gimzewski, J.K., Gerber, C., 1994. Rev. Sci. Instrum. 65 (12), 3793–3798.
Bergman, T.L., Lavine, A.S., Incropera, F.P., DeWitt, D.P., 2011. Foundamental of Heat and Mass Transfer, seventh edition. John Wiley and Sons Inc., United States.
Carrilho, E., Martinez, A.W., Whitesides, G.M., 2009. Anal. Chem. 81 (16), 7091–7095.
Carslaw, H.S., Jaeger, J.C., 1986. Conduction of Heat in Solids. Oxford University Press, Oxford.
Cho, C.-H., Cho, W., Ahn, Y., Hwang, S.-Y., 2007. J. Micromech. Microeng. 17 (9), 1810.
Dungchai, W., Chailapakul, O., Henry, C.S., 2011. Analyst 136, 77–82.
Ellerbee, A.K., Phillips, S.T., Siegel, A.C., Mirica, K.A., Martinez, A.W., Striehl, P., Jain, N., Prentiss, M., Whitesides, G.M., 2009. Anal. Chem. 81 (20), 8447–8452.
Frank, J., Wallace, J.F., Pardo, S., Parkes, J.L., 2011. J. Diabetes Sci. Technol. 5 (1), 198–205.
Fu, E., Ramsey, S., Kauffman, P., Lutz, B., Yager, P., 2011. Microfluid. Nanofluidics 10 (1), 29–35.
Gibson, Q.H., Swoboda, B.E.P., Massey, V., 1964. J. Biol. Chem. 239 (11), 3927–3934.
Ispas, C.R., Crivat, G., Andreescu, S., 2012. Anal. Lett. 45 (2–3), 168–186.
Jin, J.S., Lee, J.S., Kwon, O., 2008. Appl. Phys. Lett. 92 (17).
Kilo, C., Pinson, M., Joynes, J.O., Joseph, H., Monhaut, N., Parkes, J.L., Baum, J., 2005. Diabetes Technol. Ther. 7 (2), 283–294.
Kwak, B.S., Kim, H.O., Kim, J.H., Lee, S., Jung, H.-I., 2008. Biosens. Bioelectron. 10 (1), S10–S26.
Lacy, F., 2011. IEEE Sens. J. 11 (5), 1208–1213.
Lai, S.L., Ramanath, G., Allen, L.H., Infante, P., Ma, Z., 1995. Appl. Phys. Lett. 67 (9), 1229–1231.
Leonard, W.F., Ramey, R.L., 1966. J. Appl. Phys. 37 (9).
Li, X., Ballerini, D.R., Shen, W., 2012. Biomicrofluidics 6 (1).
Liana, D.D., Raguse, B., Gooding, J.J., Chow, E., 2012. Sensors 12 (9), 11505–11526.
Liu, H., Crooks, R.M., 2011. J. Am. Chem. Soc. 133 (44), 17564–17566.
Martin, A., 1952. The development of partition chromatographys. Nobel Lecture.
Martinez, A.W., Phillips, S.T., Butte, M.J., Whitesides, G., 2007. Angew. Chem. Int. Ed. 46 (8), 1318–1320.
Martinez, A.W., Phillips, S.T., Carrilho, E., Thomas, S.W., Sindi, H., Whitesides, G.M., 2008a. Anal. Chem. 80 (10), 3699–3707.
Martinez, A.W., Phillips, S.T., Wiley, B.J., Gupta, M., Whitesides, G.M., 2008b. Lab Chip 8, 2146–2150.
Mello-Filho, A.C., Hoffmann, M.E., Meneghini, R., 1984. Biochem. J. 218 (1) 273-0.
Muller, R.H., Clegg, D.L., 1949. Anal. Chem. 21 (9), 1123–1125.
Murugan, R., 2002. J. Chem. Phys. 117 (9).
Nie, Z., Nijhuis, C.A., Gong, J., Chen, X., Kumachev, A., Martinez, A.W., Narovlyansky, M., Whitesides, G.M., 2010. Lab Chip 10, 477–483.
Pant, M., Sharma, P., Radha, T., Sangwan, R., Roy, U., 2008. J. Biol. Sci. 8 (8), 1322–1327.
Ray, S., Mehta, G., Srivastava, S., 2010. Proteomics 10 (4), 731–748.
Scheper, T., 1999. Advances in Biochemical Engineering/Biotechnology, Thermal Biosensors Bioactivity Bioaffinity, vol. 64. Springer-Verlag, Berlin, Heidelberg.
Sung, J.H., Shuler, M.L., 2009. Biomed. Microdev. 11 (4), 731–738.
Torres, F.E., Kuhn, P., De Bruyker, D., Bell, A.G., Wolkin, M.V., Peeters, E., Williamson, J.R., Anderson, G.B., Schmitz, G.P., Recht, M.I., Schweizer, S., Scott, L.G., Ho, J.H., Elrod, S.A., Schultz, P.G., Lerner, R.A., Bruce, R.H., 2004. Proc. Natl. Acad. Sci. U. S. A. 101 (26), 9517–9522.
Wang, J., 2008. Chem. Rev. 108 (2), 814–825.
Yi, C., Lee, J.-H., Kwak, B.S., Lin, M.X., Kim, H.O., Jung, H.-I., 2014. Sens. Actuators B: Chem. 191 (0), 305–312.

M3P.047

IN-VIVO SINGLE CELL PROTEIN INTERACTION INVESTIGATION USING MICROFLUIDIC PLATFORM

B. Davaji[1], G. Biener[2], V. Raicu[2], and C.H. Lee[1]
[1]Marquette University, Milwaukee, WI, USA
[2]University of Wisconsin Milwaukee, Milwaukee, WI, USA

ABSTRACT
We have developed a microfluidic platform to immobilize single living cells at a position in a microfluidic channel for monitoring cell responses to different stimuli over time. While the cell is trapped, the device maintains control over changing the channel media and flow rate. The captured cell may be released in order to capture another cell and repeat the experiment without disturbing the setup. We have demonstrated the monitoring of an individual yeast cell, in which the captured cell is exposed to α-factor ligand.

KEYWORDS
Single cell, Microfluidic platform, silicon micromachining.

INTRODUCTION
Motivation
Investigating living cells, the building block of life, is essential to answering fundamental questions about biological function and malfunction (i.e., illness), and discovering drugs to cure diseases. Many biological investigations use large homogenous populations of cells to study their behaviors and responses to different stimuli. Such investigations require averaging the signals and statistical post processing of the data. However, it is shown that in many cases, such as gene expression, protein expression levels, and phenotypic outputs [1-2], the averaging of the signals from a population can be misleading.

The individual cell can exhibit different behavior than that of a population regardless of homogenous population selection [1]. Therefore, single cell biology is critical to overcome the limitations of studies that use cell populations. One of the requirements in such studies is to change the media in the channel without making a change in the captured cell location. A number of microfluidic technologies have been developed that contribute to single cell biology and medical genomics [3-4]. Unfortunately, most of the platforms lack full control over the trapped cell [5] and/or the fluid inside the channel [6] without disturbing the cell.

The microfluidic platform described in this report offers control over a captured cell separately from the flow direction and media change in the channel. Our device is suitable for many biological procedures at the individual cell level. The optical and electrical probing capabilities offered effectively assist the monitoring of an individual cell.

Concept
The individual cell capturing and immobilization concept is adopted from the planar patch clamp device [7-8] with some modifications. Figure 1 shows the silicon device microfluidic platform. A hole is micromachined on a thin SiN membrane which is used to trap a single cell by applying a pressure difference across the sides of the hole. A thin PDMS-Glass channel is used for compatibility with the short working distance of the high magnification microscope.

Integrated thin film resistive temperature detectors (RTDs) near the cell capturing hole on the membrane can be used for cell temperature monitoring, flow rate measuring, thermal and electrical excitation, and thermal particle cytometry [9].

As shown in Figure 2, the platform utilizes two microfluidic channels, a cell flow channel and a negative pressure channel to capture and immobilize a single cell. The microfluidic cell flow channel is fabricated on a 500 nm thick low-stress SiN membrane. At the center of the SiN membrane a trap hole (3 μm x 3 μm) is etched in the middle of the membrane, which connects the cell channel to the negative pressure channel. The cells and media are introduced in the microfluidic cell channel while negative pressure is applied to the negative pressure channel. This leads to the capture of an individual cell at the hole as illustrated in the cross-sectional view in Figure 2.

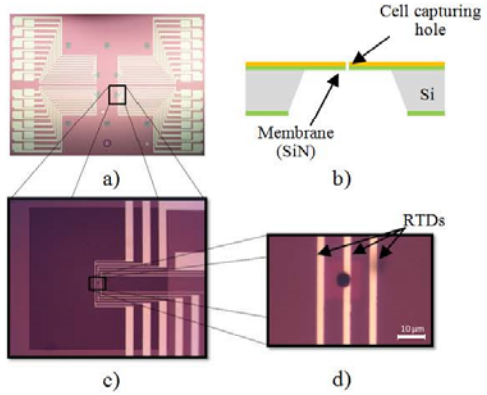

Figure 1: Microfluidic device fabricated with silicon micromachining. a) Silicon die with 4 cell trap sites, b) Cross sectional view of the membrane with cell trap site, c) Close-up image of the SiN membrane containing integrated RTD sensors, and d) Close-up image of cell trap site on membrane.

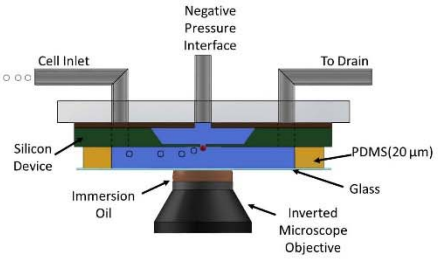

Figure 2: Cross-sectional view of the fabricated device with integrated microfluidic channels at both sides of the membrane.

We have demonstrated the ability to probe fluorescently-tagged proteins in living yeast cells (*S. cerevisiae*) using the platform. Two-photon excitation fluorescence microscopy is used to monitor the fluorescent tag interaction on the IN-VIVO single-cell.

The cell membrane is considered to be the gate to cell signaling and, as such, it requires gate keepers, which appear in the form of G protein coupled receptors (GPCR) [10]. Our platform allows the investigation of protein-protein and protein-ligand interactions at the cell membrane. The yeast cells were engineered to express the pheromone receptors Ste_2p – a GPCR –, which were fused to the green fluorescent protein (GFP_2) [11]. The cell was imaged using a two photon excitation microscope with high spectral resolution described previously [12] before and after introducing the α-factor ligand.

The conventional method requires measurements over a population of cells and use of statistical tools to recover the quaternary structure of the GPCR [13]. The use

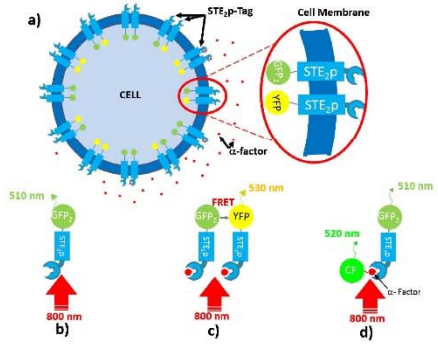

Figure 3: Concept of protein interaction probing using the two photon excitation microscopy technique is illustrated. a) Yeast cell expressing STE_{2p} with GFP2 or YFP attached. b) Fluorescent excitation concept of GFP2 to monitor spatial distribution of the protein. c) Concept of Förster Resonance Energy Transfer (FRET) technique to investigate the interaction between proteins. d) Interaction of STE_{2p}-GFP2 with α-factor (the corresponding ligand).

of a single cell technique is required in order to monitor changes in the quaternary structure or the localization of the receptor oligomers triggered by treatment with different ligands.

FABRICATION

In this section the fabrication and assembling processes of the platform shown in Figure 2 are presented in three stages: silicon device, PDMS channel, and negative pressure channel.

Silicon Device

The fabrication process starts with depositing a 500 nm SiN film on a 300 µm single crystal silicon wafer (Figure 4(a)). The membrane and the cell trap holes (i.e. , capturing sites) are printed on opposite sides of the wafer and anisotropic KOH (30% w/w) etching is used to etch the silicon and form the SiN membrane with the hole at the center as shown in Figure 4(c).

Then, a 40 nm nickel film is deposited on the wafer using thermal evaporation. Then the RTDs patterns and electrical interface contact pads are aligned and printed with cell trap holes on the SiN membrane. The metal patterns are etched using a solution of hydrochloric acid and nitric acid in DI water (1:5:5). The ratio of the solution is chosen to control the severe undercut during the metal etching.

PDMS Channel

The Polydimethylsiloxane (PDMS) channel (cell flow channel) is made by soft lithography. First, the silicon mold is fabricated by KOH silicon wet etching. The PDMS is poured over a releasing agent-coated silicon-micromachined mold. Then, the glass cover (100 µm) is placed on the PDMS and pressed against the silicon mold to make a thin microfluidic channel when cured at 70 °C for two hours. The PDMS channel on the glass cover is released from the mold by submerging in water for 24 hours. The water-soluble releasing agent dissolves in water, and the PDMS channels are lifted up from the mold.

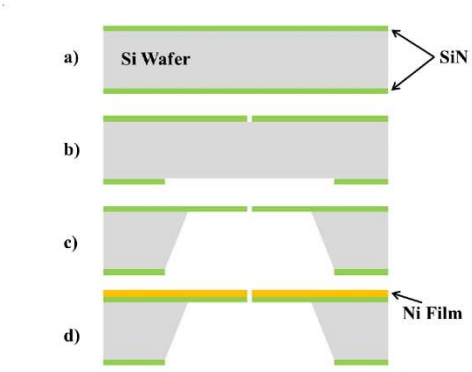

Figure 4: Process flow of the micromachined silicon device.

The released channels are rinsed in DI water, aligned, and bonded to the silicon device under the microscope.

Negative Pressure Channel

The acrylic microfluidic interface for inlets, outlets, and the negative pressure channel (Figure 2) are machined using a CO_2 laser printer. The silicon device and the PDMS channel are placed on a Plexiglas (acrylic) mount and bonded using a polyimide double-sided adhesive layer.

The fused silica capillary tubes with polyimide coating (Polymicro Technologies) are connected to the platform assembled with the PDMS channel (cell flow channel) and the acrylic mount (negative pressure channel and microfluidic interfaces). The other sides of the capillary tubes are connected to the syringes. A customized LabView program controls the syringe pumps, one for cell flow and the other for the negative pressure. All of the tubing connections within the platform are sealed with an epoxy to avoid any pressure leak during experiment.

EXPERIMENTAL RESULTS

Characterization

The flow rates in both channels have been characterized for the capturing of cells. For characterization, 10 μm polystyrene microspheres (PS beads) were used to tune the flow rates and pressure in channels for capturing the cells. The results of the flow rate characterization are shown in Figure 5.

Capturing Experiment

As mentioned above, we used yeast cells with the yeast pheromone receptor Ste2p fused to GFP_2 fluorescent proteins. The yeast cell preparation procedure was described in [11]. Yeast cells were separated from their growth medium and re-suspended in 0.1 mM KCl solution. The first step after setting up the microfluidic platform was to fill the capillary tubes of both channels with 0.1 mM KCl buffer solution. While filling the micro channels, they were monitored using a low-magnification (4X) microscope objective and transmission imaging to check for bubble formation. Bubble-free operation is essential for these experiments, since the capturing principle is based on pressure differences in the channels. The compressibility of air bubbles would change the capturing and immobilization characteristics of device.

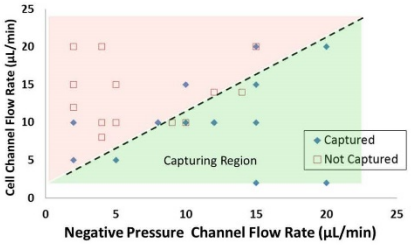

Figure 5: Cell capturing flow rate characterization. The 10 μm polystyrene beads suspended in a buffer solution are used for characterization. The capturing region is illustrated in green.

After filling the channels using the syringe pumps, the cells were introduced from a reservoir (1.5 mL tube) to the cell flow channel by changing the flow direction. After stabilizing the flow rate, a negative pressure was applied using the second syringe pump to capture a single cell, while maintaining the constant flow rate in the cell flow channel.

After the capture of a cell, excess cells and media were washed away from the microchannel by changing the cell reservoir tube to the KCl buffer tube. The flow rates in both channels were maintained during the washing process.

Using the two-photon excitation microscopy a florescent image with 1.3-nm spectral resolution was acquired to monitor the location of the GFP_2 tags and, consequently, the location of GPCRs on the cell membrane. Typical results of such an experiment are shown in Figure 6.

The florescent image provides the distribution of the GFP2 tags on the cell membrane. In some cases, the cells do exhibit florescence either due to bleaching or an error in the preparation process. Changing the flow direction in the negative pressure channel allows releasing the captured cell in such cases. Repeating the capturing procedure will enable the capture of another cell, a process that can be repeated until the right cell is found and captured.

By changing the reservoir tube, the ligand (α-factor) can be introduced into the microchannel. After exposing the cell to the ligand, the microchannel was washed with KCl buffer solution as explained above. The second florescent image was acquired using the two photon excitation microscopy. Comparing these images and distributions of

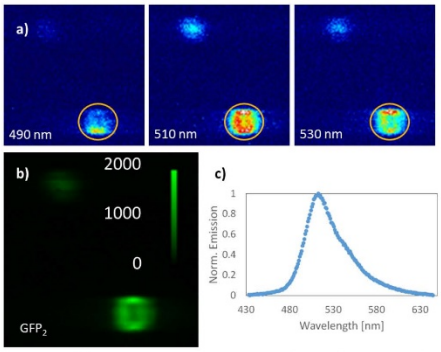

Figure 6: Florescent image of yeast cell exhibiting STE2p tagged with GFP2 trapped in a microfluidic channel captured with a two-photon excitation microscope. a) A selection of three images out of 200 captured for different wavelengths spanning the range from 430 to 650 nm, b) Fluorescent image as measured from the GFP2 tag emission and c) Spectrum of the trapped cell as measured over the area circled by the orange circle in (a). Note the square shape of the cell image, which was likely caused by optical aberrations associated with the square shape of the trapping hole.

proteins on the cell membrane will allow us in the future to investigate receptor-ligand interaction.

DISCUSSION

The pressure calibration of the capturing process and the size of the cell trap holes play key roles in performance of the microfluidic platform. By adjusting the pressures with respect to one another, we can change the flow rate of the top channel, which is required for introducing liquid samples with different viscosities.

The formation of bubbles can cause failure of the cell capturing and/or immobilization process. Air can be trapped in the dead volumes at microfluidic adaptors or interfaces and under the cell trap membrane chamber. The trapped air will result in bubble formation in channels. The compressible nature of the gas will affect the pressure in the channel and result in a significant cell capturing inefficiency.

The size of the cell trap holes needs to be selected appropriately. A larger hole can pass the cell though or trap multiple cells at once. We started with a 4 μm hole and reduced it to 3 μm to achieve higher capturing efficiency.

After capturing a cell, the protein-ligand interactions on the cell wall are monitored by comparing the fluorescent images within the ligand introduction period to the micro channel and investigating the redistribution of the GPCR's in the presence of ligands. Using a spectral unmixing method, we monitor the interaction and co-localization of the receptor and its ligand.

The microfluidic platform developed is also designed to monitor protein-protein interaction while using the microscope mentioned in conjunction with a short range process of energy transfer – called Forster resonance energy transfer, or FRET – between fluorescent tags located in the proximity of one another (i.e., less than 10 nm). This platform can be used for drug discovery and be utilized in the pharmaceutical industry. The integrated RTD sensors on the SiN membrane in the cell flow channel are also capable of monitoring the temperature change in the cell during interactions. This measurement could be beneficial for cell viability information monitoring and also performing calorimetric analysis on interactions.

CONCLUSION

The platform demonstrates the ability to immobilize individual cells while having control over the flow in a channel. The platform performs biological investigation on the individual cell level while avoiding complications and inaccuracies caused by using a population of cells. In our system, flow control issues plaguing previously developed platforms along with cell releasing difficulties are resolved.

ACKNOWLEDGEMENTS

Partial financial support for this work was provided by the National Science Foundation through the Industry/University Cooperative Research Center on Water Equipment & Policy located at the Marquette University (IIP-0968844) and by grants from the National Science Foundation (Grants PHY-1058470, IIP-1114305, and PHY-1126386) awarded to V. Raicu.

REFERENCES

[1]Shalek *et. al.,* Single-cell transcriptomics reveals bimodality in expression and splicing in immune cells, NATURE 498, 2013.

[2]Dominguez *et. al.,* Highly multiplexed quantitation of gene expression on single cells, Journal of Immunological Methods 391, 2013.

[3]Sun *et. al.,* Single-cell microfluidic impedance cytometry: a review, Microfluid Nanofluid 8, 2010.

[4]Zare *et. al.,* Microfluidic Platforms for Single-Cell Analysis, Annu. Rev. Biomed. Eng. 12, 2010.

[5]Kabiri Ameri *et. al.*, All electronic approach for high-throughput cell trapping and lysis with electrical impedance monitoring, Biosensors and Bioelectronics 54, 2014.

[6]Moon *et. al.*, Drop-on-Demand Single Cell Isolation and Total RNA Analysis, PLoS One 6(3), 2011.

[7]Mathews *et. al.*, Design and Fabrication of a Micromachined Planar Patch-Clamp Substrate with Integrated Microfluidics for Single-Cell Measurements, Journal of Microelectromechanical Systems, 15(1), 2006.

[8]Lehnert *et. al.,* Realization of hollow SiO2 micronozzles for electrical measurements on living cells, Applied Physics Letters 81, 2002.

[9]Vatha *et. al.,* A microfluidic device for thermal particle detection, Microfluid Nanofluid, 17(5), 2014.

[10]Ferré *et. al.*, G Protein–Coupled Receptor Oligomerization Revisited: Functional and Pharmacological Perspectives, Pharmacological Reviews, 66 (2), 2014.

[11]Raicu *et. al.*, Determination of supramolecular structure and spatial distribution of protein complexes in living cells, Nature Photonics, 2009.

[12]Biener *et. al.*, Development and Experimental Testing of an Optical Micro-Spectroscopic Technique Incorporating True Line-Scan Excitation, International Journal of Molecular Sciences, 2014.

[13]Raicu *et. al.*, FRET Spectrometry: A New Tool for the Determination of Protein Quaternary Structure in Living Cells, Biophysical Journal 105(9) , 2013.

CONTACT

*C.H. Lee, tel: +1-414-2884460;
chunghoon.lee@marquette.edu